PRE-STRESS LOSS DUE TO CREEP IN PRECAST CONCRETE DECKED BULB-TEE GIRDERS UNDER COLD CLIMATE CONDITIONS

By

Drew E. Vandermeer, B.S.

A Thesis Submitted in Partial Fulfillment of the Requirements

for the Degree of

Master of Science

in

Civil Engineering

University of Alaska Fairbanks

May 2019

APPROVED:

Dr. Il-Sang Ahn, Ph.D., P.E., Committee Chair

Dr. Juanyu (Jenny) Liu, Ph.D., Committee Member

Dr. Leroy Hulsey, Ph.D., P.E., S.E., Chair

Department Civil & Environmental Engineering

Dr. William "Bill" Schnabel, Ph.D., P.E., Dean,

College of Engineering and Mines

Dr. Michael Castellini, Ph.D., *Dean of the Graduate School*

Abstract

This report presents guidelines for estimating pre-stress loss in high-strength precast pre-tensioned concrete Decked Bulb-Tee (DBT) bridge girders in cold climate regions. The guidelines incorporate procedures yielding more accurate predictions of shrinkage and concrete creep than current 2017 American Association of State Highway and Transportation Officials (AASHTO) specifications. The results of this report will be of particular interest to researchers and cold climate bridge design engineers in improved predictions of design life and durability.

The use of high-strength concrete in pre-tensioned bridge girders has increased in popularity among many state highway agencies. This fact is due to its many beneficial economic and constructability aspects. The overall cost of longer girders with increased girder spacing in a bridge that is precast with high strength concrete can be significantly reduced through the proper estimating factors. Recent research indicates that the current provisions used for calculating pre-stress losses in cold regions for high-strength concrete bridge girders may not provide reliable estimates. Therefore, additional research is needed to evaluate the applicability of the current provisions for estimating pre-stress losses in high-strength concrete DBT girders. Accurate estimations of pre-stress losses in design of pre-tensioned concrete girders are affected by factors such as mix design, curing, concrete strength, and service exposure conditions. The development of improved guidelines for better estimating these losses assists bridge design engineers for such girders and provide a sense of security in terms of safety and longevity.

The research includes field measurements of an environmentally exposed apparatus set up to measure shrinkage, creep and strain in cylinders loaded under constant pressure for a full calendar year.

Table of Contents

List of Figures

Page

List of Tables

Page

Acknowledgements

There are many thanks to give in the process of developing a master's degree which go far beyond just those that I can mention. Firstly, I would like to thank God for allowing me the possibility to pursue higher education, I am truly blessed to have this opportunity. I would also like to thank my advisor and committee chair Dr. Il-Sang Ahn for his continued support, expertise, and encouragement throughout this long process. The groups that have been a big help in the development of this report are as follows: AggPro for product management, Alaska Department of Transportation Regional Lab with assistance in storage and strength tests, Jon's Machine Shop for frame manufacturing, CESTiCC for their financial backing, and all other entities involved. The faculty and staff at the University of Alaska Fairbanks, including my other committee members, have been nothing but helpful and I thank you for your belief in my efforts.

The interest I have in helping those around me goes beyond just research, there are areas in engineering that need to be pursued further in order to produce a safe and quality product. I have been gifted with the ability to invest my time into this thesis and hope that others are inspired to do the same and continue in their efforts to push engineering into the future. I am honored to bring new findings into the area of concrete creep and pre-stress loss as it pertains to construction in cold climates. Bringing new knowledge into my home state of Alaska while working for the University and seeing it implemented working as an Engineer for the State really puts a special mark on my educational and personal career, I will always cherish that fact and keep it close to my heart.

The source of strength and support from those around me has been invaluable in my efforts to produce a quality product, which takes time and sacrifice. My parents, Tim and Lynn Vandermeer, have given me all the opportunities they could provide and I am eternally grateful for their continued care, love, and support, I would be nowhere without you. I would also like to thank my loving wife Lizzy, you have been there for me through it all and always pushed me to be my best, you challenged me and I know I wouldn't be here without you, I love you.

Chapter 1 Introduction

1.1 Research Need

The popularity of using high-strength concrete for bridges has increased in recent years among many state highway agencies, such as Departments of Transportation and the Federal Highway Administration (FHWA). As of 2014, 44% of Alaska's state and local bridge inventory is concrete, but concrete accounts for approximately 80% of the new bridges built by the Alaska Department of Transportation & Public Facilities (ADOT&PF) (Daugherty and Marx 2014). The economic benefits are obtained through increased girder spacing, length, and lifespan. Due to its excellent adaptability to the constraints in Alaska, the Decked Bulb-Tee (DBT) girder is the most common type of bridge superstructure used by ADOT&PF. The DBT girder is a precast, pre-stressed concrete bulb-tee girder with a deck that is cast monolithically and pre-stressed with the girder (Oesterle et al. 2009, PCI 2011). Figure 1-1 shows the standard cross-section of Alaska-style DBT girders, where the deck width can reach 8.5 feet (ADOT&PF 2017).

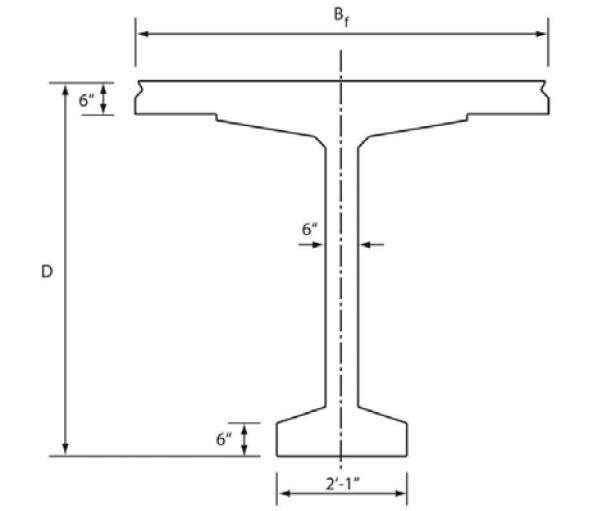

Figure 1-1: Standard Alaska-Style Precast DBT Girder Section (ADOT&PF 2017)

The long-term durability and wear-resistance of DBT girders to the Alaskan environment has proven to be outstanding. During the last ten years, approximately 80% of the new bridges constructed in Alaska have been bulb-tee girders. There has been almost no girder-related maintenance required on the 273 bridges of this style built in Alaska since 1973 (Daugherty and Marx 2014).

A DBT girder utilizes pre-stressing force applied to the girder by pre-stressing strands inside the girder during the fabrication. The pre-stressing force lets a DBT girder span a long distance. The amount of pre-stressing force in the entire life of the girder ensures the serviceability and safety of the bridge. As other types of pre-stressed concrete girders, the pre-stressing force initially applied during fabrication of a DBT girder decreases. The amount of force decreased, known as "pre-stress loss," is caused by several mechanisms when the bridge is both under construction and in service.

The pre-stress applied to a bridge girder counteracts the dead and live loads, in order to keep the tensile stress of the girder (i.e., the bottom flange) less than a specified tensile stress limit in the design. Meanwhile, the magnitude of pre-stress force in a girder decreases over time; from the fabrication of a girder to the end of the bridge's service life. The amount of pre-stress change, or pre-stress loss, should be well-known for girder design to assure the serviceability and safety of the bridge over the structure's life.

Since the climate conditions vary among the United States' locations, a more accurate representation of pre-stress loss with emphasis on temperature and relative humidity is required to assure accuracy. This is especially true for those in cold climate regions since the low temperature nature of the environment can have big impacts on the material properties of concrete and pre-stressing strands. Data for pre-stress losses in the design of pre-stressed concrete girders in cold climates are minimal and therefore require additional research to provide such information for better understanding of cold climate effects.

In Alaska, long-term pre-stress losses are different from other states due to;

- Different aggregate: the influence of different aggregate on the elastic modulus and creep coefficient of concrete was noted in Tadros et al. (2003).
- Few DBT girder fabricators in Alaska: there have been only three fabricators, with most of the work performed by one fabricator in Anchorage; so the material quality and workmanship can be relatively uniform among girders.
- Shorter time between fabrication and placement of girders: typically the time period in a storage yard is 60 days[1] in Alaska. Storage time is much longer in other states.
- Cold climates and extreme annual temperature variation in Alaska.

[1] From a DBT girder fabricator in AggPro in Anchorage, AK. Girders have been known to be placed two weeks after being cast while others sit in storage through the winter.

1.2 Objective and Scope of the Study

The goal of this research is to develop more accurate design parameters for estimating pre-stress losses in DBT girders due to concrete creep in cold climates. In the design of DBT girders, the amount of pre-stress force determines short-term and long-term stresses in concrete. If the pre-stress loss is underestimated, the concrete of a girder at midspan may experience the tensile stresses that exceed the bottom flange tension limit of concrete, which can compromise the durability and long-term performance of the girder. If the pre-stress loss is overestimated, however, more pre-stressing strands will be required than necessary, which may increase the cost of girder fabrication, reduce the maximum span length, or increase the number of girders. The accurate estimation of pre-stress losses, therefore, is essential in the design process.

Pre-stress loss can vary dramatically depending on its thermal environment, which directly affects its curing process. While this subject has been long studied by many researchers, it is hard to find research focused on DBT girders. Specifically, in-situ measurement of pre-stress loss data for DBT girders over a long period of time is extremely rare or does not exist. As the major portion of time-dependent pre-stress loss is due to concrete creep, the major part of the research focused on this specific mechanism.

The objectives of the present research are:

1. Acquiring a better understanding of concrete creep in cold climate regions. Since concrete creep depends on concrete mix design and environmental conditions, a physical concrete creep test in ambient environment of cold climate is done to accurately evaluate concrete creep. The study contained two identical concrete creep test setups; one outdoors in the natural Alaskan environment, while the second is in a lab indoors with controlled conditions.

2. Understanding specific design issues for DBT girders that are related to time-dependent pre-stress losses. The difference in design and construction between DBT girders and conventional pre-stressed girders should be well understood, since the majority of existing pre-stress loss provisions have been developed for conventional pre-stressed girders.

3. Proposing time-dependent pre-stress loss provisions for DBT girders in cold climate regions. Within the framework of current provisions in AASHTO LRFD, design recommendations are proposed.

1.3 Scope of This Report

This report presents all of the work performed in this project, including a literature review, the design and construction of concrete creep test frames, experiment procedures, concrete creep measurement results, and design implication.

In Chapter 2, the results of literature review are provided. In particular, design provisions for pre-stress losses from different design specifications and guidelines are compared. The provisions in AASHTO LRFD are discussed in details.

In Chapter 3, the design and fabrication of concrete frame are described. The specimen preparation and concrete creep test procedures are also explained. Sensors and a data acquisition system used for long-term creep measurement are presented.

In Chapter 4, the strain measurement results are presented. Also, the change of concrete compressive strength and elastic modulus are described. Additional measurements including temperature and relative humidity are summarized.

In Chapter 5, the measured pre-stress losses due to concrete creep are provided. These measured losses are compared with those in several design provisions. Design implications from the measured pre-stress losses are discussed.

In Chapter 6, summary of findings and conclusions are presented.

Chapter 2 Literature Review

2.1 Background

Over the past 20 years, the use of precast modular components to accelerate bridge construction has increasingly gained attention in the United States. Pre-cast concrete components are separately transported and assembled at the construction site, minimizing cast-in-place concrete work. Since the time period occupying the construction site can be substantially reduced, pre-cast modular construction allows bridge engineers to minimize accidents in the work zone, reduce traffic disruptions, and increase the speed of construction, all while maintaining construction quality, and minimizing the life-time costs and environmental impact (Shahawy 2003, PCINE 2014). The Linn Cove Viaduct in North Carolina (Figg and Pate 2004) and the Getty Museum People-Mover Guideway in California (Josten et al. 1995) are good examples where pre-cast concrete components have been used to substantially minimize environmental impact during the construction of substructures. In cold climate regions, accelerated bridge construction (ABC) is a particularly important strategy due to the short construction season (ADOT&PF 2017).

The environment where concrete cures and concrete structures are placed is one of the important factors that control the mechanical properties of the concrete. Just after the completion of construction, concrete bridges in cold climate regions are exposed to severely cold weather in the winter. Figure 2-1 shows daily average temperature and ambient relative humidity of several cities in cold climate regions (ClimaTemps 2016; Current Results Nexus 2016a; NOWData). The average winter (December – February) temperature is -6.7 °F in Fairbanks, AK, 29.4 °F in Spokane, WA, and 22.4 °F in Helena, MT. For the entire U.S., excluding Hawaii and Alaska, the average winter temperature is 33.2 °F (Current Results Nexus 2016b). Also, the ambient relative humidity has a significant influence on concrete creep (Park and Paulay 1975). Creep strains are low when the relative humidity is high, because creep is reduced if water loss from the member is restricted. During a typical construction season (June – October), the average relative humidity is 58.2% in Fairbanks, AK, 52.7% in Spokane, WA, and 51.8% in Helena, MT. In the AASHTO LRFD Bridge Design Specifications (AASHTO LRFD), the average annual ambient relative humidity in Fairbanks and Spokane is greater than 70% (AASHTO 2017). The concrete creep strains in such regions could be different from those anticipated in AASHTO LRFD.

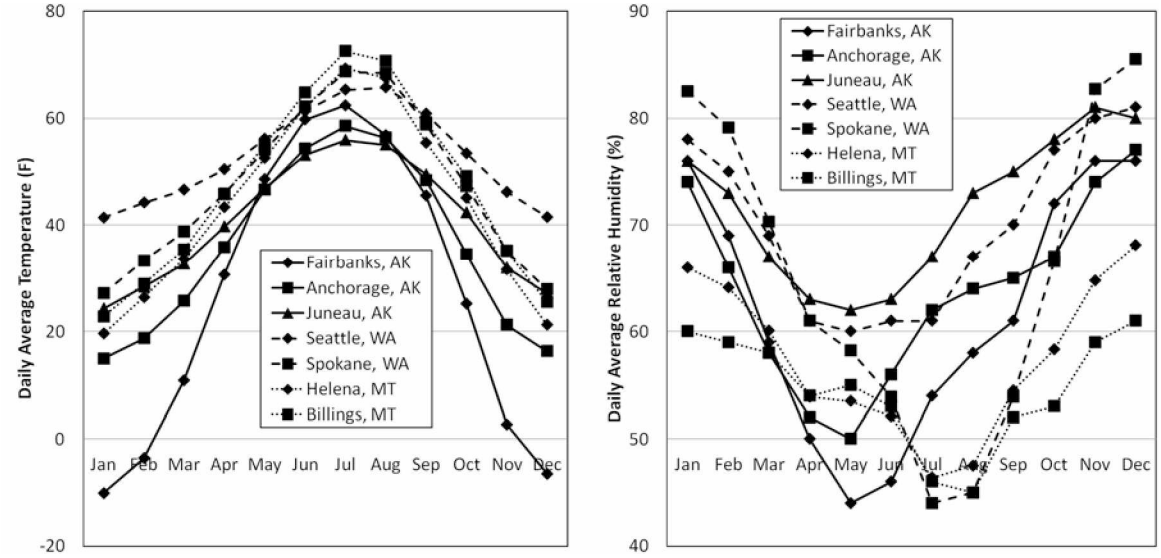

Figure 2-1: Daily Average Temperature and Daily Average Relative Humidity of Several Cities in Cold Climate Regions

When designing a concrete bridge there are many factors that must be take into account to ensure safety and longevity. The most important of these aspects includes pre-stress loss, environmental characteristics, curing conditions, and method of testing. Theoretically, total loss of pre-stress is the reduction of tension from the time strands are tensioned until the end of service life of the pre-stressed concrete member (Tadros et al. 2003). This includes both instantaneous and time-dependent losses and, for the pre-stressing steel, stress gains. Losses due to creep, shrinkage, and relaxation are time-dependent, whereas losses due to anchorage set, friction, and elastic shortening are instantaneous. The main resources that designers choose to use comes from the American Association of State Highway and Transportation Officials (AASHTO), the National Cooperative Highway Research Program (NCHRP), and some of their own state funded research operations which usually give insight into that particular geographic location. Upon studying how these organizations configure their work based on cold locations, the estimations of pre-stress loss do not emphasize the effects of ambient temperature and relative humidity with their temperature effects, which can have dramatic and permanent effects of the concrete.

In Alaska, the extreme environment makes it especially difficult to predict the pre-stress losses of a high-strength DBT girder. The time-dependent losses for standard precast, pre-

tensioned members subject to normal loading and environmental conditions can be found in the AASHTO LRFD section 5.9.3 regarding pre-stress loss (AASHTO 2017). In most cases this section would be useful, however, Alaska has never fit under the normal environmental conditions classification. The instantaneous loss can sometimes be identified under more controlled circumstances, due to the manufacturers pre-casting the girders indoors depending on the need. Although, the long term effects are more relative to the transfer and natural environment that the girders are in. The effects of ambient temperature and relative humidity need an emphasis on how it impacts pre-stress loss estimations.

The total pre-stress loss is separated into two groups: (1) instantaneous losses and (2) long-term time-dependent losses (AASHTO 2017). Losses due to anchorage set, friction, and elastic shortening are grouped as an instantaneous loss; losses due to concrete creep, concrete shrinkage, and relaxation of pre-stressing strands are classified as time-dependent losses. Figure 2-2 demonstrates the change in pre-stress force that occurs during bridge construction activities.

- A – C: Pre-stress loss due to pre-stressing bed anchorage seating, relaxation between initial tensioning and transfer, and temperature change in strand embedded in concrete. The losses from the bed anchorage seating (A – B) are not present in either pre-stressing strands or concrete.
- C – D: Instantaneous pre-stress loss at transfer due to elastic deformation and self-weight.
- D – E and F – G: Time-dependent pre-stress loss due to shrinkage and creep of girder concrete and relaxation of pre-stressing strands.
- E – F: Increasing tensile stress due to superimposed dead loads (SIDL).

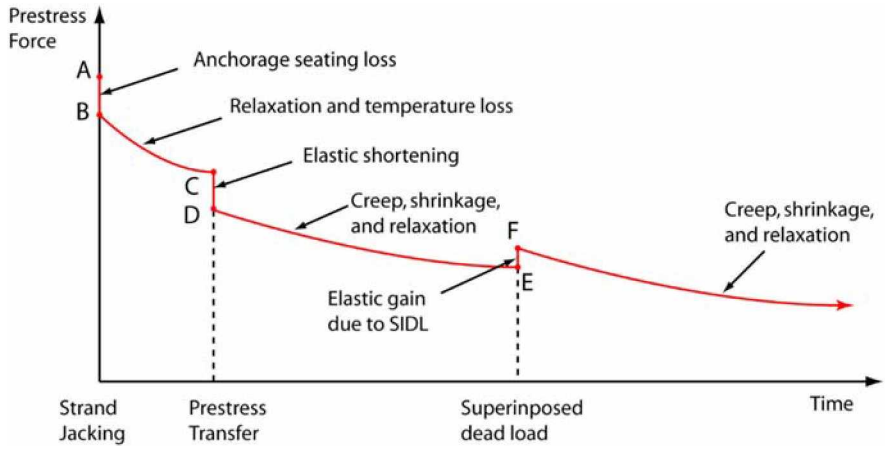

Figure 2-2: Pre-stressing Strand Force Changes with Time [modified from (Tadros et al. 2003) to represent DBT girders]

At transfer, compressive stresses are imposed to the concrete. In the current AASHTO LRFD (AASHTO 2017), the maximum allowable compressive stress at pre-stress transfer is $0.65 f'_{ci}$, where, f'_{ci} is concrete strength at transfer[2]. Figure 2-3 shows corresponding compressive stress changes at the bottom fiber concrete (tension side when subject to gravity loads) of a girder. When superimposed dead loads (SIDL) are placed, tensile stress increases both in the pre-stressing strands and the concrete. This induces stress "gain" in the pre-stressing strands (see Figure 2-2) and additional tensile stress at the bottom of the girder (see Figure 2-3). The tension side of the girder experiences only an increase in tensile stress and pre-stress "gains" do not equate to a reduction in pre-stress losses over time.

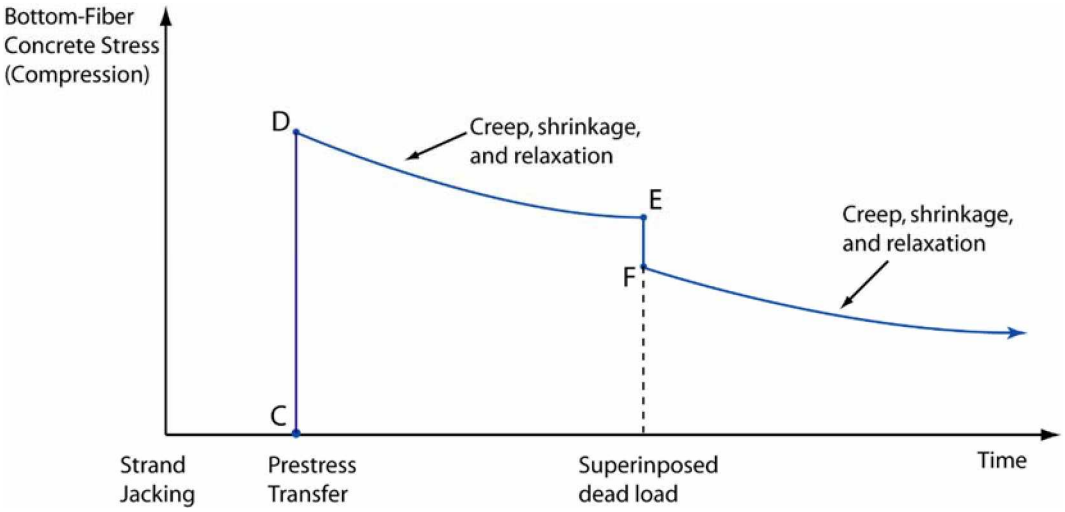

Figure 2-3: Bottom-Fiber Compressive Stress Changes [modified from Garber et al. (2013) to represent DBT girders]

Concrete shrinkage, concrete creep, and relaxation of pre-stressing strands are three major mechanisms contributing to time-dependent pre-stress losses. Among them, pre-stress loss due to creep is the most significant. For instance, the percentages of pre-stress losses due to creep, shrinkage, and relaxation to the total time-dependent losses were 68%, 24%, and 8%, respectively, for two example bridges in Tadros et al. (2003) and Roller et al. (2011). Due to

[2] This revision was made in 2016 Interim

creep, concrete strain under a constant stress increases with time. This occurs because the elastic modulus of the concrete under a constant stress decreases with the rate of loading.

Figure 2-4 shows the concrete stress-strain relationships that depend on the rate of loading (Rüsch 1960). When hardened concrete cylinders were loaded with a slow rate of loading (longer than 1 hour), the strength of concrete decreased compared to the strength observed from a loading occurring in minutes, which is typical for a concrete cylinder test. Collins and Mitchell (1997) reported that the strength reduction was about 20% of the 28-day strength. Also, concrete typically gains 20 to 40% in strength due to continuing hydration. These two phenomena compensate for each other, resulting in a conservative assumption on the 28-day concrete strength, so the strength reduction caused by long-term loading was not considered in the design (Collins and Mitchell 1997).

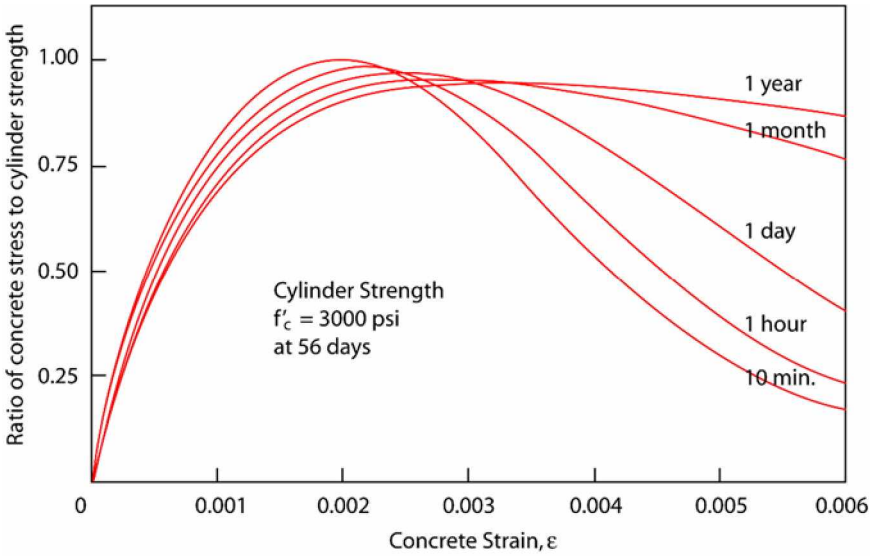

Figure 2-4: Stress-Strain Relationships for Eccentric Compression after Various Durations of Loading at Constant Strain Rates (Rüsch 1960)

Concrete creep in stress-strain relationships is demonstrated in Figure 2-5, shown below (Rüsch 1960). When a stress is applied to a concrete cylinder with a rate of $t = 20\,\text{min}$. and held constant for a long time, the strain increases as the stress-strain relationship changes with time. Theoretically, the creep stops as the strain reaches the creep limit, a stress-strain relationship for a load with a rate of $t = \infty$. For estimating concrete creep, therefore, the stress-strain relationship of concrete at different ages and under different stress histories should be known.

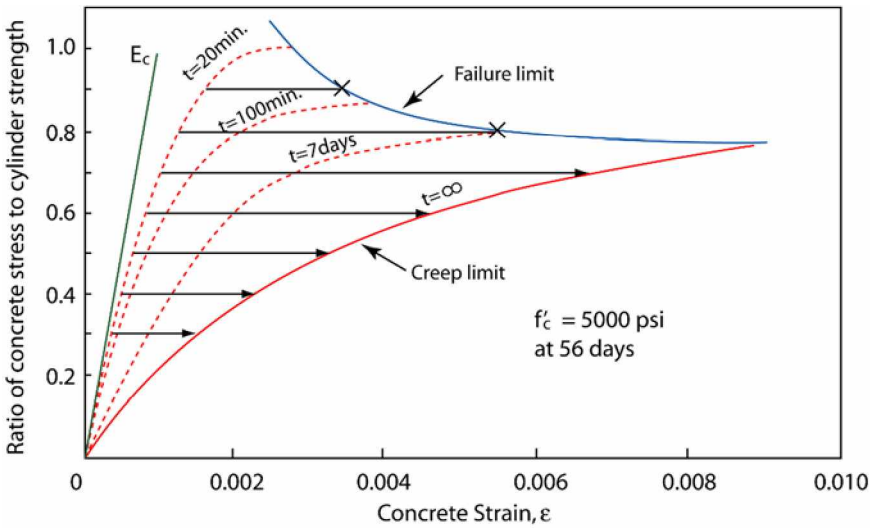

Figure 2-5: Influence of Load Intensity and Duration on Concrete Strain (Rüsch 1960)

The creep deformation of concrete with time under constant axial compressive stress is illustrated in Figure 2-6 (Park and Paulay 1975). The creep would proceed at a decreasing rate with time. If the load is removed, the elastic strain is immediately recovered. However, the elastic recovery is less than the initial elastic strain, because the elastic modulus of concrete increases with age[3]. The creep strain occurring over a given period of time is proportional to the applied stress if the stress level is not high. Concrete creep strain is the permanent strain that remains after concrete that was loaded for some time was then unloaded. For the usual range of concrete stress used in structural design, the assumption of a linear relationship between creep strain and applied stress is acceptable.

[3] After the start of concrete hardening, the stress-strain relationship under short-term loading is different from the stress-strain relationship under long-term loading for the same concrete.

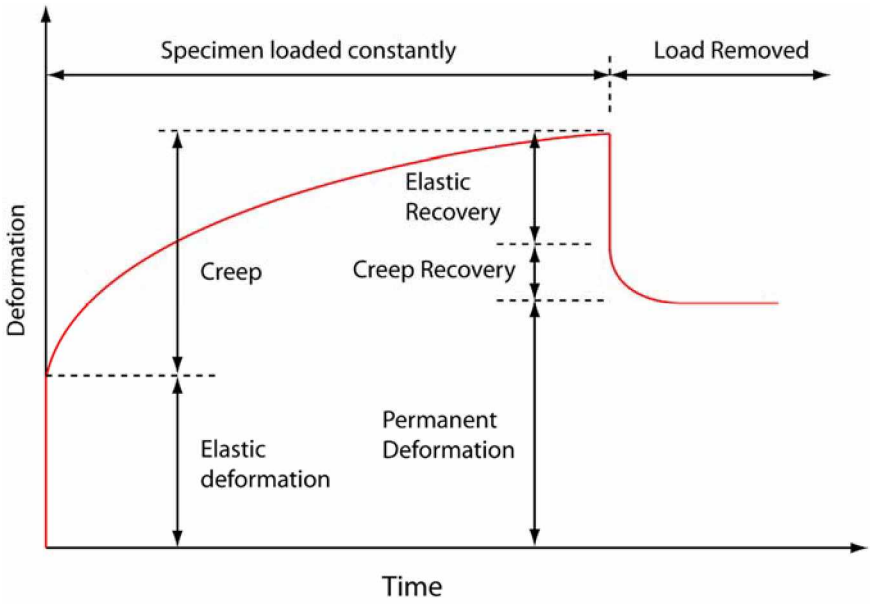

Figure 2-6: Typical Creep Curve with Constant Axial Compressive Stress (Park and Paulay 1975)

The stress-strain relationship of concrete can be represented by various models, and a linear elastic relationship in Eq. (2-1) can be used if the stress is low, $f_c < 0.6 f_c'$ (Collins and Mitchell 1997).

$$f_c = E_c \varepsilon_{cf} \tag{2-1}$$

where,

f_c = the concrete stress

f_c' = the maximum stress (strength),

ε_{cf} = the concrete strain caused by f_c

E_c = the tangent modulus when $\varepsilon_{cf} = 0$.

In AASHTO LRFD (AASHTO 2017), Eq. (2-2) is used for the estimation of E_c.

$$E_c = 120,000 K_1 w_c^{2.0} \left(f_c'\right)^{0.33} \qquad (ksi) \tag{2-2}$$

where

K_1 = correction factor for source of aggregate

$w_c^{2.0}$ = unit weight of concrete (kcf)

The difference between this secant modulus and the tangent modulus is negligible for the concrete used in typical pre-stressed concrete (Collins and Mitchell 1997). The total concrete strain due to a sustained stress $f_{c,long}$ can be expressed as the sum of an elastic strain $\varepsilon_{c,el}$ and a creep strain $\varepsilon_{c,c}$ in Eq. (2-3):

$$\varepsilon_{c,long} = \varepsilon_{c,el} + \varepsilon_{c,c} = \varepsilon_{c,el} + \phi(t,\tau)\varepsilon_{c,el} = \frac{f_{c,long}}{E_c}\left[1+\phi(t,\tau)\right] \tag{2-3}$$

where

$\phi(t,\tau)$ = creep function

t = the age of the concrete

τ = the age when the stress $f_{c,long}$ is applied

The creep function can be expressed in Eq. (2-4) as (Menn 1986):

$$\phi(t,\tau) = \phi_n k(\overline{\tau}) f(t-\tau) \tag{2-4}$$

where

ϕ_n = the creep coefficient that depends on material properties and environmental conditions

$k(\overline{\tau})$ = a correction factor for the age of concrete at time of loading

$f(t-\tau)$ = the time-varying behavior of creep and depends on an effective thickness parameter.

There are various factors that affect concrete creep and shrinkage, and Table 2-1 shows the ones in ACI 209.2R-08 *Guide for Modeling and Calculating Shrinkage and Creep in Hardened Concrete* (ACI 2008).

Table 2-1: Factors Affecting Concrete Creep and Shrinkage (ACI 2008)

Factors			Variables considered
Concrete (creep and shrinkage)	Concrete composition	Cement paste content	Type of cement
		Water-cement ratio	Slump
		Mixture proportions	Air content
		Aggregate characteristics	Fine aggregate percentage
		Degrees of compaction	Cement content
	Initial curing	Length of initial curing	Moist cured
			Steam cured
		Curing temperature	Moist cured
			Steam cured
		Curing humidity	Relative humidity
Member geometry and environment (creep and shrinkage)	Environment	Concrete temperature	Concrete temperature
		Concrete water content	Ambient relative humidity
	Geometry	Size and shape	Volume-surface ratio or minimum thickness
Loading (creep only)	Loading history	Concrete age at load application	Moist cured
			Steam cured
		During of loading period	Sustained load
		Duration of unloading period	—
		Number of load cycles	—
	Stress conditions	Type of stress and distribution across the section	Compressive stress
		Stress/strength ratio	Stress/strength ratio

Since the adoption of the current pre-stress loss provisions in the AASHTO LRFD, the accuracy and usability of the provisions have been called into question. For example, in a study comparing measured and calculated pre-stress losses, a significant discrepancy was found in the time-dependent losses of high-strength concrete bulb-tee girders (Roller et al. 2011). Brewe observed that the AASHTO LRFD refined method underestimates the total pre-stress losses for all beams by an average of 22% (Brewe et al. 2008). Garber discussed that the current refined estimation method resulted in underestimation of the pre-stress loss by nearly half (Garber et al. 2013). Mertol et al. investigated creep and shrinkage of high-strength concrete of which compressive strengths were 10 ksi, 14 ksi, and 18 ksi (Mertol et al. 2010). It was shown that the creep coefficient in AASHTO LRFD (AASHTO 2017) was closer to the measured value for moist-cured HSC specimens but overestimated the measured value for heat-cured HSC specimens. For shrinkage strain, AASHTO LRFD provided reasonably good predictions compared to the measured strains except that the predicted shrinkage strains are higher than the

measured values at an early age. In addition, there was less shrinkage for heat-cured specimens than for the moist-cured cylinders. The difference in the shrinkage having different strength (10 ksi to 18 ksi) was small.

Based on measured pre-stress loss data, different methods for estimating pre-stress losses are compared in Figure 2-7 (Garber et al. 2016). The PCI simplified method and 2004 AASHTO LRFD provisions are conservative in the estimation of the final pre-stress loss; whereas, the other methods generate many cases where measured pre-stress losses are significantly larger than estimated losses. It was mentioned that the current provisions are less conservative, possibly more accurate, and significantly more complex without accurately predicting pre-stress losses.

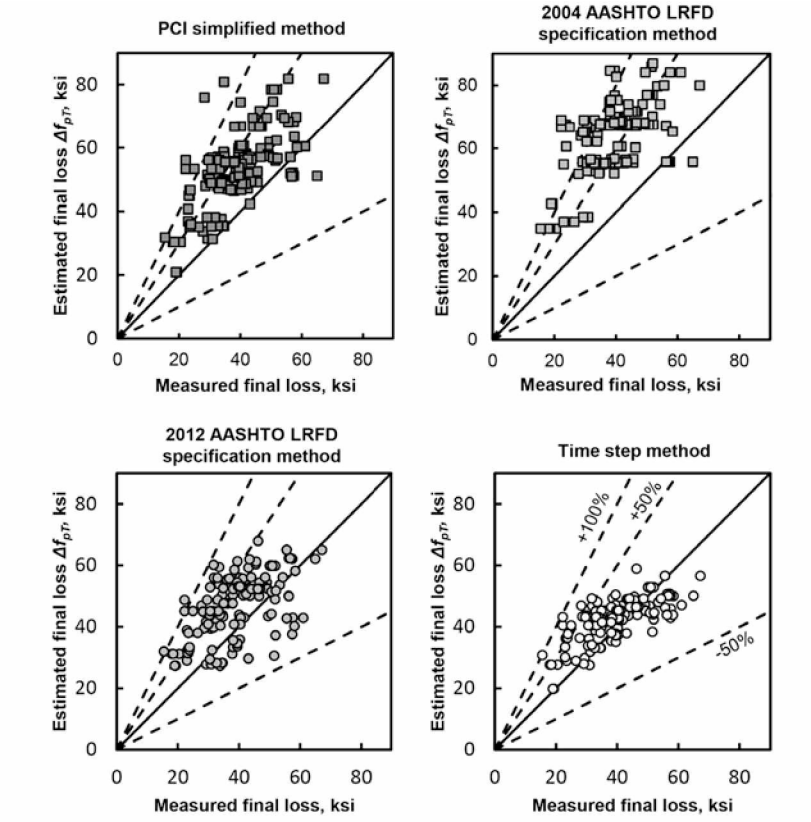

Figure 2-7: Estimated and Measured Pre-stress Losses (Garber et al. 2016)

2.2 Design Provisions in AASHTO LRFD (2017)

The pre-stress loss provisions in AASHTO LRFD were based on findings in NCHRP Project 18-07 (AASHTO 2017, Tadros et al. 2003). The total pre-stress loss is represented in Eq. (2-5) as:

$$\Delta f_{pT} = \Delta f_{pES} + \Delta f_{pLT} \tag{2-5}$$

where,

Δf_{pES} = instantaneous loss due to elastic shortening in members and

Δf_{pLT} = the sum of time-dependent losses.

For the estimation of the time-dependent losses, two methods were provided: approximate estimation and refined estimation methods. The approximate estimation method was developed for pre-stressed, I-beams and inverted tee beams with which a concrete deck was compositely built. Furthermore, it was assumed that moment from live load was about 1/3 of the total load moments. Therefore, the application of the approximate estimation method to DBT girders is questionable, and modification of the method may be necessary.

2.2.1 Instantaneous Pre-stress Losses

Interpretation of concrete strain prior to transfer, especially in high-strength concrete, is rather complicated. When pre-stressing force is released to the concrete and the temperature of the concrete is still elevated due to hydration and curing, the amount of pre-stressing force applied to the girder is significantly impacted by the temporary high temperature. Eq. (2-6) represents strand stress loss due to a temperature rise, ΔT (Tadros et al. 2003):

$$\Delta f_{pt} = \alpha_s E_p \Delta T \tag{2-6}$$

where,

Δf_{pt} = pre-stress changes (loss or gain) due to temperature change

α_s = the coefficient of the thermal expansion of steel

E_p = modulus of elasticity of pre-stressing strands

Pre-stress loss due to the elastic shortening of pre-stressing strands in Eq. (2-7) is shown as: [AASHTO 5.9.3.2.3a-1]:

$$\Delta f_{pES} = \frac{E_p}{E_{ct}} f_{cgp} \tag{2-7}$$

where,

Δf_{pES} = pre-stress loss due to elastic shortening (ksi)

E_p = modulus of elasticity of pre-stressing steel (ksi)

E_{ci} = modulus of elasticity of concrete at transfer or time of load application (ksi)

f_{cgp} = concrete stress at the center of gravity of pre-stressing tendons due to the pre-stressing force immediately after transfer and the self-weight of the member at the section of maximum moment (ksi)

Historically, the conservative approach is to account for the effect of elastic deformation to occur at all stages of loading in the calculation of elastic shortening and creep losses considering only the pre-stress force present after transfer. The pre-stress may be assumed to be 90% of the initial pre-stress before transfer and the analysis is iterated until acceptable accuracy is achieved. When using transformed section properties, the pre-stressing strand and the concrete are treated together as a composite section. The effective stress in these strands consists of the sum of the Δf_{pES} values that must be included. However, analysis with gross (or net) section properties involves using the effective stress in the strands at any given stage of loading to determine the pre-stress force and resulting concrete stresses.

2.2.2 Time-Dependent Pre-stress Losses

In the refined estimation method, the time-dependent pre-stress loss is calculated from Eq. (2-8) [AASHTO 5.9.3.4.1-1].

$$\Delta f_{pLT} = \left(\Delta f_{pSR} + \Delta f_{pCR} + \Delta f_{pR1}\right)_{id} + \left(\Delta f_{pSD} + \Delta f_{pCD} + \Delta f_{pR2} - \Delta f_{pSS}\right)_{df} \quad (2\text{-}8)$$

where

(Δf_{pSR})= pre-stress loss due to shrinkage of girder concrete between transfer and deck placement (ksi)

(Δf_{pCR}) = pre-stress loss due to creep of girder concrete between transfer and deck placement (ksi)

(Δf_{pR1}) = pre-stress loss due to relaxation of pre-stressing strands between time of transfer and deck placement (ksi)

(Δf_{pR2}) = pre-stress loss due to relaxation of pre-stressing strands in composite section between time of deck placement and final time (ksi)

(Δf_{pSD}) = pre-stress loss due to shrinkage of girder concrete between time of deck placement and final time (ksi)

(Δf_{pCD}) = pre-stress loss due to creep of girder concrete between time of deck placement and final time (ksi)

(Δf_{pSS}) = pre-stress gain due to shrinkage of deck in composite section (ksi)

$(\Delta f_{pSR} + \Delta f_{pCR} + \Delta f_{pR1})_{id}$ = sum of time-dependent pre-stress losses between transfer and deck placement (ksi)

$(\Delta f_{pSD} + \Delta f_{pCD} + \Delta f_{pR2} - \Delta f_{pSS})_{df}$ = sum of time-dependent pre-stress losses after deck placement (ksi)

For the estimation of each component in time-dependent pre-stress losses, the concrete strain is estimated based on the stress-strain relationship of slow-loading which can be represented by elastic modulus, $E_c^{"}$, in Eq. (2-9): (Tadros et al. 2003):

$$E_c^{"} = \frac{E_{ci}}{1 + \chi \psi_b (t_f, t_i)} \tag{2-9}$$

where,

E_{ci} = the concrete elastic modulus at pre-stress transfer,

$\chi = 0.7$ = the relaxation coefficient, and

$\psi_b (t_f, t_i)$ = the creep coefficient.

The creep coefficient in Eq. (2-10) is the ratio of creep strain at time $t = t_f$ to elastic strain when a load is applied at time $t = t_i$ and held constant (Tadros et al. 2003).

$$\psi_b (t_f, t_i) = \frac{\varepsilon_{cc}}{\varepsilon_e} = \psi_u \cdot \gamma_{cr} = 1.9 \cdot \left(k_{td} k_s k_{hc} k_f t_i^{-0.118} \right) \tag{2-10}$$

where,

ψ_u = an ultimate creep coefficient

k_{td} = the time-development factor

k_s = the factor for the effect of the volume-to-surface ratio

k_{hc} = the humidity factor

k_f = the factor for effect of concrete strength

Correction factors are used in various prediction methods to modify the ultimate values of creep coefficient and shrinkage strain of concrete for any period of time. Factors are

introduced to account as much as possible for the average conditions commonly encountered in practices; such as 70% annual average ambient relative humidity, V/S ratio of 3.5in., loading age of 1 day for precast pre-tensioned members and 7 days for cast-in-place deck slabs, and accelerated curing for 1 day or moist curing for 7 days. (Tadros et al. 2003)

For the ambient relative humidity, the range of 30% to 80% encountered in the United States can be applied to the humidity factors for shrinkage and creep in Eq. (2-11) and Eq. (2-12) (Tadros et al. 2003):

$$\text{Shrinkage: } k_{hs} = 2.00 - 0.0143H \tag{2-11}$$

$$\text{Creep: } k_{hc} = 1.56 - 0.008H \tag{2-12}$$

where,

H = relative humidity (%)

The pre-stress loss due to shrinkage of girder concrete between the time of transfer and the time of deck placement shall be determined in Eq. (2-13) and Eq. (2-14) [AASHTO Equations 5.9.5.4.2a-1 and 5.9.5.4.2a-2] as:

$$\Delta f_{pSR} = \varepsilon_{bid} E_p K_{id} \tag{2-13}$$

$$K_{id} = \frac{1}{1 + \frac{E_p}{E_{ci}} \frac{A_{ps}}{A_g} (1 + \frac{A_g e_{pg}^2}{I_g})[1 + 0.7\psi_b(t_f, t_i)]} \tag{2-14}$$

where,

ε_{bid} = concrete shrinkage strain of girder between the time of transfer and deck placement per Eq. 5.4.2.3.3-1 (in. / in.)

K_{id} = transformed section coefficient that accounts for time-dependent interaction between concrete and bonded steel in the section being considered for time period between transfer and deck placement

e_{pg} = eccentricity of pre-stressing force with respect to the centroid of girder (in.); positive in common construction where it is below girder centroid

$\psi_b(t_f, t_i)$ = girder creep coefficient at final time due to loading introduced at transfer per Eq. 5.4.2.3.2-1

t_f = final age (day)

t_i = age of concrete at time of transfer (day)

The pre-stress loss due to shrinkage of girder concrete between the time of deck placement and the final time found in Eq. (2-15) and Eq. (2-16) [AASHTO Equation 5.9.3.4.3a-1 and 5.5.9.4.3a-2] shall be determined as:

$$\Delta f_{pSD} = \varepsilon_{bdf} E_p K_{df} \tag{2-15}$$

$$K_{df} = \frac{1}{1 + \frac{E_p}{E_{ci}} \frac{A_{ps}}{A_c}(1 + \frac{A_c e_{pc}^2}{I_c})[1 + 0.7\psi_b(t_f, t_i)]} \tag{2-16}$$

where,

ε_{bdf} = shrinkage strain of girder between time of deck placement and final per Eq. 5.4.2.3.3-1

K_{df} = transformed section coefficient that accounts for time-dependent interaction between concrete and bonded steel in the section being considered for time period between deck placement and final time

e_{pc} = eccentricity of pre-stressing force with respect to centroid of composite section (in.) positive in typical construction where pre-stressing force is below centroid of section

A_c = area of section calculated using the gross composite concrete section properties of the girder and the deck and the deck-to-girder modular ration (in.^{2})

I_c = moment of inertia of section calculated using the gross composite concrete section properties of the girder and the deck and the deck-to-girder modular ration (in.^{4})

The pre-stress loss due to creep of girder concrete between the time of transfer and the time of deck placement in Eq. (2-17) [AASHTO Equation 5.9.3.4.2b-1] shall be determined as:

$$\Delta f_{pCR} = \frac{E_p}{E_{ci}} f_{cgp} \psi_b(t_d, t_i) K_{id} \tag{2-17}$$

where,

Δf_{pCR} = pre-stress loss due to creep of concrete between time of transfer and deck placement

$\psi_b(t_d, t_i)$= girder creep coefficient at time of deck placement due to loading per Eq. 5.4.2.3.2-1

t_d = age at deck placement (day)

The pre-stress loss due to creep of girder concrete between time of deck placement and final time in Eq. (2-18) [AASHTO Equation 5.9.5.4.3b-1] shall be determined as:

$$\Delta f_{pCD} = \frac{E_p}{E_{ci}} f_{cgp}\left[\psi_b(t_f,t_i) - \psi_b(t_d,t_i)\right]K_{df} + \frac{E_p}{E_c}\Delta f_{cd}\psi_b(t_f,t_d)K_{df} \quad (2\text{-}18)$$

where,

Δf_{pCD} = the change in pre-stress (loss is positive, gain is negative) due to creep of girder concrete between time of deck placement and final time

Δf_{cd} = change in concrete stress at centroid of pre-stressing strands due to long-term losses between transfer and deck placement, combined with deck weight and superimposed loads (ksi)

$\psi_b(t_f,t_d)$ = girder creep coefficient at final time due to loading at deck placement per Eq. 5.4.2.3.2-1

The pre-stress loss due to relaxation of pre-stressing strands between the time of transfer and the time of deck placement shall be determined in Eq. (2-19) [AASHTO Equation 5.9.3.4.2c-1] as:

$$\Delta f_{pR1} = \frac{f_{pt}}{K_L}\left(\frac{f_{pt}}{f_{py}} - 0.55\right) \quad (2\text{-}19)$$

where,

Δf_{pR1} = The pre-stress loss due to relaxation of pre-stressing strands between time of transfer and deck placement, may be assumed equal to 1.2ksi for low-relaxation strands.

K_L = factor accounting for type of steel taken as 30 for low relaxation strands and 7 for other pre-stressing steel, unless more accurate manufacturer's data are available

f_{pt} = stress in pre-stressing strands immediately after transfer, taken not less than $0.55\,f_{py}$ in Eq. 5.9.3.4.2c-1

A more accurate prediction of relaxation loss between transfer and deck placement is given in Eq. (2-20) (Tadros et al. 2003):

$$\Delta f_{pR1} = \left[\frac{f_{pt}}{K_L'}\frac{log(t)}{log(t_i)}\left(\frac{f_{pt}}{f_{py}} - 0.55\right)\right]\left[1 - \frac{3(\Delta f_{pSR} + \Delta f_{pCR})}{f_{pt}}\right]K_{id} \quad (2\text{-}20)$$

where,

K_L' = factor accounting for type of steel, equal to 45 for low relaxation steel

K_{id} = factor accounting for restraint of concrete member caused by bonded reinforcement = 0.8

t = time between strand tensioning and deck placement (day) = 120 days

t_i = 0.75 day

$$\left[1-\frac{3(\Delta f_{pSR}+\Delta f_{pCR})}{f_{pt}}\right]=0.67$$

The pre-stress loss due to relaxation of pre-stressing strands in composite section between time of deck placement and final time, Δf_{pR2}, shall be determined in Eq. (2-21) [AASHTO Equation 5.9.3.4.3c-1] as:

$$\Delta f_{pR2}=\Delta f_{pR1} \tag{2-21}$$

The pre-stress gain due to shrinkage of deck composite section, Δf_{pSS}, shall be determined in Eq. (2-22) and in Eq. (2-23) [AASHTO Equation 5.9.3.4.3d-1 & 5.9.3.4.3d-2] as:

$$\Delta f_{pSS}=\frac{E_p}{E_c}f_{cdf}K_{df}\left[1+0.7\psi_b(t_f,t_d)\right] \tag{2-22}$$

$$\Delta f_{cdf}=\frac{\varepsilon_{ddf}A_dE_{cd}}{[1+0.7\Psi_d(t_f,t_d)]}\left[\frac{1}{A_g}-\frac{e_{pc}e_d}{I_c}\right] \tag{2-23}$$

where,

Δf_{cdf} = change in concrete stress at centroid of pre-stressing strands due to shrinkage of deck concrete (ksi)

ε_{ddf} = shrinkage strain of deck concrete between placement and final time per Eq. 5.4.2.3.3-1 (in./in.)

A_d = area of deck concrete (in.^{2})

E_{cd} = modulus of elasticity of deck concrete (ksi)

e_d = eccentricity of deck with respect to the gross composite section, positive in typical construction where deck is above girder (in.)

$\Psi_d(t_f,t_d)$ = creep coefficient of deck concrete at final time due to loading introduced shortly after deck placement

2.3 Other Design Provisions

For pre-stress loss estimation, three methods have been used: lump-sum estimates, rational approximate methods, and detailed time-dependent analyses. The approximate estimation method of time-dependent losses (section 5.9.3.3) in AASHTO LRFD and the total-loss method in the PCI Design Handbook are lump-sum estimate methods (AASHTO 2017, PCI 2010). The refined estimation of time-dependent losses method (section 5.9.3.4) in AASHTO LRFD and a method in the PCI Design Handbook can be classified as rational approximate methods. Detailed time-dependent analyses may provide accurate prediction of pre-stress losses. Some of these methods are presented in the PCI Bridge Design Manual (PCI 2000). In the present study, the following methods are of primary concern.

- 2004 AASHTO Lump-sum method
- 2004 AASHTO Refined method
- 2017 AASHTO Approximate estimation
- 2017 AASHTO Refined estimation

In NCHRP report 496, the final form of the approximate method of pre-stress loss formula is shown as (Tadros et al. 2003) in Equation (2-24) through (2-26):

$$\Delta f_{pLT} = 10.0\frac{f_{pi}A_{ps}}{A_g}\gamma_h\gamma_{st} + 12.0\gamma_h\gamma_{st} + 2.5 \tag{2-24}$$

$$\gamma_h = 1.7 - 0.01H \tag{2-25}$$

$$\gamma_{st} = \frac{5}{1+f_{ci}'} \tag{2-26}$$

where,

γ_h = correction factor for relative humidity of the ambient air

γ_{st} = correction factor for specified concrete strength at time of pre-stress transfer to concrete member

A_{ps} = area of pre-stressing steel (in^2)

f_{pi} = pre-stressing steel stress immediately prior to transfer (ksi)

The following assumptions were made to arrive at the approximate method coefficients.

(a) Pre-stress losses are calculated for conditions at the maximum positive moment section

(b) No mild steel reinforcement exists at that section

(c) Elastic losses at transfer or elastic gains due to application of external loads are not considered.

(d) Pre-stress is transferred to the concrete at 1 day in accelerated plant curing conditions.

(e) The cast-in-place deck weight (composite construction) is applied to the precast concrete section without any shoring after at least 28 days from the time of pre-stress transfer.

(f) V/S ratio for the girder cross section is 3 in. to 4 in.

In the third edition of the AASHTO LRFD specifications, pre-stress losses due to concrete creep and shrinkage were determined from Eq. (2-27) and Eq. (2-28) (AASHTO 2004):

$$\Delta f_{pCR} = 12.0 f_{cgp} - 7.0 \Delta f_{cdp} \tag{2-27}$$

$$\Delta f_{pSR} = 17.0 - 0.15H \tag{2-28}$$

where,

f_{cgp} = the concrete stress at the center of gravity of the pre-stressing

Δf_{cdp} = the concrete stress change due to permanent loads

H = average relative humidity (%).

The *Alaska Bridges and Structures Manual* (ADOT&PF 2017) was mainly based on the 6th edition of the AASHTO LRFD (2012), but provisions for the estimation of time-dependent pre-stress losses for DBT girders in Eq. (2-29) were adopted from the lump-sum method in the 3rd edition (or before) of the AASHTO LRFD. Specifically, the equation of average loss for single T or double T girders was adopted with a pre-stress loss reduction of -8 ksi for low-relaxation strands. In this equation, the sum of time-dependent pre-stress losses is expressed as a function of concrete strength, f_c'.

$$\Delta f_{pLT} = 33\left[1 - 0.15\left(\frac{f_c' - 6}{6}\right)\right] - 2 \quad (ksi) \tag{2-29}$$

The 28 day compressive strength of concrete in structural elements can be found in the ADOT&PF tables in Chapter 14 regarding structural concrete (ADOT&PF 2017). Normal weight concrete varies between 145 pcf for cast-in-place concrete, and 155 pcf for precast

concrete excluding the weight of the internal steel reinforcement. The common sizes for the pre-stressing strands used in bridge construction are 0.5 and 0.6 inches in diameter. For girders within Alaska, the diameter of the pre-stressing strands in pre-tensioned girders is 0.5 inches, while the diameter is typically 0.6 inches for girders fabricated outside Alaska.

Chapter 3 Concrete Creep Test Setup

The amount of concrete creep that a particular concrete experiences is difficult to estimate accurately unless concrete cylinder tests are conducted to determine the creep characteristics. Without such tests, accuracies of better than ±30% should not be expected (Collins and Mitchell 1997). From the measurement of small size test specimens, it was observed that the most of pre-stress loss occurred between 140 and 168 days, and the loss increases significantly within the first 6 months (Brewe et al. 2008).

In the present research, two concrete creep test frames were fabricated based on ASTM C 512 "Standard Test Method for Creep of Concrete in Compression" (ASTM 2015). One test frame was placed in the structural engineering laboratory at University of Alaska Fairbanks (UAF) and the other frame was located outside a building on the UAF campus under ambient environment conditions. The effects on concrete creep from the cold climate were evaluated by comparing the measured strain changes from the two test frames for 11 months (7/26/2017 – 6/21/2018).

3.1 Concrete Creep Test Frame

Two concrete creep test frames were designed based on ASTM C 512 (ASTM 2015). One test apparatus was set up in the laboratory while the other remained exposed to the outdoor weather. The design for the apparatus is shown in Figure 3-1 with a maximum capacity of 192,000 lbf., and a maximum stress to the frame of 6,795 psi. In each of the test frames, two 6″×12″ cylindrical specimens were placed on top of one another with 1″ thick circular steel plates as spacers and tested under the same compression while an additional two specimens were placed unloaded near the frame.

The load was applied by means of a hydraulic jack, with a maximum capacity of 120,000 lbf., and monitored by a calibrated load cell. When the desired load is reached, the nuts on the threaded rods are turned so that they are snugly pressing against the plate underneath the hydraulic jack, holding the plate in position and the applied load remains continuous and steady. After the nuts are securely positioned, the jack can be removed from the test frame and used to set the load on another test frame. After the jack is removed, the 9 sets of springs (D2 inner and D2 outer types) in the frame maintain the load applied to the specimens consistently. Standard railroad springs, which are much less expensive than custom-made springs, were used at the base

of the frame as to apply equal force upward. This design has the advantage of when a smaller load is applied, a smaller number of springs are used as to maintain the applied load more accurately.

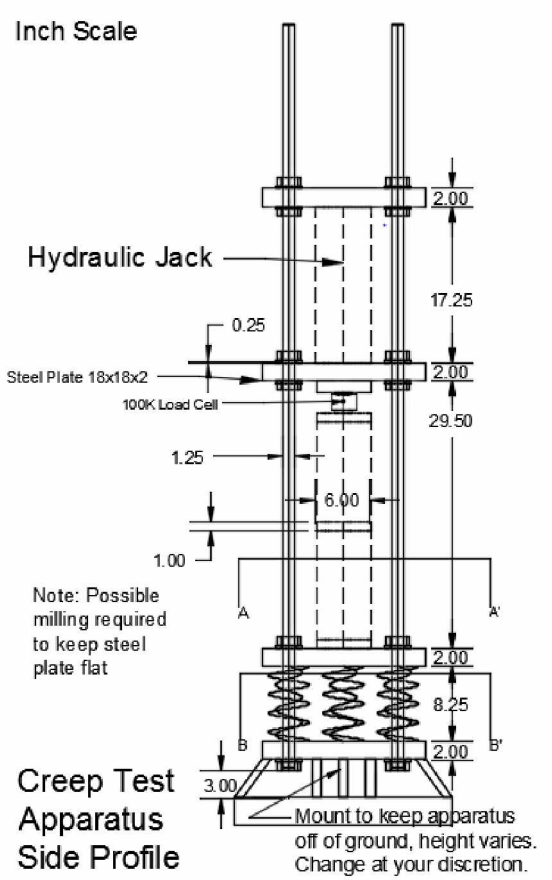

Figure 3-1: Creep Test Apparatus

Each spring set consists of two springs. The spring constant of the outer spring, k_1, is 9,778 lbf/in, while the spring constant of the inner spring, k_s is 3,520 lbf/in. When they are used as a set, the combined is 13,298 lbf/in, and the solid capacity is 21,345 lbf[4]. Under the maximum load, the set of springs deforms 1.61 inches. If all nine sets of springs are used, the maximum load, $C_{\max}$, that the springs can hold can be calculated to 192,000 lbf. The maximum stress, σ_{MAX}, that can be applied to a 6"×12"cylindrical concrete specimen in the creep frame can be calculated as 6,795 psi. In consideration that the concrete test specimens may be loaded up to

[4] Personal e-mail communication with a vendor.

50% of its compressive strength in the creep test, this creep apparatus can be used to test concretes with a maximum ultimate compressive strength of 13,590 psi.

When the concrete specimens are loaded in the creep frame, each of the four steel rods will carry one quarter of total load. The steel rods are 1.25 in. in diameter and are made of a high-strength alloy steel with a yield strength of 105,000 psi. If the concrete specimens were loaded up to the maximum capacity of the creep apparatus of 192,000 lbf, the maximum stress in the steel rods would be equal to 48,300 psi. This maximum possible stress in the steel rod is less than half of the yield strength of the steel of 105,000 psi.

As the concrete specimens are loaded in the creep frame, the rectangular steel plates, which are in between each cylinder, are slightly deflected. To keep the loading surfaces flat and the test specimens vertical when the load is applied, four 1-inch thick circular steel plates with a diameter of 6 inches are placed on the top and bottom of the stack of concrete test specimens and as in between the cylinders.

As the concrete specimens creep under the sustained load in the creep frame, the load applied on the concrete will be reduced. The load relaxation due to the creep deformation of the concrete specimens can be calculated by multiplying the total creep deformation by the total spring constant of the springs, as follows:

Load Relaxation = (Total Spring Constant) × (Creep Deformation)
= (Total Spring Constant) × (Creep Strain) × number of specimens × 12 in.

When all nine sets of springs are used, the total spring constant is equal to 119,682 lbf/in. Table 3-1 presents the load relaxation of the creep frame for various values of creep strains for the case when all nine sets of springs are used. Also, two test setup cases, two specimens and three specimens, are compared. Depending on the creep strain and the number of specimens, re-adjustment of load may be necessary to maintain the load constant on the concrete specimens.

Table 3-1: Load Relaxation in the Creep Apparatus due to Creep Strain of Concrete

Creep Strain	5.0×10^{-5}	1.0×10^{-4}	5.0×10^{-4}	1.0×10^{-3}	2.0×10^{-3}
Load Relaxation (lbf) : 2 specimens	140	280	1400	2800	5600
Load Relaxation (lbf) : 3 specimens	210	420	2100	4200	8400

3.2 Concrete Cylinder Specimens

A single large batch of cylinders, used for compression and stress-strain tests, were made at AggPro in Anchorage, Alaska during a girder pour for the 76th Avenue Undercrossing Girders on July 12th at 10:00am. The design concrete strength was $f'_{ci} = 7000\,psi$ at stress transfer and $f'_c = 8500\,psi$ at 28 days which can be found in the submitted and approved girder plan in Appendix A.

The concrete mix design was submitted to and approved by ADOT&PF. The water reducing admixture should be noted to effect the total creep, basic and drying creep, at an increase by 20% at the same water-cement ratio (ACI 2005), however, this calculation was not utilized for our purposes.

The mix ingredients are described as follows:

- Cement

  ABI Type III Cement were used in the batches.

- Coarse Aggregate

  The coarse aggregate used was AASHTO Gr. # 67 with a saturated surface dry (SSD) Specific Gravity of 2.70, Absorption Percent of 0.69, and a Dry-Rodded Unit Weight of 110.7

- Intermediate Aggregate

  The coarse aggregate used was AASHTO Gr. # 8 with a SSD Specific Gravity of 2.69, Absorption Percent of 0.62, and a Dry-Rodded Unit Weight of 110.3

- Fine Aggregate

  The fine aggregate used was AASHTO Gr. # M6 with a SSD Specific Gravity of 2.64, Absorption percent of 1.39, and a Fineness Modulus of 2.76

- Water-Reducing Admixture

The water-reducing admixture used included BASF PS 1466: a ready-to-use high-range water-reducing admixture effective in assisting with workability.

The grain size distribution chart for the materials pit that produced the aggregates for the concrete mix design are seen in Figures 3-2 through 3-4.

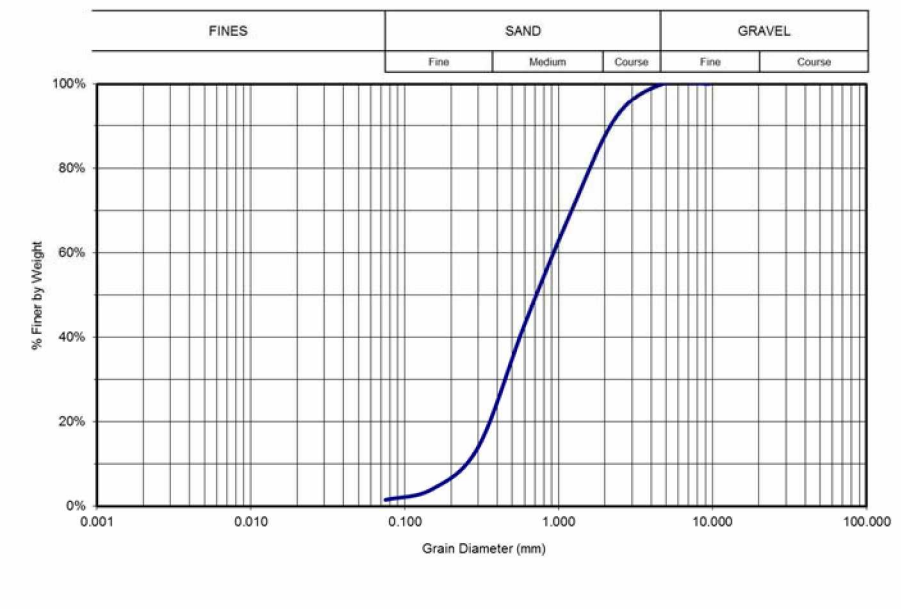

Figure 3-2: Fine Concrete Aggregate Grain Size Distribution

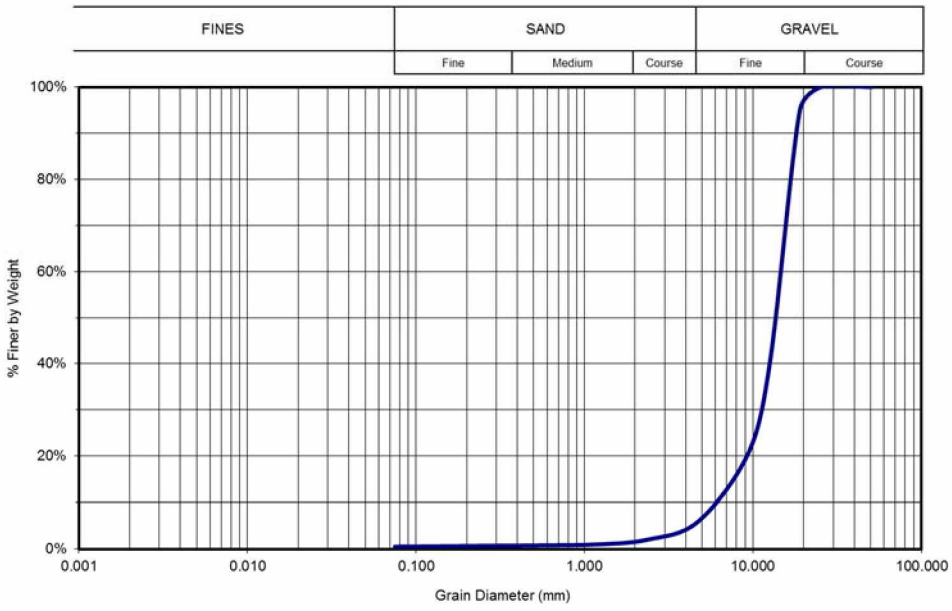

Figure 3-3: Coarse Concrete Aggregate Grain Size Distribution

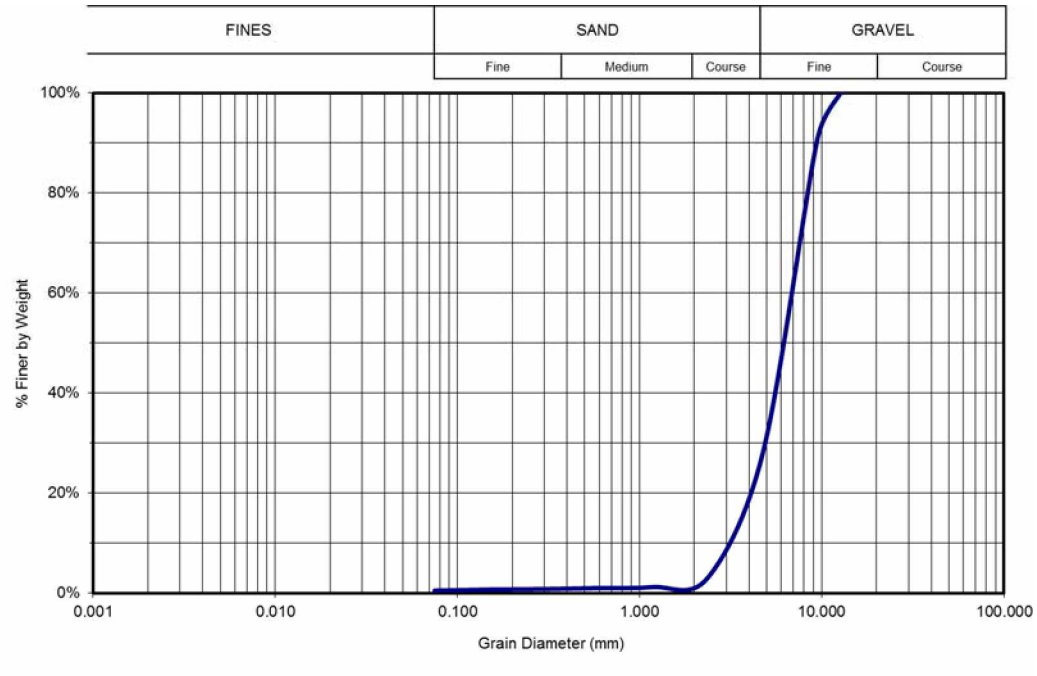

Figure 3-4: 3/8" Aggregate Grain Size Distribution

The concrete specimens were created in conformance with ASTM standard C31 "Making and Curing Concrete Test Specimens in the Field" utilizing a tamping rod as seen in Figure 3-5 (ASTM 2012). During the girder pour, 24 cylinders of size 4″×8″ and 15 cylinders of size 6″×12″ were made and cured on site. Thermistors were placed inside the cylinders carefully as to not create voids. Figure 3-6 shows the completion of the fieldwork with the sensors in position. The superintendent of operations from Aggpro also made 3 cylinders, following the metal mold and vibratory method, to be steam cured along with the girder to approximate a similar 7-day steam cured strength. The following morning the vibratory cylinders were broke to test compression strength on the steam-cured specimens to ensure minimum strength. An employee from DOWL HKM, who specializes in quality assurance for concrete, also ran field tests for slump (9 inches), percent air entrained (2.5%), unit weight (152.2 pcf), and recordings of ambient temperature (57°F) and concrete temperature (64°F) were recorded[5].

[5] From a data sheet from DOWL HKM. Attached in Appendix B.

Figure 3-5: Making Concrete Test Specimens in the Field

Figure 3-6: Completion of Making Concrete Cylinders in the Field

Transportation of the concrete cylinders from Aggpro in Anchorage to Fairbanks followed ASTM C31 section 11 "Transportation of Specimens to Laboratory". The cylinders were capped and placed at the bottom of a 5 gallon bucket as to remain flat, then sand was poured around as to maintain a solid, vertical surrounding. The transportation time specified

shall not exceed 4 hours according to the specification, however, ADOT&PF in Alaska realizes that this feat is an impossibility in such a large state for certain locations. After leaving Anchorage around 10am and arriving in Fairbanks roughly 6 hours later, the cylinders were stripped of their molds and placed in a lime bath at the ADOT&PF Northern Region Materials Lab.

3.3 Sensors and Data Acquisition System

Two pairs of gage points with a gage distance of 8 inches were placed in each concrete test specimen. A Demountable Mechanical Strain Gauge (DEMEC) was used to measure the change in distance between the gage points, which is the creep of concrete.

Once the concrete has gained some initial strength, holes are drilled into the cylinders to allow for the gauge-points to be placed. An electric drill is used after the spacing has been marked out utilizing a masonry bit per ASTM C426. Aluminum Putty Epoxy from JBWeld was also used to ensure the stabilization of the gauge plugs to shrink with the concrete. Once the epoxy hardened the gauge-points were placed finger tight and were to not be moved after.

Once the cylinders reached the optimum number of days, they were prepared for the creep test. Placement of the cylinders into the loading frame required preparation of the gauge points and leveling the top and bottom with a diamond tipped saw. Holes were drilled into the specimens at roughly 1” from the top and bottom, and approximately 8” apart from each other to allow for the DEMEC strain gauge to accurately measure the creep. After the holes were drilled out to proper depth, an air compressor cleaned out the dust while gauge plugs with JBWeld epoxy were used to maintain a constant position within the cylinders, which can be seen in Figure 3-7. The thermistors are located in the center of the cylinder, as seen in Figure 3-8, with the ends protected and secured in place. Gauge points with a half spherical shape are then screwed inside the plugs to allow an accurate center to center measurement.

Figure 3-7: Specimens Epoxied with Gauge Plugs

Figure 3-8: Specimens Pre-Loading Set Up with Thermistors

The wiring was connected to a CR1000 wiring panel located inside a weather proof case along with a storage device for readouts of the load cell and thermistor every 5 seconds. The devices before final set up of the outdoor frame can be seen in Figure 4-2. The load cells were calibrated before use to ensure accuracy.

3.4 Ambient Temperature and Relative Humidity Data

During each physical measurement of the cylinders, outside temperature and relative humidity were recorded. Also, more robust weather data was obtained from the closest, in-service weather station on West Ridge of UAF campus. The station, FAOA2 College Observatory, is located at the Elvey building, providing an adequate comparison for obtaining records.

As the temperature seasonally changes, the thermal contraction and expansion of the steel as well as the concrete must be accounted for. The contraction of the steel rods can induce additional stress as it causes the plates to be closer together, therefore creating an additional force on the concrete cylinders. The internal concrete force that limits the potential of total creep due to the change in temperature at a reference temperature of 22 Celsius is approximately -519$\mu\varepsilon$. If the change in temperature is adjusted to 0 Celsius, the potential internal concrete force is approximately -222$\mu\varepsilon$, however, these value are not considered for our calculations and is an area for a future study. The calculation for the steel rods and the concrete cylinders is listed in Table 3-2.

Table 3-2: Calculations and Equations for Various Measured Constants

Radius of Concrete	$r_c = 3\ in$	Change in Temperature	$\Delta T = 51.44^\circ\ C$
Radius of Steel Bar	$r_s = \frac{1.25}{2} = 0.625\ in$	Force	$F = 80{,}000\ lbf$
Area of Steel	$A_{rod} = 152.17\ in^2$	Outer Spring Constant	$k_1 = 9{,}778\ \frac{lbf}{in}$
Area of Concrete	$A_{Concrete} = 96.21\ in^2$	Inner Spring Constant	$k_2 = 3{,}520\ \frac{lbf}{in}$

Thickness of Steel Plate	$t_s = 2\ in$	Spring Constant	$k_t = 13{,}298\ \frac{lbf}{in}$
Length between Cylinders	$l_1 = 24.00\ in$	Modulus of Elasticity for Concrete	$E_C = 4.5 * 10^6\ psi$
Length between Spring	$l_2 = 8.25\ in$	Modulus of Elasticity for Steel	$E_S = 29 * 10^6\ psi$
Coefficient of Thermal Expansion of Concrete	$\alpha_C = 9.9 * 10^{-6}\ \frac{in}{in}\ ^\circ C$	Coefficient of Thermal Expansion of Steel	$\alpha_S = 11.7 * 10^{-6}\ \frac{in}{in}\ ^\circ C$
Length of Rod	$L_S = 38.25\ in$	Length of Concrete	$L_C = 24\ in$
Concrete Thermal Expansion	$\delta_C = \frac{P * L_C}{A_C * E_C} = 0.00023$	Steel Thermal Expansion	$`\delta_S = \frac{P * L_S}{A_S * E_S} = 0.00033$
$\Delta S = (\alpha_s \Delta T)(l_1 + l_2 + 3t) - \frac{F(l_1 + l_2 + 3t)}{E_S * A_{rod} * 4}$		$\Delta C = (\alpha_C \Delta T)(l_1) + \frac{F(l_1)}{E_C * A_C} + \frac{F}{K}$	
$(\alpha_s \Delta T)(l_1 + l_2 + 3t) - \frac{F(l_1 + l_2 + 3t)}{E_S * A_{rod} * 4} = (\alpha_C \Delta T)(l_1) + \frac{F(l_1)}{E_C * A_C} + \frac{F}{K}$			
$F = \left[(\alpha_s \Delta T)(l_1 + l_2 + 3t) - (\alpha_C \Delta T)(l_1) - \left(\frac{l_1}{E_C * A_C}\right) - \left(\frac{l_1 + l_2 + 3t}{E_S * A_{rod} * 4}\right)\right] * [E_S * A_{rod} * 4 + E_C * A_C + K]$			
Internal Concrete Force	$\varepsilon_c = (\alpha_C \Delta T) + \frac{F}{E_C A_C} = -519 \mu\varepsilon$	Internal Steel Force	$\varepsilon_s = (\alpha_S \Delta T) + \frac{F}{E_S A_S} = -593 \mu\varepsilon$

Chapter 4 Experimental Programs

In the two creep test frames, two concrete cylinders stacked together were loaded with a target compression of 80,000 pounds on the 13th day after molding (7/25/2017). The target compression is roughly 33% of the compressive strength of the specimens on the 14th day following ASTM C512 (ASTM 2015). Once the target compression was reached, the steel plates of the frame were tightened in place, leveled, and the hydraulic jack was demounted. Circular steel and rubber plates were placed in between the cylinders to equally distribute the load. Figures 4-1 and 4-2 show the two concrete creep frames under loading with the jack still in position.

Figure 4-1: Specimens Loading Set Up Inside Frame

Figure 4-2: Specimens Loading Set Up Outside Frame

4.1 Compressive Strength of Concrete

The scheduling for the compressive strength of the specimens were 3, 7, 14, 28, 56, 90, 189, and 365 days. The cylinders were kept in a lime bath at the Regional lab at ADOT&PF in Fairbanks. Three cylinders are broken to failure in each test day following the ASTM standard C39 (ASTM 2018). An example of the loading apparatus can be seen in Figure 4-3 for the 3-day break of a 4″×8″ cylinder.

The average value of the compressive strength tests from three cylinders at 28-day break will be taken as the compressive strength of the concrete. Figures 4-4 through 4-10 show the results of the strength tests for 3, 7, 14, and 28-day tests of the 4″×8″ cylinders. The cylinders can be seen breaking more equally over the area of the ruptured in their earlier breaks, however, as the concrete gets harder, it starts to somewhat shear off rather than break cleanly. This trend could verify the values of the breaks obtained and gives incite as to the strength of materials.

Figure 4-3: 3-Day Break Cylinder Strength Test Loading

Figure 4-4: 3-Day Break Strength Test Results 1 through 3

Figure 4-5: 7-Day Break Cylinder Strength Test Loading

Figure 4-6: 7- Day Break Strength Test Results 1 through 3

Figure 4-7: 14-Day Break Strength Test Results 1 through 3

Figure 4-8: 28-Day Break Cylinder Strength Test Loading

Figure 4-9: 28- Day Break Strength Test Results 1 through 3 in Frame

Figure 4-10: 28-Day Breaks 1 Through 3

Table 4-1 shows the measured concrete strength. A relationship between the average compressive strength and time can be seen in Figure 4-11, with the trend line behaving as expected increasing up to a maximum after a longer period left to cure. As time increases, the average compression strength increases up to the 56 day break. At 90 days the strength of the concrete decreases, however, at the 189 and 365 day breaks determined the strength increased to its local maximum. The specified 28-day strength was 8,000 psi and the probable 28-day strength was 10,000 psi in the concrete mix design report reported by the fabricator. From the strength test result, the 28-day strength was 9,119 psi which was less than the probable strength, but it was greater than the specified strength.

Table 4-1: Compressive Strength Test Results

Time (Days)	Test #1 (psi)	Test #2 (psi)	Test #3 (psi)	Average (psi)
3	6,909	6,750	6,788	6,816
7	7,935	8,156	7,957	8,016
14	8,761	8,654	8,545	8,654
28	9,609	9,206	8,543	9,119
56	10,317	9,597	10,569	10,161
90	9,845	9,927	9,467	9,746
189	11,993	11,175	11,625	11,598
365	11,719	12,146	11,873	11,913

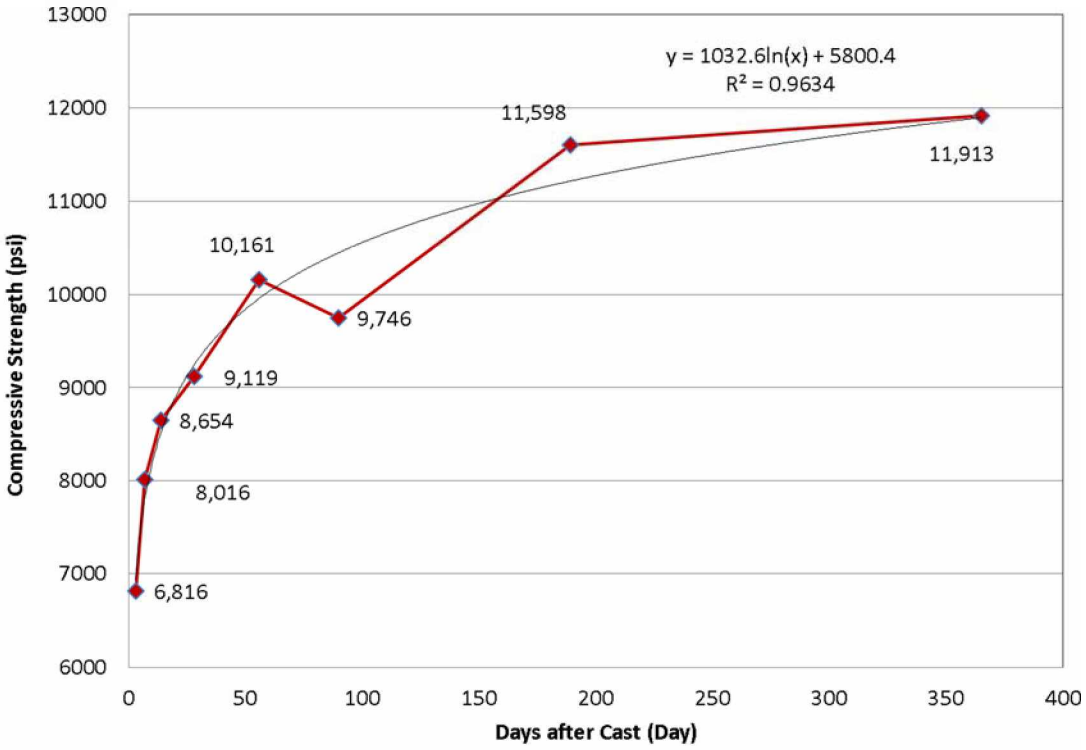

Figure 4-11: Compressive Strength (psi) vs. Time (Days)

4.2 Elastic Modulus of Concrete

The stress-strain tests of the cylinders were carried out by a Forney compression machine in the Structural Materials Lab at UAF, which can be seen in Figure 4-12 following the ASTM C469 "Standard Test Method for Static Modulus of Elasticity and Poisson's Ratio of Concrete" (ASTM 2014). The compressometer is used to measure the stress-strain of the cylinder as it is loaded utilizing a digital readout. The first loading trial is not recorded, per ASTM C469, and the following two readings are then measured and recorded. The following Figures 4-13 through 4-16 show the stress-strain in graphical format for the 14, 29, 189, and 365 day tests.

Figure 4-12: Stress-Strain Test using Forney Compression Machine & Compressometer

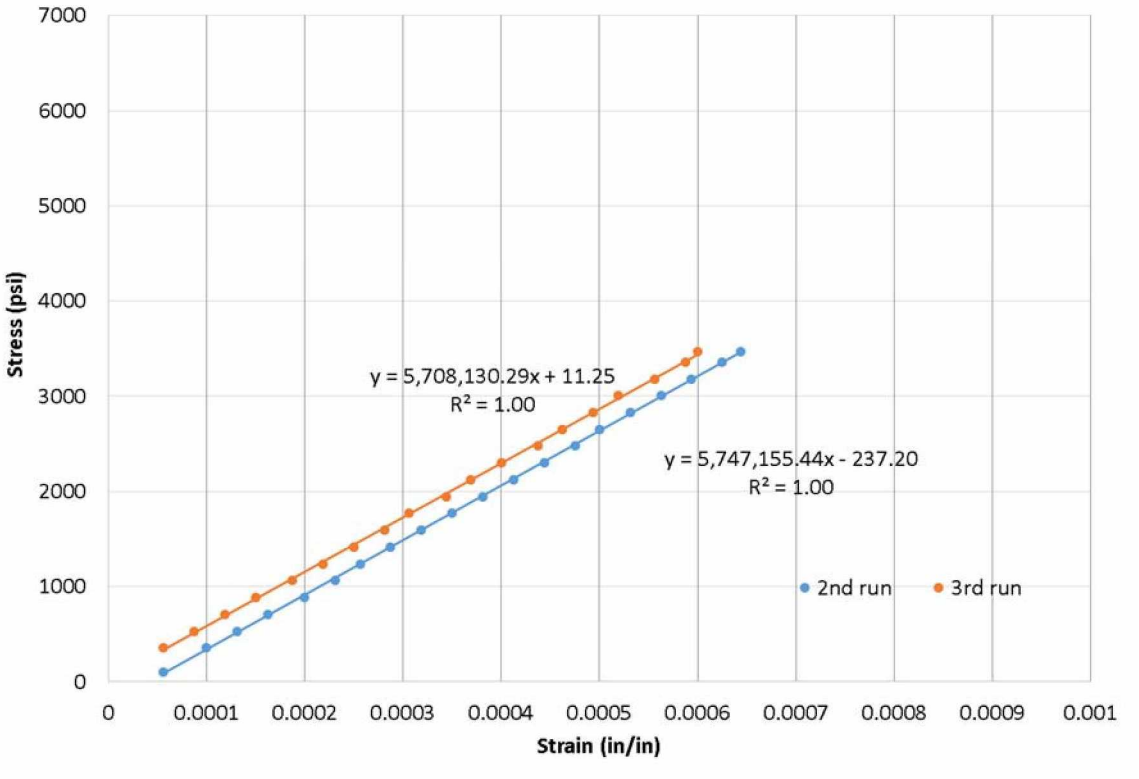

Figure 4-13: 14-day stress-strain test

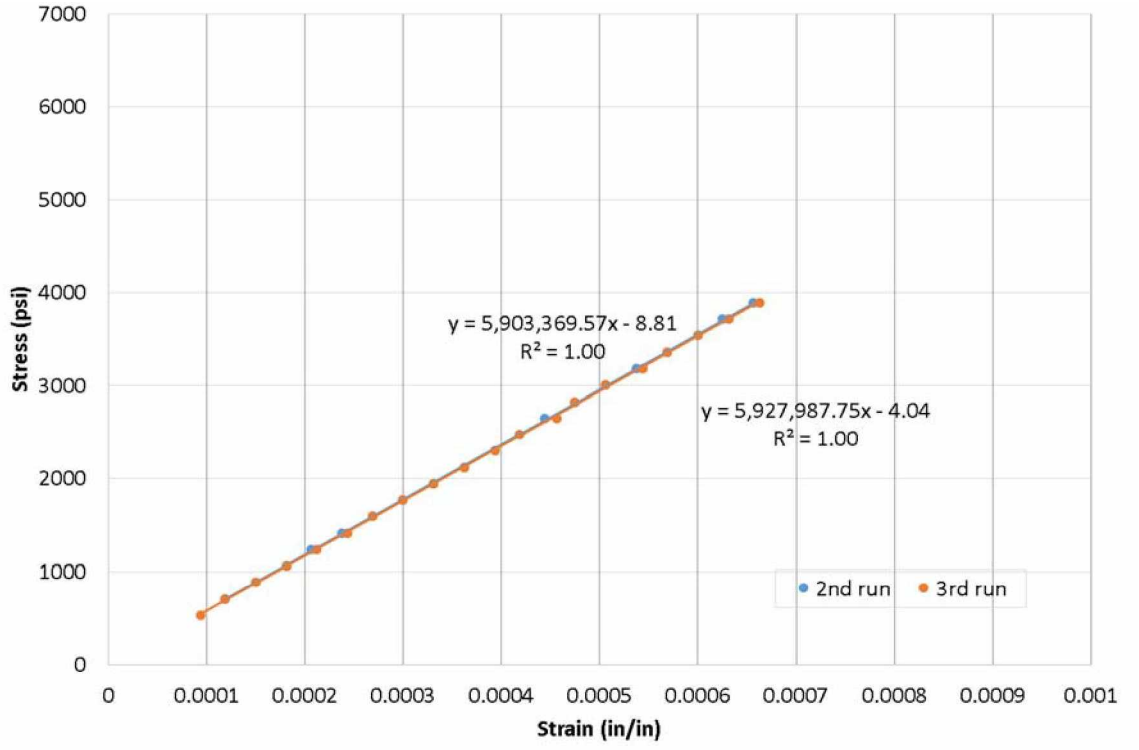

Figure 4-14: 29-day stress-strain test

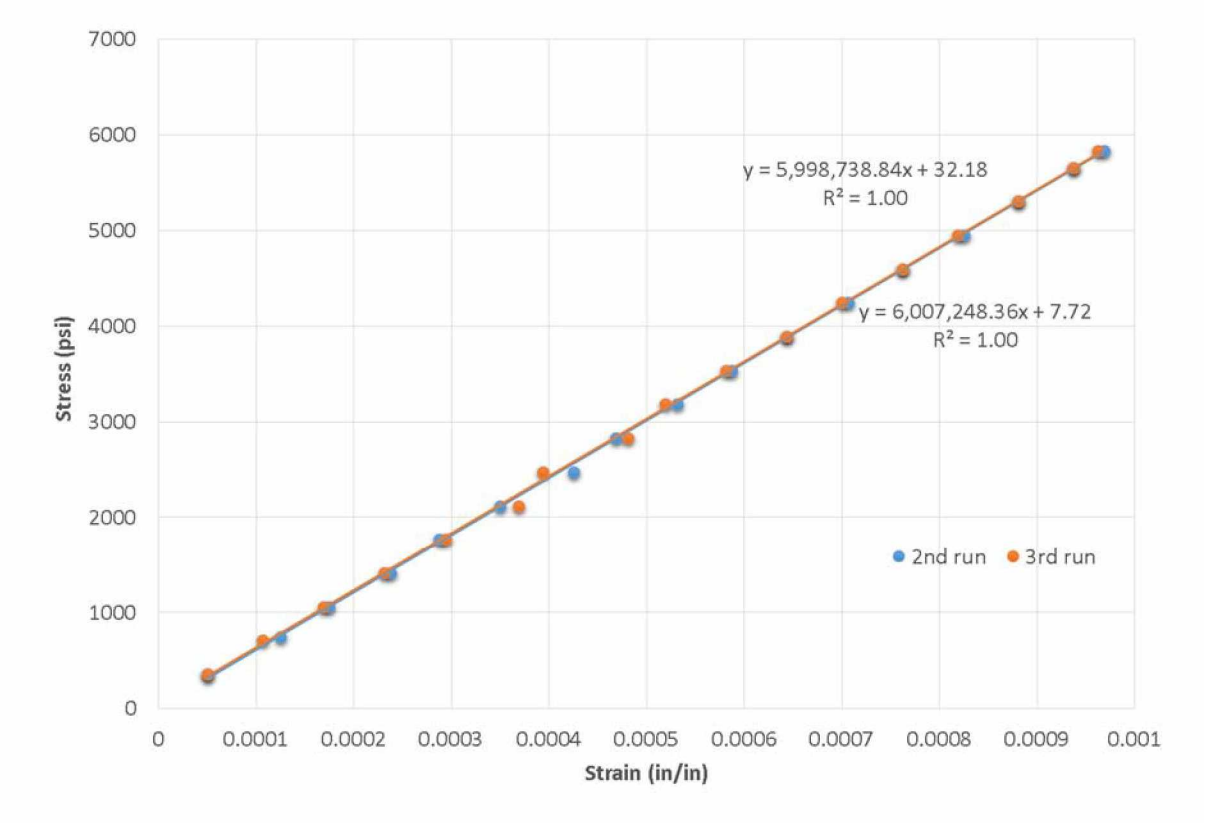

Figure 4-15: 189-day stress-strain test

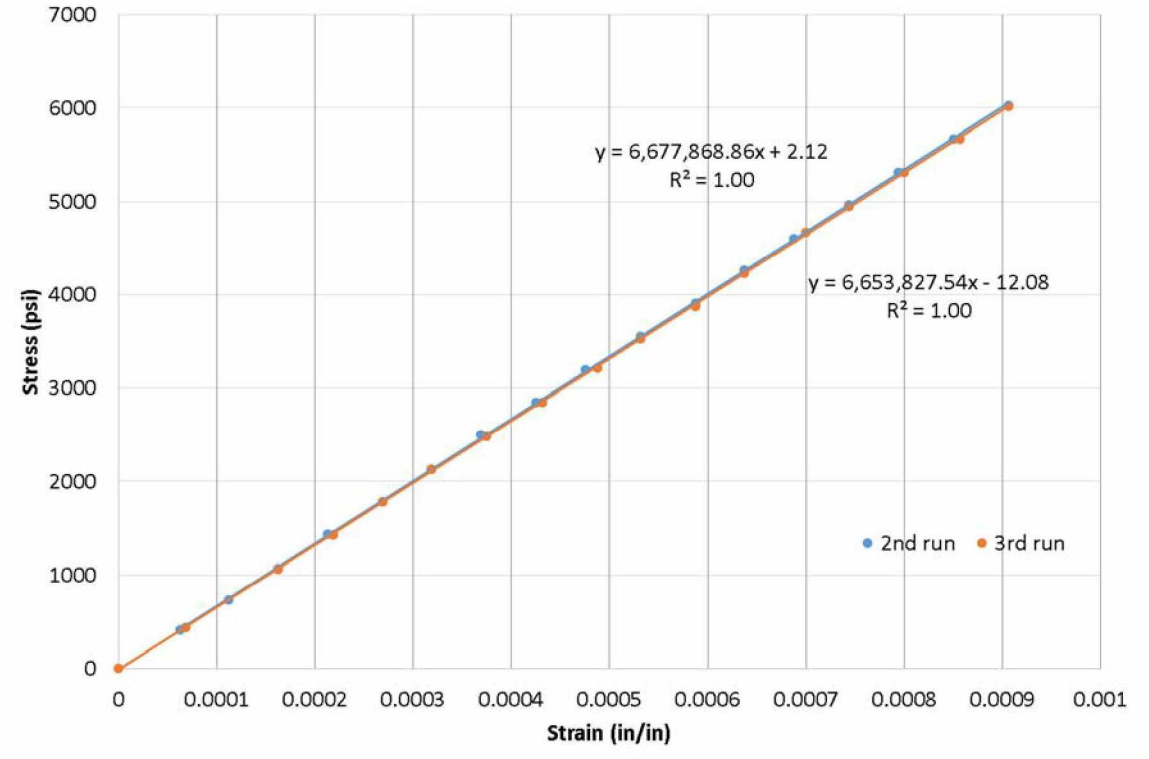

Figure 4-16: 365-day stress-strain test

In Table 4-2, measured elastic modulus values are summarized and they are compared with calculated values based on measured concrete compressive strength. The values in "AASHTO (8th)" were calculated from Eq. (4-1) while the values in "AASHTO (7th)" were calculated from a traditional equation in Eq. (4-2) (AASHTO 2014, 2017).

$$E_c = 120,000 K_1 w_c^{2.0} f_c'^{0.33} \quad (4\text{-}1)$$

$$E_c = 33,000 K_1 w_c^{1.5} \sqrt{f_c'} \quad (4\text{-}2)$$

where,

K_1 = correction factor for source of aggregate (1.0 unless determined by physical test)

w_c = the unit weight of concrete (kcf)

f_c' = the compressive strength of concrete (ksi)

The unit weight of concrete used in the calculation was $w_c = 151.5 pcf$ from the concrete design mix document. The average concrete strength measured from 4″×8″ specimens in Table 4-1 was also used in the calculation.

Table 4-2: Comparison of Concrete Elastic Modulus (psi)

Day	2nd run	3rd run	Average	AASHTO (8th)	AASHTO (7th)
3				5,188,768	5,069,952
7				5,474,098	5,489,181
14	5,747,155	5,708,130	5,727,643	5,614,096	5,688,318
28	5,927,988	5,903,370	5,915,679	5,712,081	5,687,718
56				5,919,643	6,326,301
90				5,838,807	5,987,411
189	6,007,248	5,998,739	6,002,994	6,183,729	6,634,937
365	6,677,869	6,653,828	6,665,848	6,238,637	6,705,112

In Figure 4-17, the measured and calculated elastic moduli are compared. At 28 days, the calculated values are comparable with the measured one, but they become different as the day approaches 365 days. The calculated value based on AASHTO 7th ed. is closer to the measured value at 365 days.

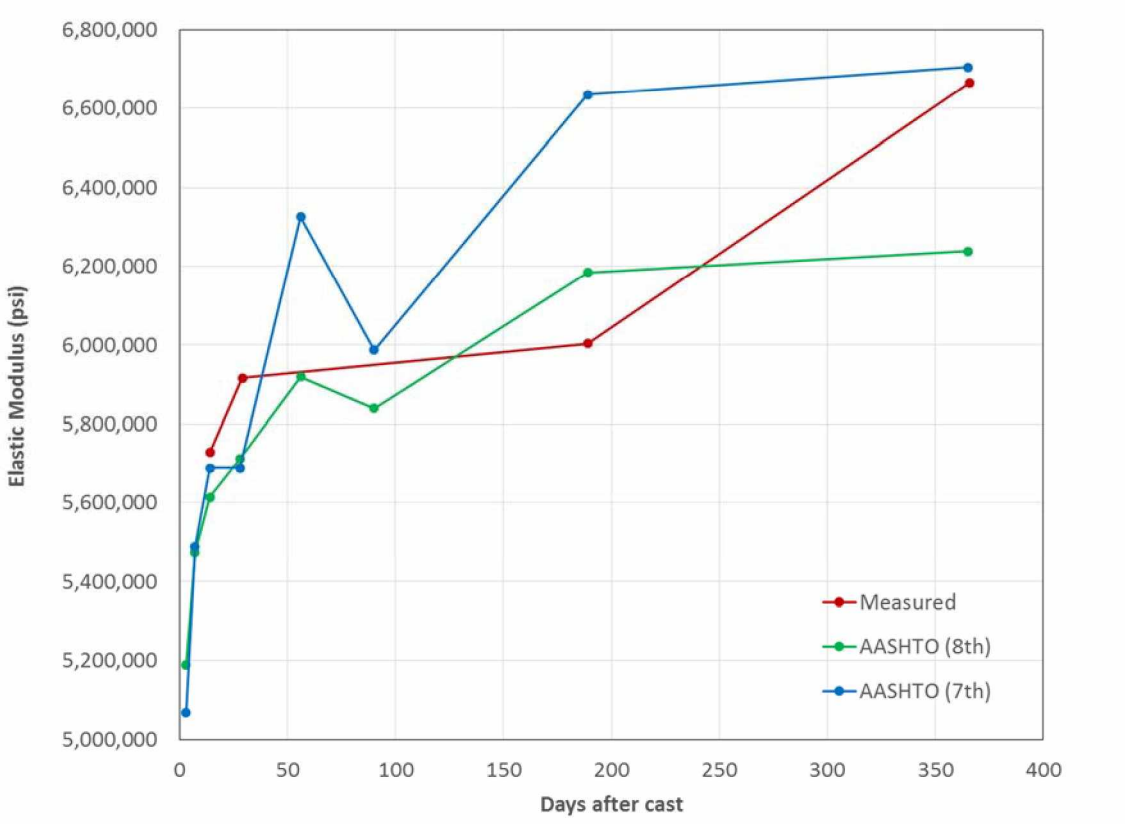

Figure 4-17: Comparison of elastic modulus

4.3 Strain Measurement Results

The indoor and outdoor strain measurements were collected one after the other and at the same time of day in the beginning of the experiment to ensure consistency. The measurements were more susceptible to movement within the first few weeks of the concrete curing, and thus they were gathered more frequently. After approximately one month, the measurements were collected twice per day, then after three months, roughly one measurement per week. The ambient temperature and relative humidity were recorded at the beginning and end of the measurements taken from a standing gauge and averaged to display a graphical output. The on-board internal unit also collected the inner temperature of the specimens, which was used later in comparison. The entire measured data were collected and stored in Appendix B.

Figure 4-18 shows various strain values related to creep and shrinkage strains. The total strain is the sum of creep strain, initial strain or elastic strain, and shrinkage strain if there is no temperature changes. The creep strain consists of basic creep and drying creep strains. The shrinkage strain is the sum of autogenous shrinkage strain and drying shrinkage strain.

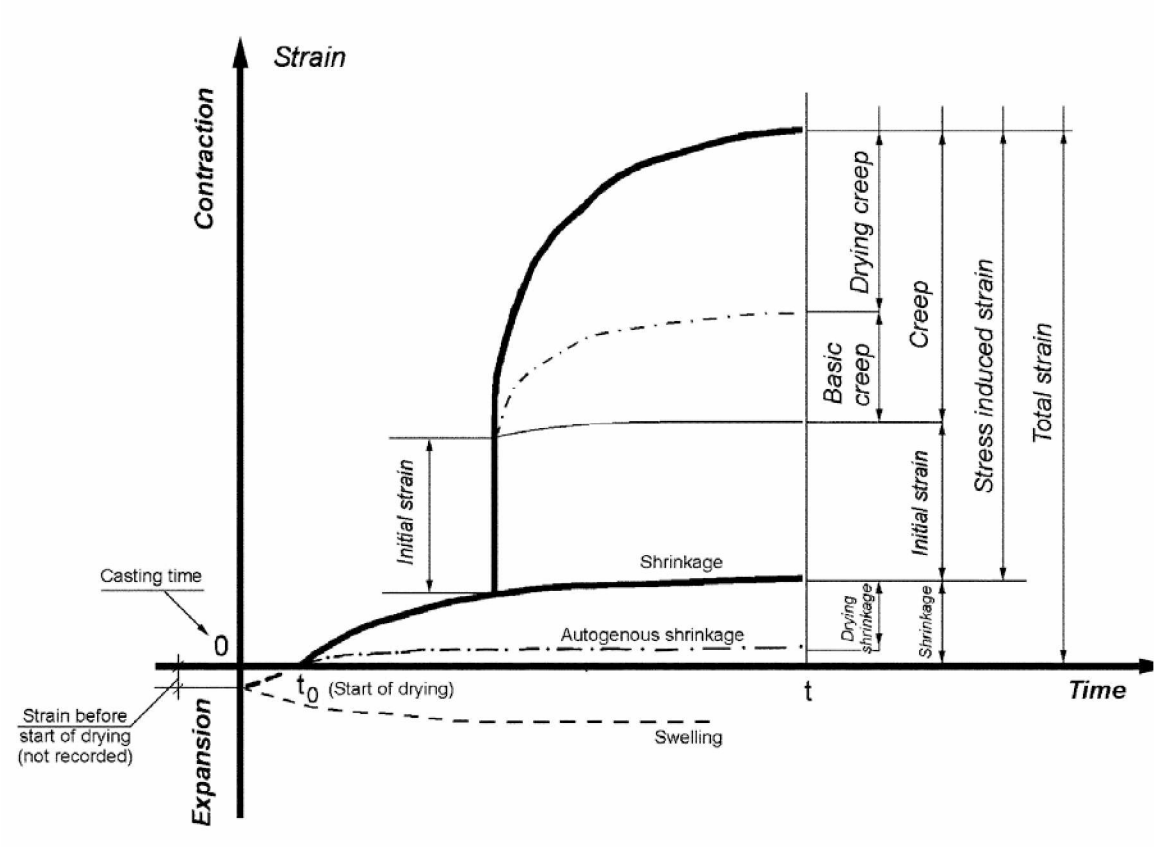

Figure 4-18: Relationship between various measured and derived strain values (ACI 2005)

Following the definition in Figure 4-18, strains measured from the specimens in the creep frames correspond to the total strain, while strains measured from the unloaded specimens are shrinkage strains.

4.3.1 Total Strain Measurement

For each specimen, two measurement lines were prepared on the opposite side of specimen's cylindrical surface and named as Top (T) and Bottom (B) although they were on the side surface. At each measurement line, measurements were repeated three times, and their average value was taken.

The loaded control frame set up that was placed indoors consisted of specimens V-3 and V-1. Figure 4-19 shows the total strain measured at V-1T (Top measurement line in specimen V-1). The total strain starts at roughly a change of 500$\mu\varepsilon$ to 1000$\mu\varepsilon$ for the first 50 measurements while V-1B starts at roughly a change of 800$\mu\varepsilon$ to 1300$\mu\varepsilon$ in Figure 4-20. The reason why the values differ when it is the same specimen is not completely clear, but it could be due to

orientation of the cylinder and uneven loading along its cross section. Figure 4-21 shows the total strain at V-3B ranging from approximately 500$\mu\varepsilon$ to 900$\mu\varepsilon$ for the first 50 measurements, but displays more of a linear trend rather than exponential as expected. Measurement at V-3T was not used due to inconsistent information. The graphical overlays of the indoor loaded specimens can be seen in Figure 4-22, showing an overall exponential trend in the beginning of the collected measurements, with a linear trend that tapers out until unloading.

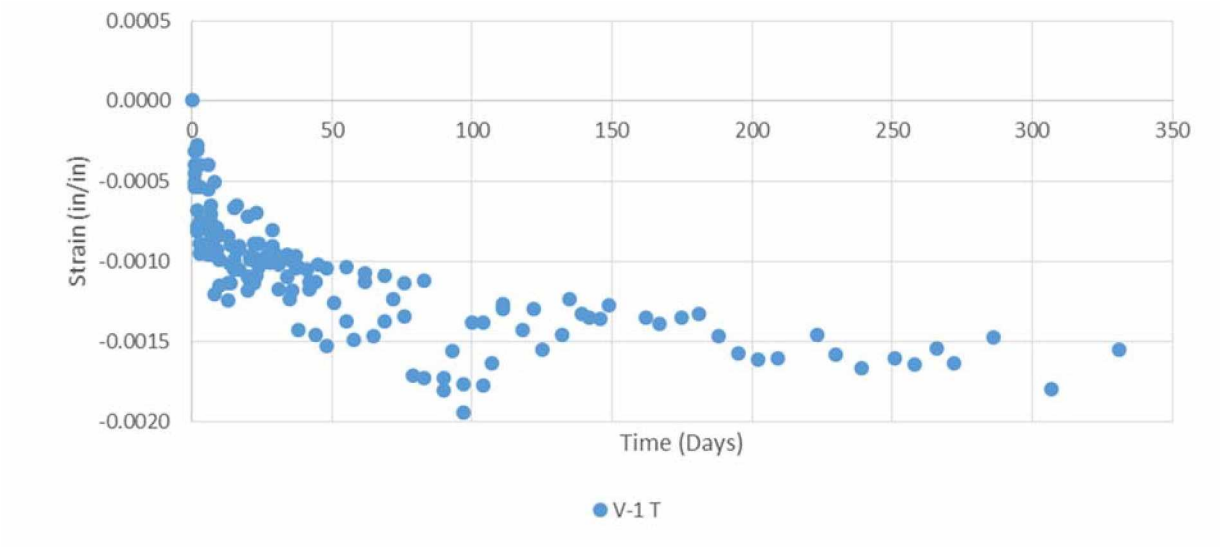

Figure 4-19: V-1 Top (Loaded, Indoor)

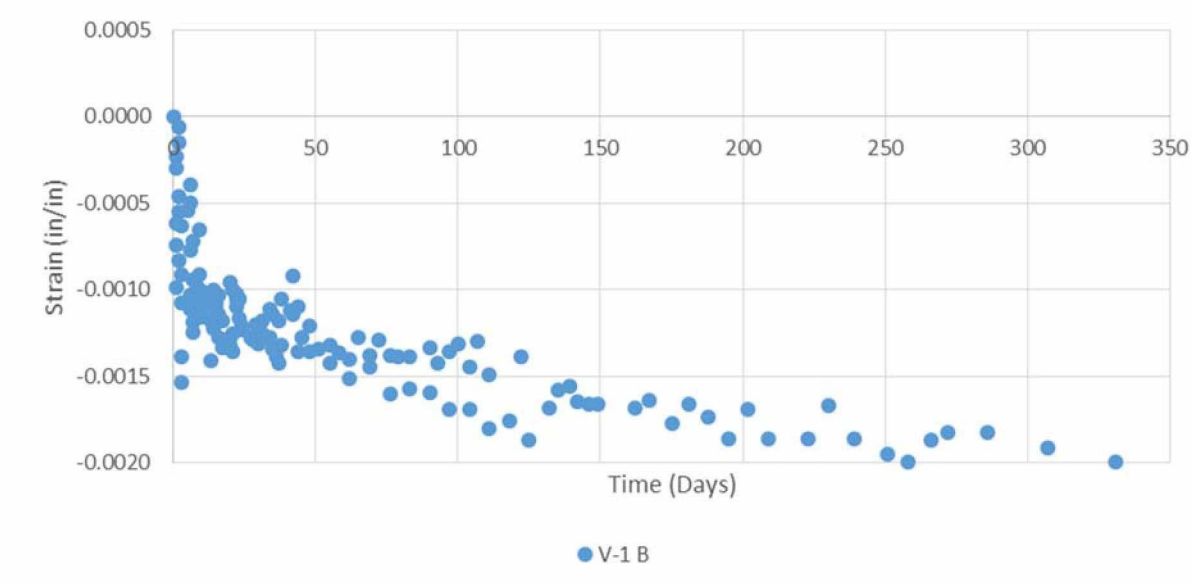

Figure 4-20: V-1 Bottom (Loaded, Indoor)

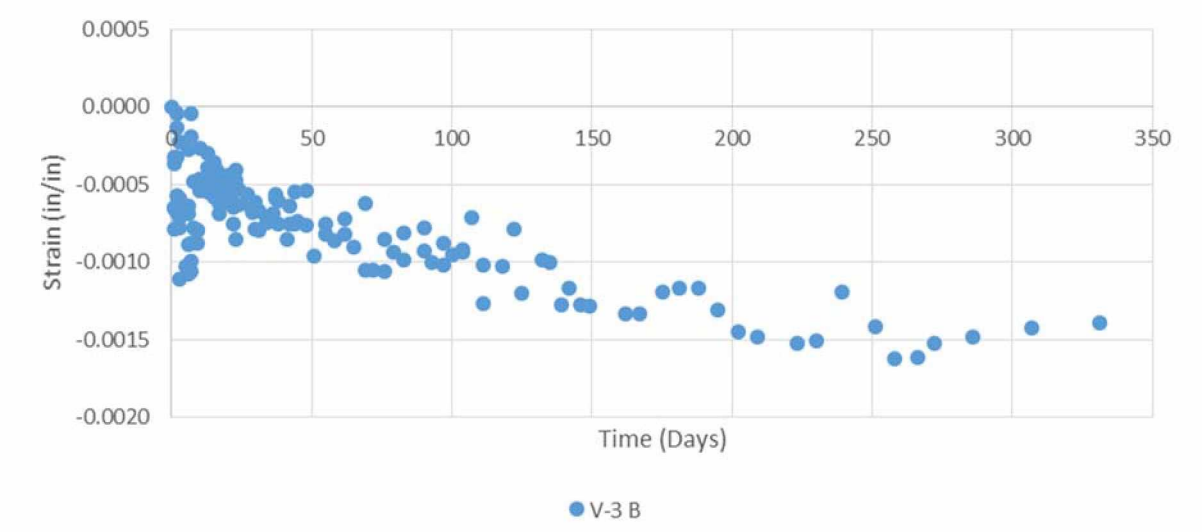

Figure 4-21: V-3 Bottom (Loaded, Indoor)

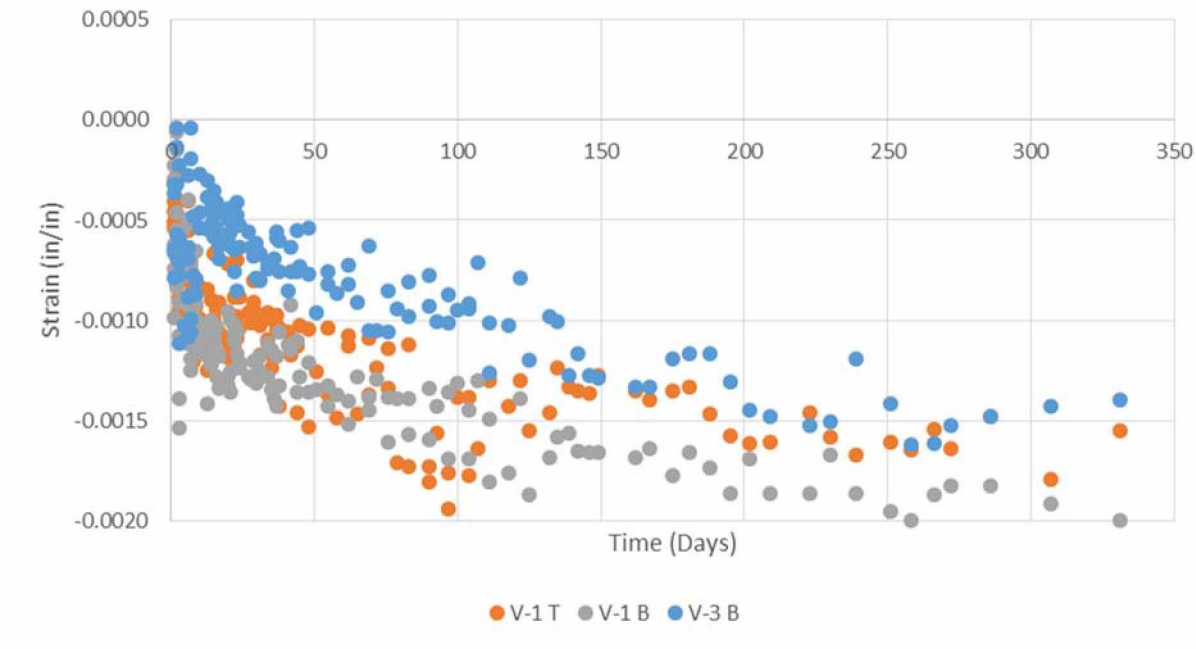

Figure 4-22: Indoor Loaded Strain

Figures 4-23 through 4-26 show the total strain measured from the specimens exposed to the natural environment. Measurement at V-4T in Figure 4-23 shows a more gradual exponential trend for the first 100 days with a change of roughly 120$\mu\varepsilon$, while specimen V-4B in Figure 4-24 shows a steeper exponential trend with a change of roughly 1650$\mu\varepsilon$. The other outdoor specimen V-6B in Figure 4-25 shows a similar trend to V-4B with a steep exponential tendency the first 50 days and tapers out with a change of approximately 1000$\mu\varepsilon$. The graphical overlay of the

outdoor loaded specimens in Figure 4-26 shows the same exponential trend for the first 100 days with values from 750$\mu\varepsilon$ to 1750$\mu\varepsilon$.

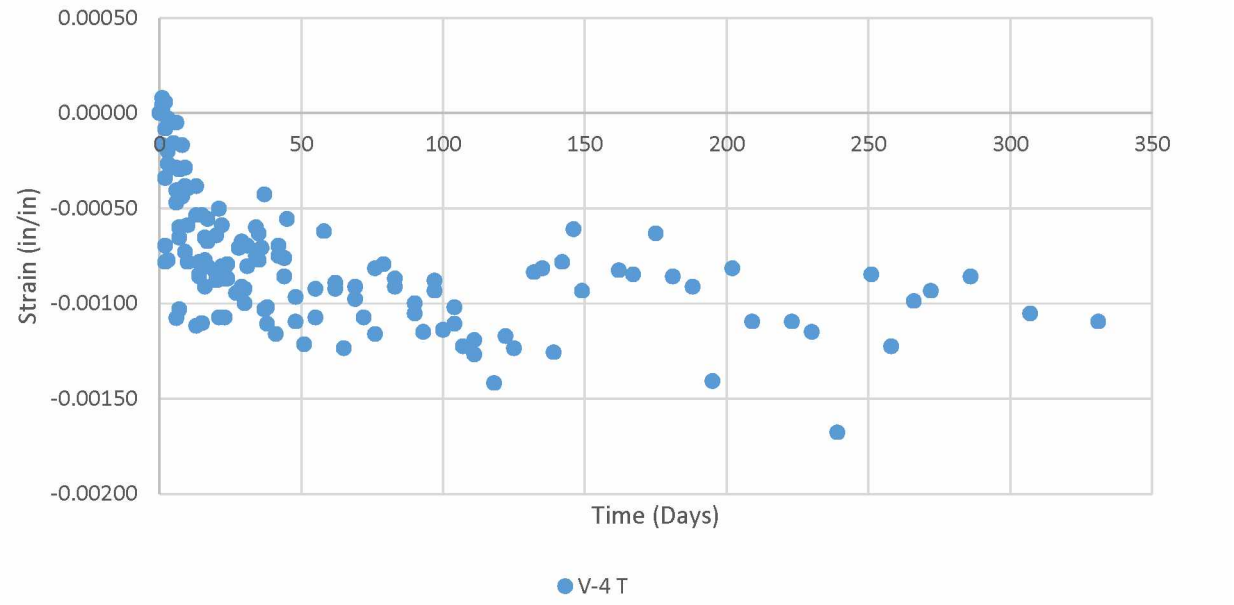

Figure 4-23: V-4 Top (Loaded, Outdoor)

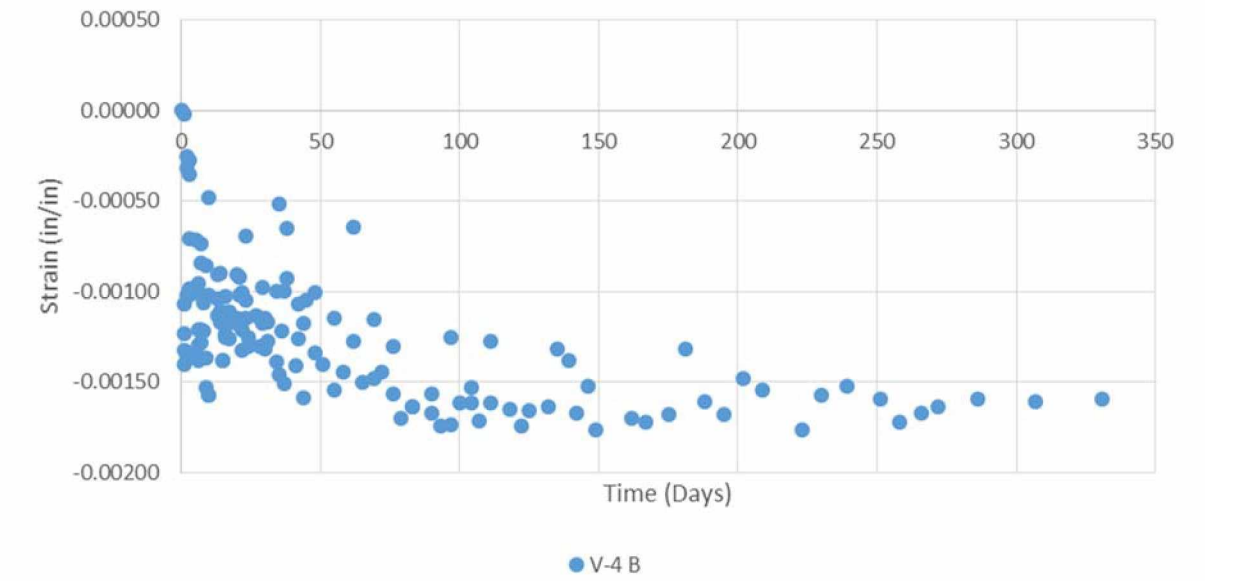

Figure 4-24: V-4 Bottom (Loaded, Outdoor)

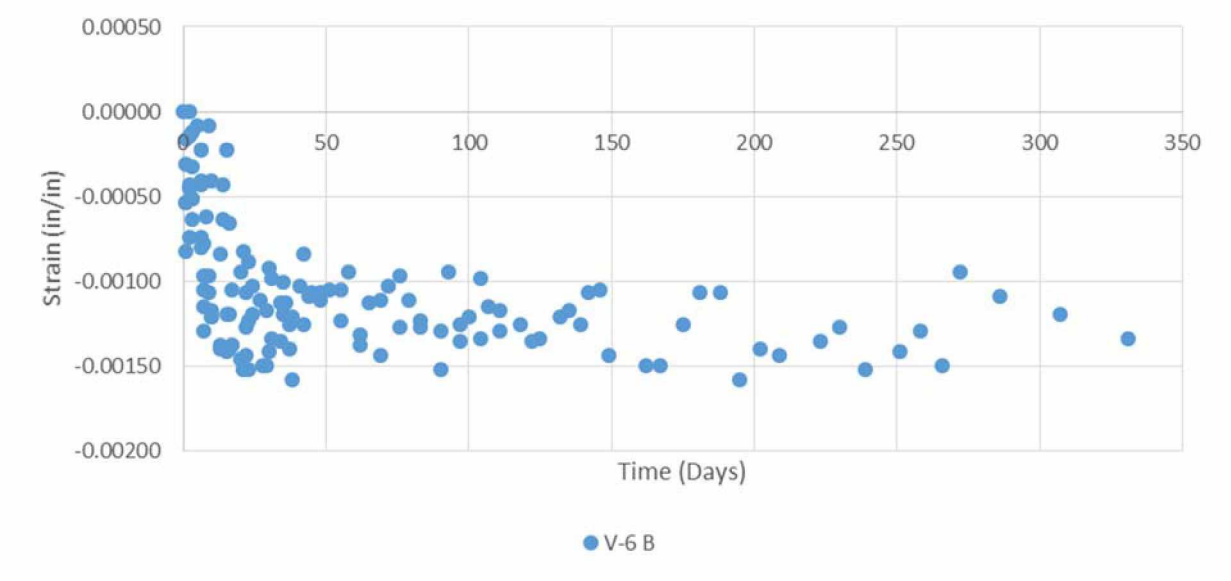

Figure 4-25: V-6 Bottom (Loaded, Outdoor)

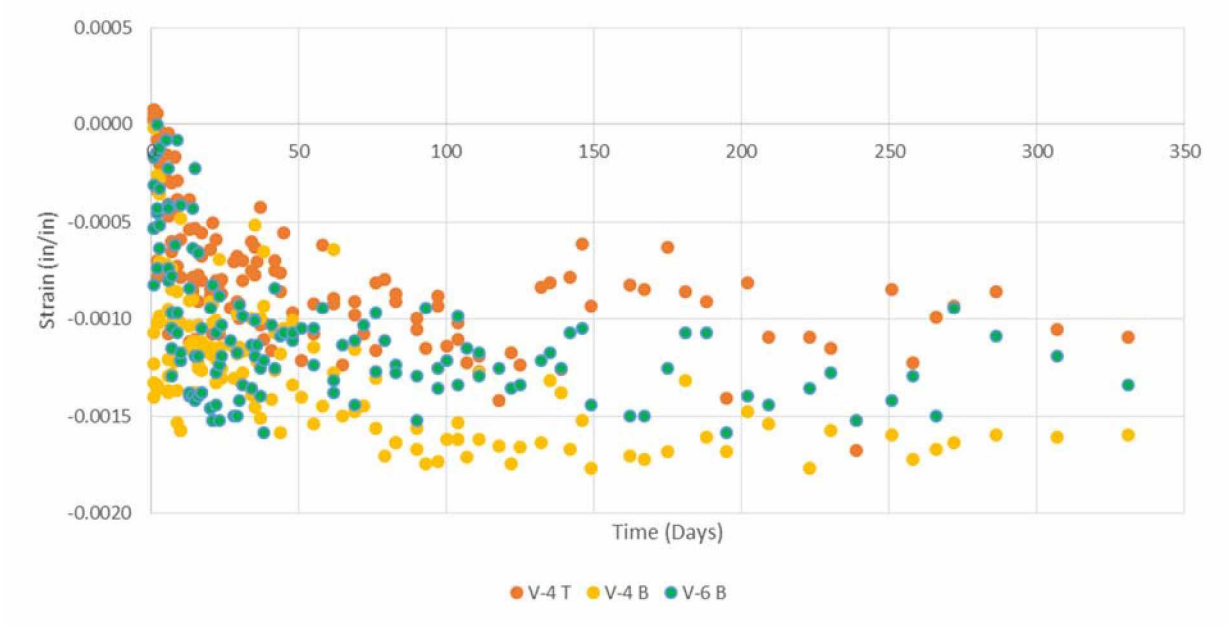

Figure 4-26: All Outdoor Loaded Cylinders

Figures 4-27 and 4-28 show the average of measured total strains at three measurement positions. In addition, a trend line is added to each Figure to show a different pattern between indoor and outdoor total strains. Between 0 and 50 days, the total strains from the outdoor frame was greater than the ones from the indoor frame. Between 50 and 100 days, two curves from the two frames are similar in their patterns and values. After 100 days, the total strain from the indoor frame slowly increased reaching 1600 and 1700 $\mu\varepsilon$ after 250 days. However, the total

strain from the outdoor frame did not change mush. They varied between 1000 and 1500 $\mu\varepsilon$ and the averaged total strain was 1300 $\mu\varepsilon$ after 250 days.

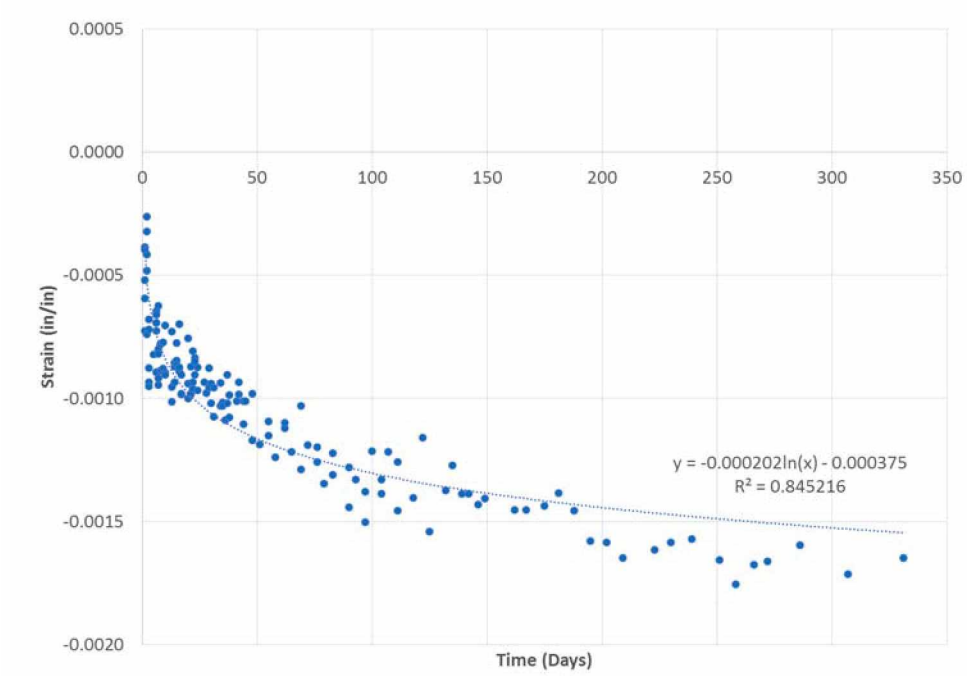

Figure 4-27: Indoor Loaded Comparison

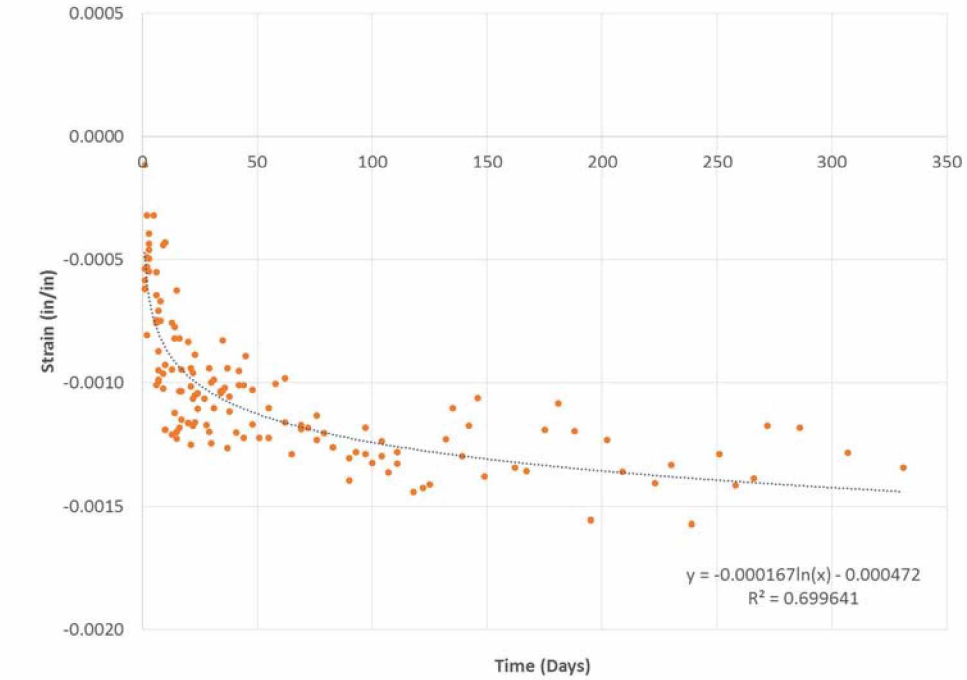

Figure 4-28: Outdoor Loaded Comparison

In Figures 4-29 and 4-30, a logarithmic scale was used to draw the total strain in the indoor and outdoor frames. A parabolic curve was used to generate a trend line with a constraint of having -0.0005 as a y-intercept which corresponded to the initial strain. When the two trend lines were compared, the sign of the second order term was different. It is -0.000114 for the indoor frame and it was +0.000016 for the outdoor frame. Thus, the strain increased much greater and faster in the indoor frame than the outdoor frame.

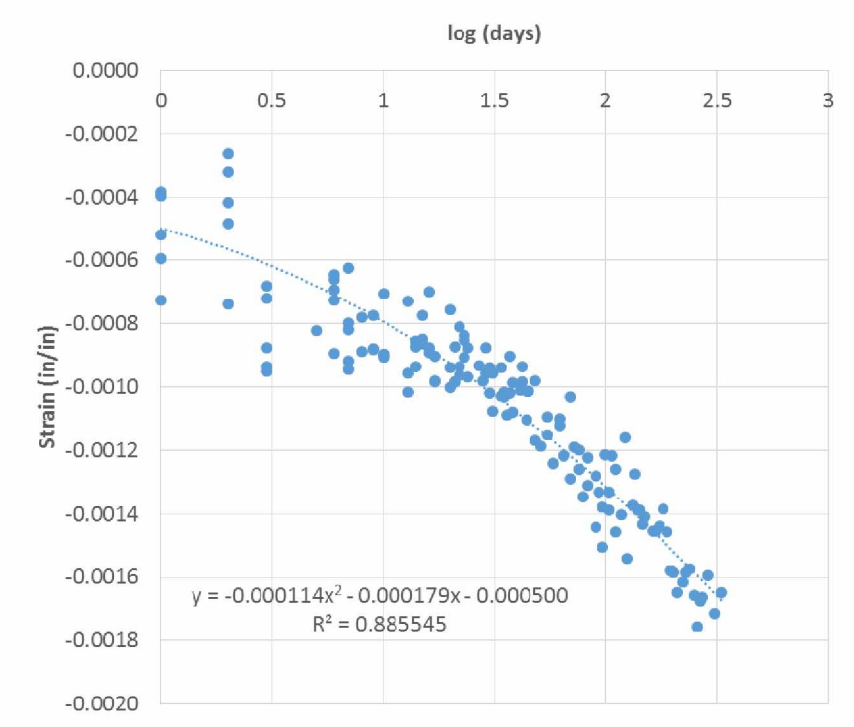

Figure 4-29: Indoor Total Strain in log(days)

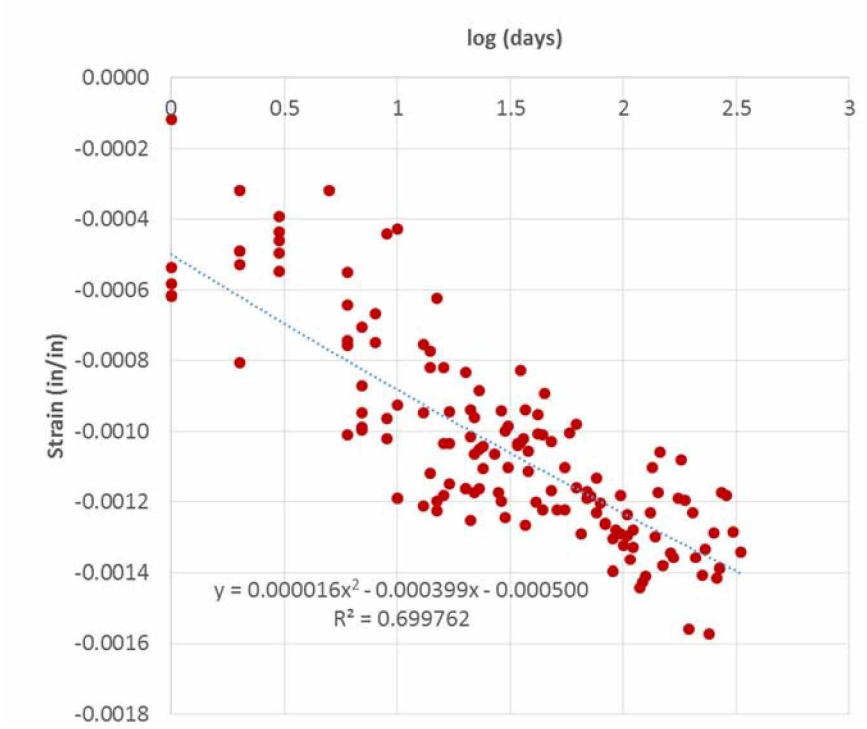

Figure 4-30: Total Strain in log(days)

4.3.2 Shrinkage Measurements

Shrinkage strains were measured from two unloaded specimens for each frame. The specimens were the same in size as the loaded cylinders and located next to the indoor and outdoor frames. The shrinkage strain from indoor specimens is shown in Figure 4-31, showing a change of roughly 500$\mu\varepsilon$ in the first 50 days, then a steadily increasing trend until measurements stop to a maximum of 1000$\mu\varepsilon$. The outdoor specimens in Figure 4-32 show a similar trend within the first 50 days at roughly 500$\mu\varepsilon$, however, the data does not steadily decrease like the indoor specimens after this point but tapers off until no change can be seen. This long term effect of shrinkage may be due to the weather outdoors varying between warm and cold, while the indoor specimens did not fluctuate. In order to verify this effect the temperature and relative humidity of the ambient air and the inside the specimens must be analyzed.

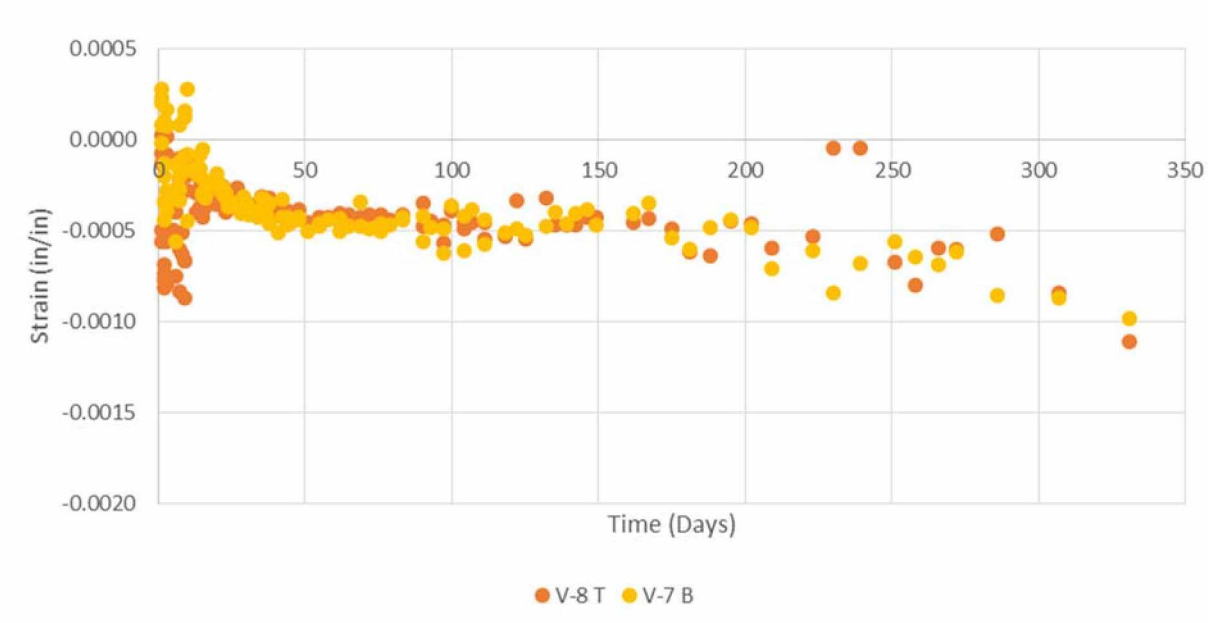

Figure 4-31: Indoor Unloaded Strain

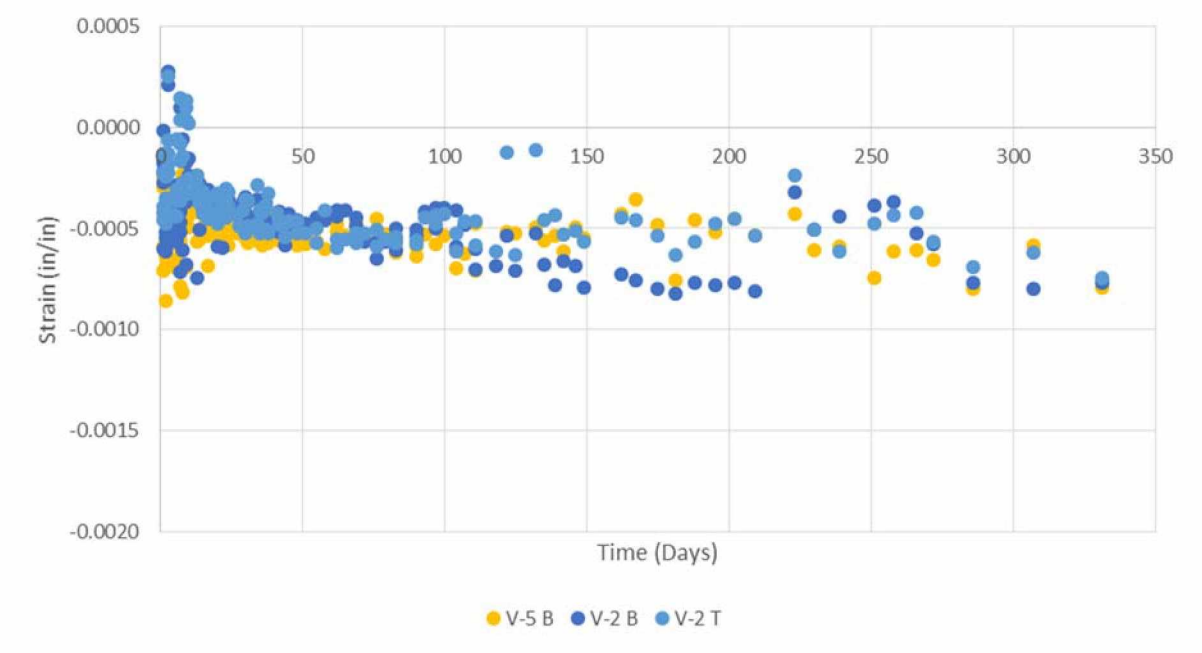

Figure 4-32: Outdoor Unloaded Strain

4.3.3 Temperature and Relative Humidity Data

Temperature and relative humidity are the factors identified as the main cause of concrete creep and shrinkage, as the concrete has not yet fully hardened before being exposed to non-ideal environments (ACI 2008). For the indoor specimens, the ambient temperature and relative humidity were measured from a digital weather station. They were recorded at the beginning and end of the measurements. Also, a thermistor was installed one of the specimens to monitor internal temperature. Figure 4-33 shows the ambient temperature and internal temperature measured for the entire time period. A relatively uniform temperature was maintained with the average ambient temperature at roughly 22.4°C and the average internal temperature at 22.67°C. The change of relative humidity is compared with the average total strain in Figure 4-34. It can be seen that the air was dry for the time period of the test, and it became very dry between days 100 – 331. The average relative humidity of this time period was 8.9%.

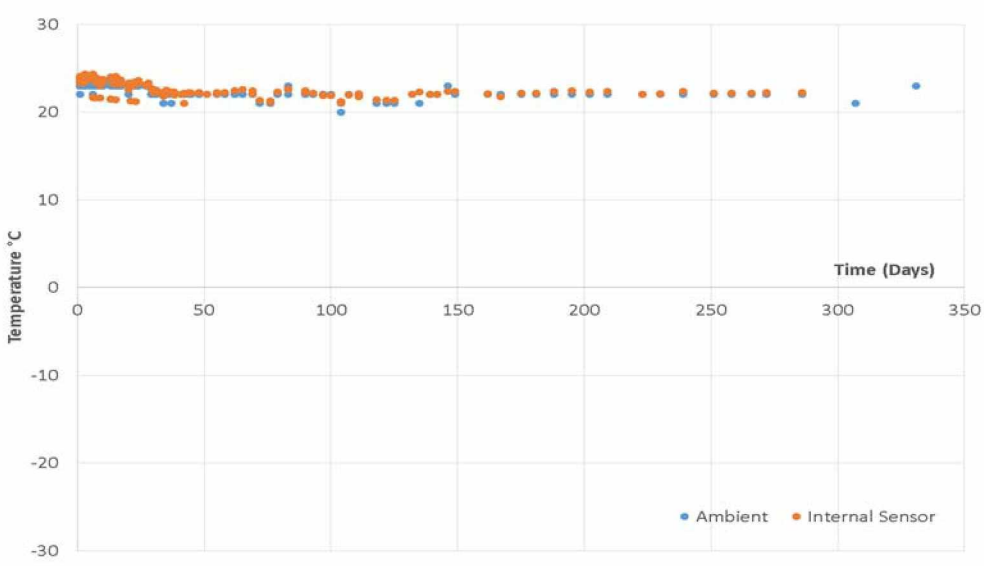

Figure 4-33: Indoor Measured Temperature

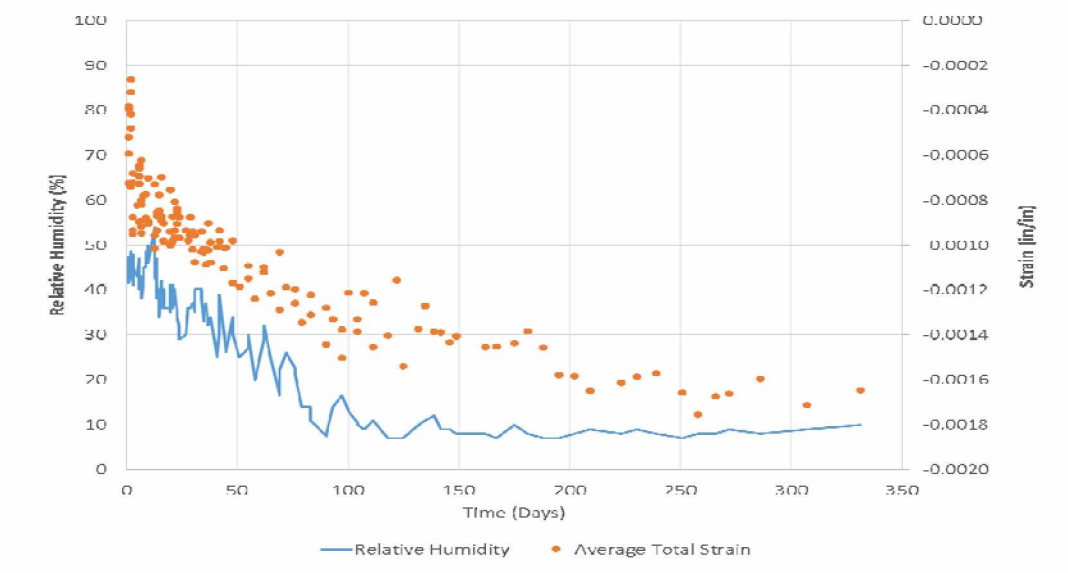

Figure 4-34: Indoor Relative Humidity and Strain Comparison

Figure 4-35 shows the three types of temperature collection for the outdoor specimens: a weather station on the Elvey Building (Meso West) on West Ridge of the UAF Campus, an internal sensor, and an onboard weather station to collect ambient air temperature. From the Figure it can be seen that the natural swing from higher to lower to higher temperatures reveals a full season outdoors with a high of roughly 28 and a low of -30°C. Due to daily temperature fluctuation, it can be seen that the three temperature readings varied. Specifically, the difference is substantial when the temperature dropped below 0°C in days 100 and 250.

Figure 4-36 shows the change of relative humidity. The average total strain was drawn together for comparison. Between days 100 and 250, the relative humidity became high, and the overall change of the total strain became small. From this comparison, it can be seen that the total strain in the outdoor frame became smaller due to high relative humidity during the winter season. The outdoor daily maximum and minimum temperature for selected periods are shown in Figures 4-37 and 4-38, displaying an overall trend for the seasonal change in an Alaskan environment.

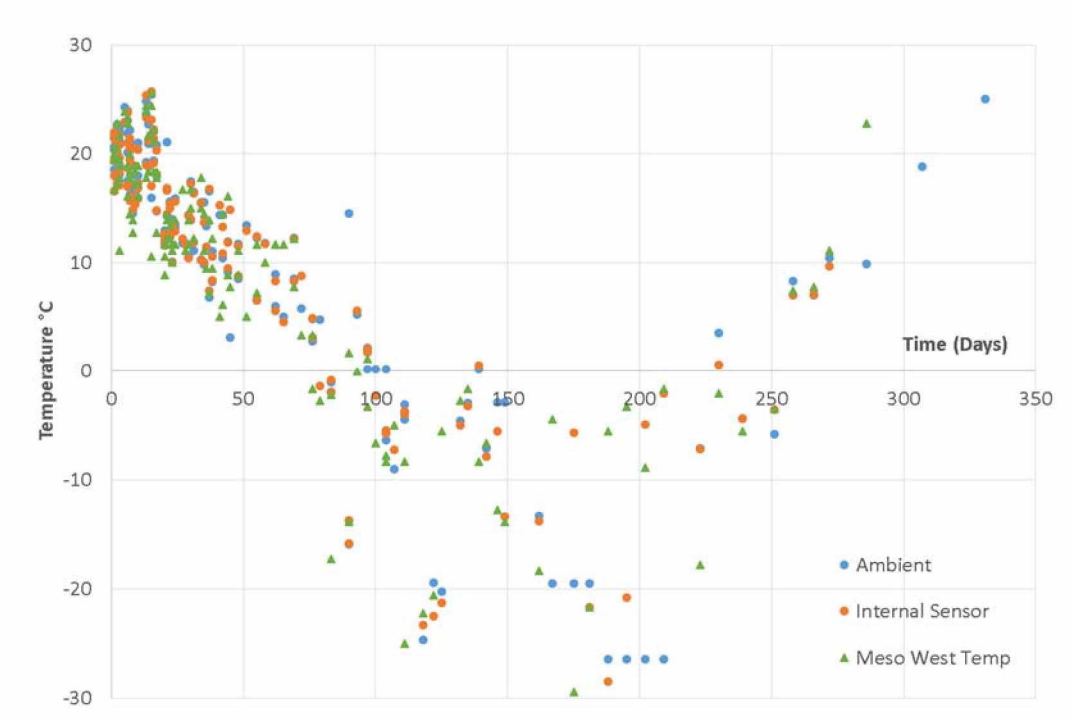

Figure 4-35: Outdoor Measured Temperature

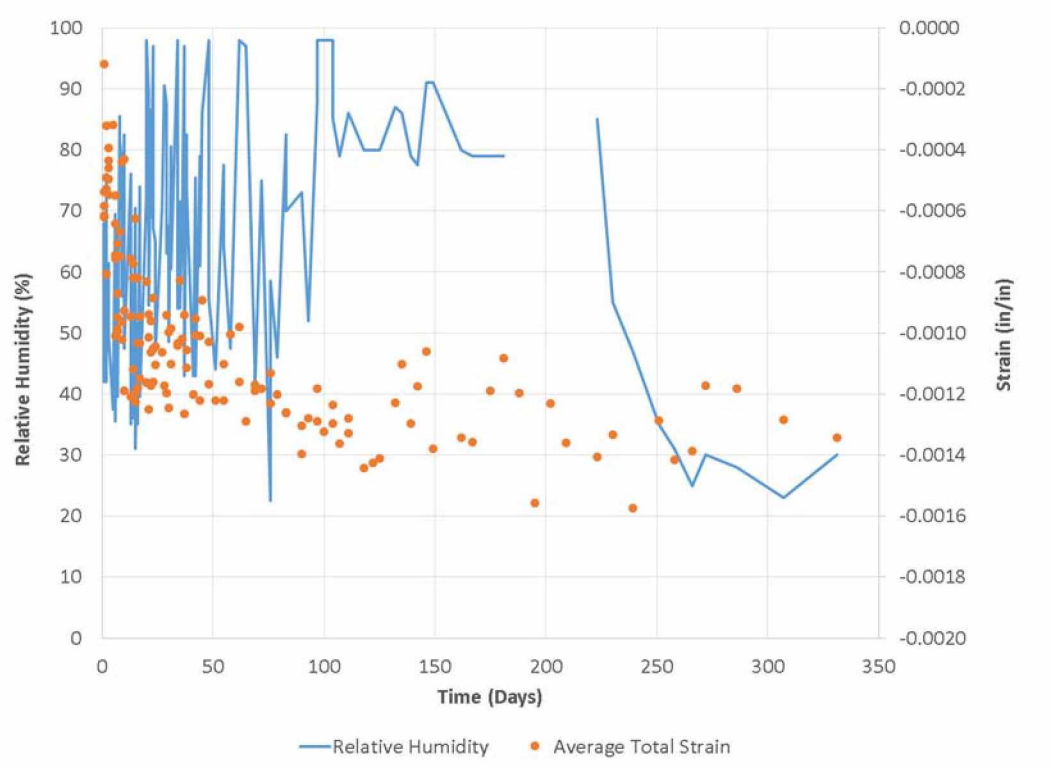

Figure 4-36: Outdoor Relative Humidity and Strain Comparison

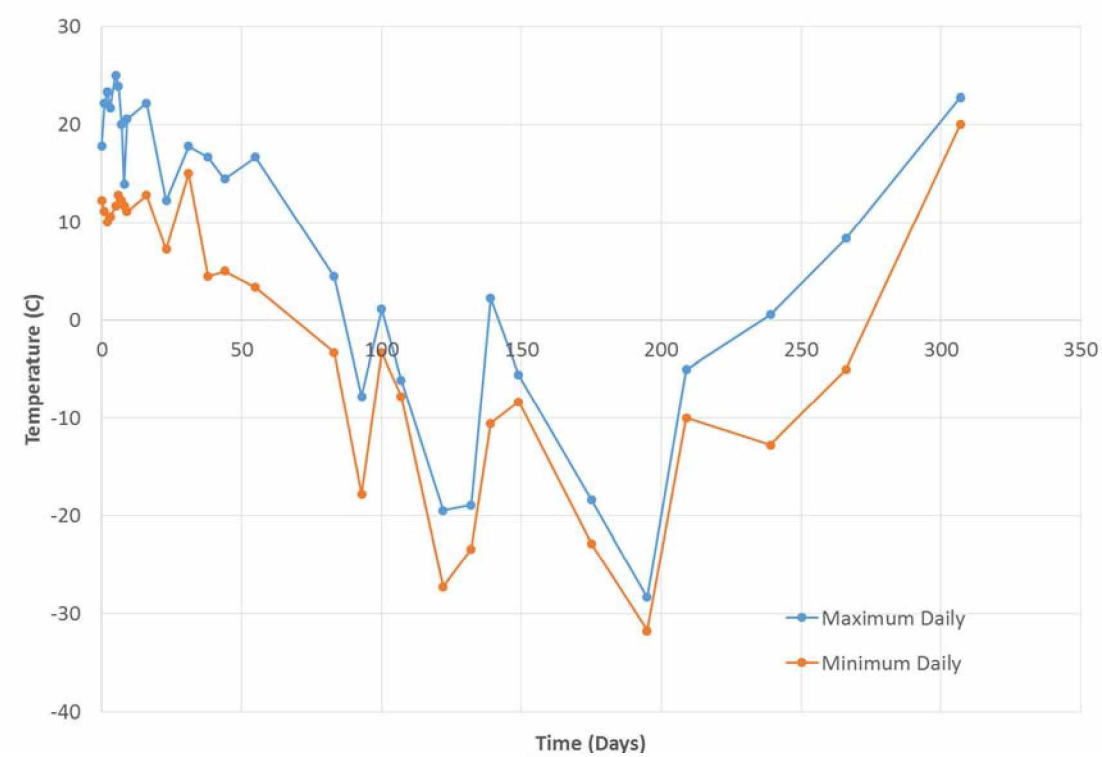

Figure 4-37: Outdoor Temperature Daily Maximum and Minimum

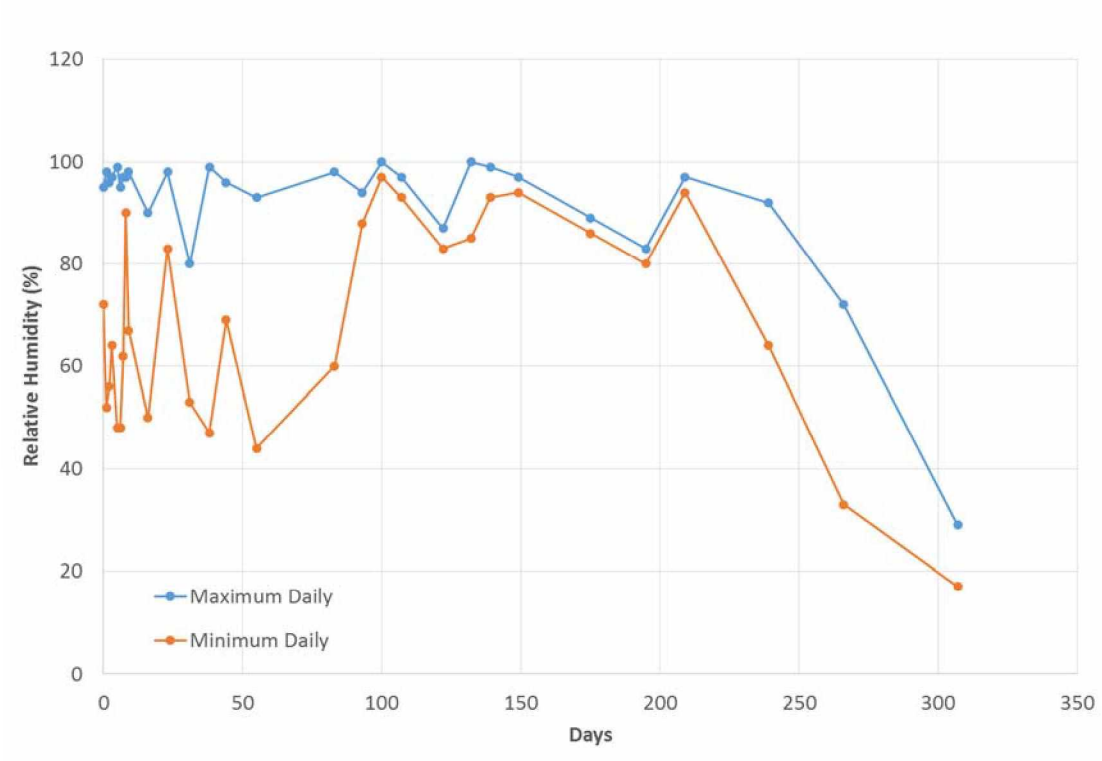

Figure 4-38: Outdoor Relative Humidity Daily Maximum and Minimum

Chapter 5 Design Implication

In this chapter, the measured total strains were compared with predicted values from several shrinkage and creep models. Used models were ACI 209R-92, Bažant-Baweja B3, CEB MC90-99, and GL 2000 models in ACI 209.2R-08 (ACI 2008). In addition, the models used in the AASHTO LRFD were included for comparison (AASHTO 2017). The model that fit best with the measured data was used to predict pre-stress loss.

5.1 Concrete Shrinkage and Creep Models

While shrinkage and creep may vary with local conditions, research has shown that short-term shrinkage and creep measurements improve the predictions regardless of location (Bažant 1987, Bažant and Baweja 2000, Aguilar 2005). For this reason, the ACI committee recommends short-term testing to determine the shrinkage, creep, and elastic modulus of the concrete to improve the predictions of the long-term deformations of the concrete.

The collection of shrinkage and creep data from around the world was initially done by Bažant and Panula and placed in a databank, which was then extended by the ACI and CEB. The issues with the databank include but are not limited to, which data sets should be used, the description of the concrete, European cement concretes versus United States, and experiments using smaller specimens. Several models, compromising between accuracy and convenience, have been proposed for the prediction of creep, drying shrinkage, and total strains under load. The idea being that an engineer with little to no specialized knowledge of shrinkage and creep can still use these models. The user friendly modeling includes specifications of the concrete to make the prediction such as its age at loading, ambient relative humidity, duration of loading, specimen size, among others. However, it has been recognized by the committee that the stiffness of the aggregate significantly effects the shrinkage and creep of concrete (ACI 2008). Some models account for this effect while others use concrete strength as an adjustment. If no mechanical characteristics of the concrete are available, rely on mixture proportion information alone may not account for the behavior due to aggregate properties.

Various models were selected to be used for comparison, mainly; the ACI 209R-92 (ACI 1992), the Bažant-Baweja B3 developed by Bažant and Baweja (1995, 2000), the CEB Model Code 1990-99 (CEB MC90-99)(Muller and Hillsdorf 1990, CEB 1999), and the GL2000 developed by Gardner and Lockman (2001). The comparison of the various models using

experimental data complicates the result by the lack of agreement on selection of the appropriate data and on the method used to compare the correlation, Table 5-1 lists the individual model's applicable range for different input variables.

Table 5-1: Parameter Ranges of Each Model

Input variables	Model				
	ACI 209R-92	Bažant-Baweja B3	CEB MC90	CEB MC90-99	GL2000
f_{cm28}, MPa (psi)	—	17 to 70 (2500 to 10,000)	20 to 90 (2900 to 13,000)	15 to 120 (2175 to 17,400)	16 to 82 (2320 to 11,900)
a/c	—	2.5 to 13.5	—	—	—
Cement content, kg/m^3 (lb/yd^3)	279 to 446 (470 to 752)	160 to 720 (270 to 1215)	—	—	—
w/c	—	0.35 to 0.85	—	—	0.40 to 0.60
Relative humidity, %	40 to 100	40 to 100	40 to 100	40 to 100	20 to 100
Type of cement, European (U.S.)	R or RS (I or III)	R, SL, RS (I, II, III)	R, SL, RS (I, II, III)	R, SL, RS (I, II, III)	R, SL, RS (I, II, III)
t_c (moist cured)	≥ 1 day	≥ 1 day	< 14 days	< 14 days	≥ 1 day
t_c (steam cured)	1 to 3 days	—	—	—	—
t_o	≥ 7 days	$t_o \geq t_c$	> 1 day	> 1 day	$t_o \geq t_c \geq 1$ day

5.1.1 ACI 209R-92 Model

The ACI Committee 209R-92 developed a prediction model of creep, shrinkage, and temperature effects in concrete structures (ACI 2008). Their method is concerning normal weight concrete, roughly below 6000psi, however, the variables methodology still applies to high strength concrete which has a compressive strength greater than 6000psi. Some of the advantages of this model include its simplicity and it's relatively easy to adjust to match short-term test data. The disadvantages include its limitations in accuracy when accommodating member size and it is empirical based and does not model shrinkage or creep phenomena. The input values required are only age of concrete when drying starts, age of concrete at loading, curing method, relative humidity expressed as a decimal, volume-surface ratio, and cement type. The model doesn't calculate compliance but calculates the creep coefficient, which may introduce problems with an assumed value for elastic modulus. The formula for shrinkage time function and shrinkage strain are in Eq. (5-3) and (5-4),

$$f(t,t_c) = \left[\frac{(t-t_c)^{\alpha}}{(f+(t-t_c)^{\alpha})}\right] \tag{5-3}$$

$$\varepsilon_{sh}(t,t_c) = \frac{(t-t_c)^{\alpha}}{f+(t-t_c)^{\alpha}}\varepsilon_{shu} \tag{5-4}$$

where,

ε_{shu} = Ultimate Shrinkage Strain = 347μ

α = Air Content Expressed as Percentage = 1.0

f = Number of Days = 35

The variables f and α, are considered constants for a given member shape and size. The creep coefficient time function and the creep coefficients are shown in Eq. (5-5) and (5-6),

$$f(t-t_0) = \left[\frac{(t-t_0)^{\Psi}}{(d+(t-t_0)^{\Psi})}\right] \tag{5-5}$$

$$\phi(t,t_0) = \left[\frac{(t-t_0)^{\Psi}}{(d+(t-t_0)^{\Psi})}\right]\phi_u \tag{5-6}$$

where,

ϕ_u = Ultimate Shrinkage Strain = 2.35γ_c

γ_c = Unit Weight of Concrete = 146 lb/ft^3

Ψ = Fine Aggregate Percentage = 0.6

d = Number of Days = 10

5.1.2 Bažant-Baweja B3 Model

The B3 Bažant-Baweja model is the latest variant in a number of shrinkage and creep prediction methods developed. This current model derives from a simpler and more theoretically justified version than previous models and is based on a mathematical description of over 10 physical phenomena affecting creep and shrinkage (Bažant 2000). This particular model has been found to be useful for those dealing with complex as well as simple structures. The compliance function is utilized to reduce the risk of errors due to inaccurate values of the elastic modulus. The factors taken into account include age of concrete when drying starts, age of concrete at loading, aggregate and cement content, cement type, concrete mean compressive strength at 28 days, curing method, relative humidity, shape of specimen, volume-surface ratio, and water content in concrete. The mean shrinkage strain and shrinkage time function are calculated by Eq. (5-7) and (5-8),

$$\varepsilon_{sh}(t,t_c) = -\varepsilon_{sh\infty}k_h tanh\left[\frac{(t-t_c)}{\tau_{sh}}\right]^{0.5} \tag{5-7}$$

$$S(t-t_c) = tanh\left[\frac{(t-t_c)}{\tau_{sh}}\right]^{0.5} \tag{5-8}$$

where,

t = Age of Concrete (days)

t_c = Start of Drying (days)

$\varepsilon_{sh\infty}$ = Ultimate Shrinkage Strain = -779μ

k_h= Ambient Relative Humidity Factor

$S(t - t_c)$ = the time curve

$(t - t_c)$ = is the time from the end of the initial curing

τ_{sh} = shrinkage half time given in days

The compliance function for basic creep is given by Eq. (5-9),

$$C_0(t, t_0) = q_2 Q(t, t_0) + q_3 ln[1 + (t - t_0)^n] + q_4 ln\left(\frac{t}{t_0}\right) \quad (5\text{-}9)$$

where,

q_2 = Aging Viscoelastic Term = 1.103μ (1/psi)

q_3 = Non-Aging Viscoelastic Term = 0.020μ (1/psi)

q_4 = Aging Flow Term = 5.106 x 10^{-8} (1/psi)

$Q(t, t_0) = Q_f(t_0)\left[1 + \left\{\frac{Q_f(t_0)}{Z(t,t_0)}\right\}^{r(t_0)}\right]^{\frac{-1}{r(t_0)}}$ = Aging Viscoelastic Term Part 1

$Z(t, t_0) = (t_0)^{-m} ln[1 + (t - t_0)^n]$ = Aging Viscoelastic Term Part 2

m = Constant = 0.5

n = Constant = 0.1

$r(t_0)$ = Constant = 10.333

$Q_f(t_0)$ = Constant = 0.246

5.1.3 CEB MC90-99 Model Solution

The CEB MC90-99 model is a revised version that takes into account both normal and high-strength concrete. In terms of creep and shrinkage-sensitive structures, this method is more widely used over the ACI 209R-92 model. However, the correction term used for relative humidity in the creep equation is extremely sensitive to any variation in relative humidity. This method requires the age of concrete when drying starts and at loading, concrete mean compressive strength at 28 days, relative humidity, volume-surface ratio, and cement type. It must be noted that European models were considered when optimizing the model, meaning that the model underestimates the shrinkage of North American concretes, and substantially

underestimates the shrinkage of concretes containing basalt aggregates (ACI 2008). The shrinkage strain and shrinkage time function are calculated by Eq. (5-10) and (5-11),

$$\varepsilon_{sh}(t,t_c) = \varepsilon_{cso}\beta_s(t-t_c) \tag{5-10}$$

$$\beta_s(t-t_c) = \left[\frac{\left\{\frac{(t-t_c)}{t_1}\right\}}{\left\{350\left[\frac{\left(\frac{V}{S}\right)}{\left(\frac{V}{S}\right)_0}\right]^2 + (t-t_c)/t_i\right\}}\right]^{0.5} \tag{5-11}$$

where,

ε_{cso} = Notional Shrinkage Coefficient = -453μ

$\frac{V}{S}$ = Volume to Surface Ratio = 4in

$\left(\frac{V}{S}\right)_0$ = Volume to Surface Ratio = 2in

$(t-t_c)$ = Duration of Drying (Days)

The creep coefficient and creep coefficient time function are calculated by Eq. (5-12) and (5-13),

$$\phi_{28}(t,t_0) = \phi_0\beta_c(t-t_c) \tag{5-12}$$

$$\beta_c(t-t_0) = \left[\frac{\frac{(t-t_0)}{t_1}}{\left\{\beta_H + \frac{(t-t_0)}{t_1}\right\}}\right]^{0.3} \tag{5-13}$$

where,

β_H = Relative Humidity Adjustment Factor = 570.445

ϕ_0 = Notional Shrinkage Coefficient = 2.524

t_0 = Age of Loading = 14 Days

5.1.4 GL2000 Model Solution

The GL2000 model was developed by Gardner and Lockman (2001) and is a modification made to conform to the ACI 209 model guidelines. The model is convenient to use because other than compressive strength, it only requires input data that are available to the engineer at time of design. The method requires age of concrete when drying starts and when loaded, relative humidity, volume-surface ratio, cement type, and concrete mean compressive strength at 28 days. The shrinkage strain and shrinkage time function are calculated by Eq. (5-14) and (5-15),

$$\varepsilon_{sh}(t,t_c) = \varepsilon_{shu}\beta(h)\beta(t-t_c) \quad (5\text{-}14)$$

$$\beta(t-t_c) = \left[\frac{(t-t_c)}{\left\{t-t_c+77\left(\frac{V}{S}\right)^2\right\}}\right]^{0.5} \quad (5\text{-}15)$$

where,

ε_{shu} = Ultimate Shrinkage Strain = 867μ

$\beta(h)$ = Ambient Relative Humidity Factor = 0.717

The basic creep coefficient is calculated by Eq. (5-16),

$$\phi_{28}(t,t_0) = 2\left[\frac{(t-t_0)^{0.3}}{\{((t-t_0)^{0.3}+14)\}}\right] + \left[\frac{7}{t_0}\right]^{0.5}\left[\frac{(t-t_0)}{\{(t-t_0)+7\}}\right]^{0.5} \quad (5\text{-}16)$$

5.1.5 AASHTO LRFD Model Solution

The AASHTO LRFD Model was utilized as a basis for calculation since they are one of the more major influences when it comes to design characteristics of pre-stress loss. The shrinkage is calculated using Eq. (5-17) while the creep coefficient and compliance derive from Eq. (5-18) and (5-19) as follows;

$$\varepsilon_{bid} = k_{shape} * k_{hs} * k_f * k_{eva} * 48 * 10^{-3} \quad (5\text{-}17)$$

$$\psi_{creep} = 1.9 * k_{shape} * k_{hc} * k_f * k_{eva} * t_{ini}^{-0.118} \quad (5\text{-}18)$$

$$J_{t,t_0} = J_{t_0,t_0} + \frac{\psi_{creep}}{E_{cmto}} \quad (5\text{-}19)$$

where,

k_{shape} = Volume-Surface Factor

k_{hc} = Humidity Factor for Creep

k_{hs} = Humidity Factor for Shrinkage

k_f = Concrete Strength Factor

k_{eva} = Time Development Factor

t_{ini} = Age at Loading

E_{cmto} = Measured Mean Elastic Modulus

5.1.6 Model Graphical Comparison

The five models were used to predict the total strain of the indoor and outdoor frames. The total strains were calculated from the loading day (14 day) to 365 day based on the measured material properties. All required parameters used in the models were from the concrete mix design document and test results in the present study. Table 5-2 shows selected material properties used in the models.

Table 5-2: Selected Parameters in the Models

Parameter	Value	Remark
unit weight of concrete	$\gamma_c = 152 pcf$	concrete mix document
Concrete compressive strength	$f_c^{'} = 8000 psi$	specified 28day strength
	$f_{c\_14d}^{'} = 8654 psi$	measured 14day strength
	$f_{c\_28d}^{'} = 9119 psi$	measured 28day strength
Elastic modulus	$E_{c\_14d} = 5727643 psi$	measured 14day modulus
	$E_{c\_28d} = 5915679 psi$	measured 28day modulus
Relative humidity	$RH=0.4$	Indoor frame
	$RH=0.686$	Outdoor frame
Volume-surface ratio	*1.3 in.*	6″×12″ cylinder
Stress applied	$f_{start} = 2829 psi$	initial load (80kips)
	$f_{end} = 2476 psi$	final load (70kips)

Figure 5-1 shows the total strains calculated from the models with measured total strains for the indoor frame. A relative humidity of $RH=0.4$ and an applied stress of $f_{start} = 2829 psi$ are used in the models. The ACI model has values exceeding the others until day 50, showing that it is more sensitive in short term shrinkage measurements indoors. It is also noted that in the shrinkage comparison the values until day 28 are zero for all except the GL2000, this is because the difference in the age of concrete at loading being 7 days versus 28 days. For shrinkage strains, after the initial changes settle out, the models seem to have a similar trend line over long terms, except the GL2000 with a slightly steeper trend. The measured total strains match well with the CEB MC90-99 model. Also the AASHTO LRFD model has the smallest slope so that long-term prediction from this model is substantially smaller than others.

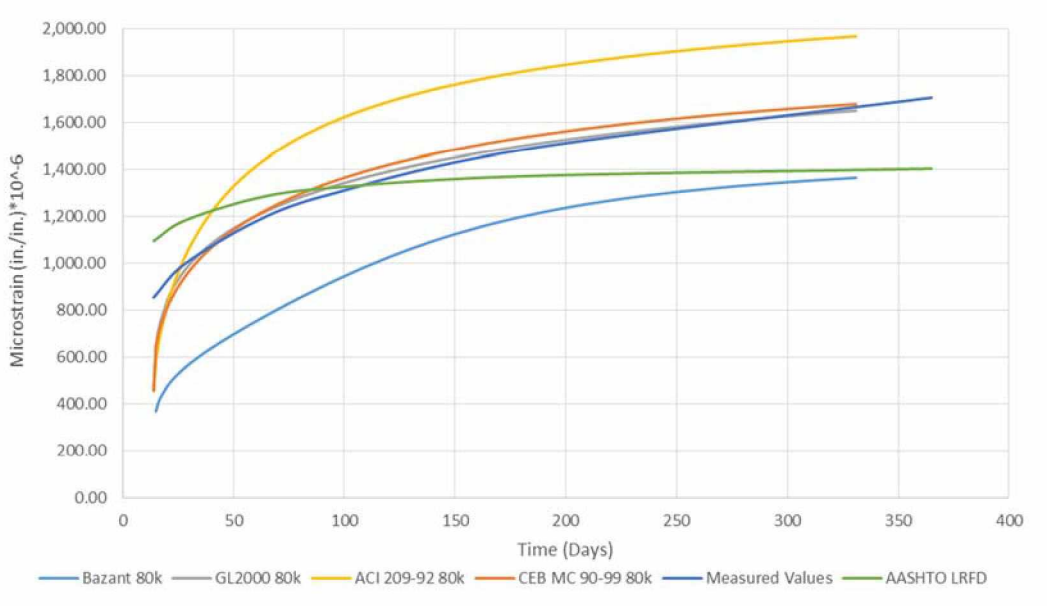

Figure 5-1: Total Strain Comparison (Indoor, 80kip)

In Figure 5-2, total strains from the models are compared with the measured strains. A relative humidity of $RH=0.686$ and an applied stress of $f_{start}=2829\,psi$ are used in the models. The Bažant-Baweja B3 model can be seen as underestimated while the GL2000 models show a closer trend as time goes on. The two that are most related are the ACI 209-92 and GL2000 model, which are seen as a more conservative estimation short term. Specifically, the measured total strains match well with the ACI 209-92 model in a wide range.

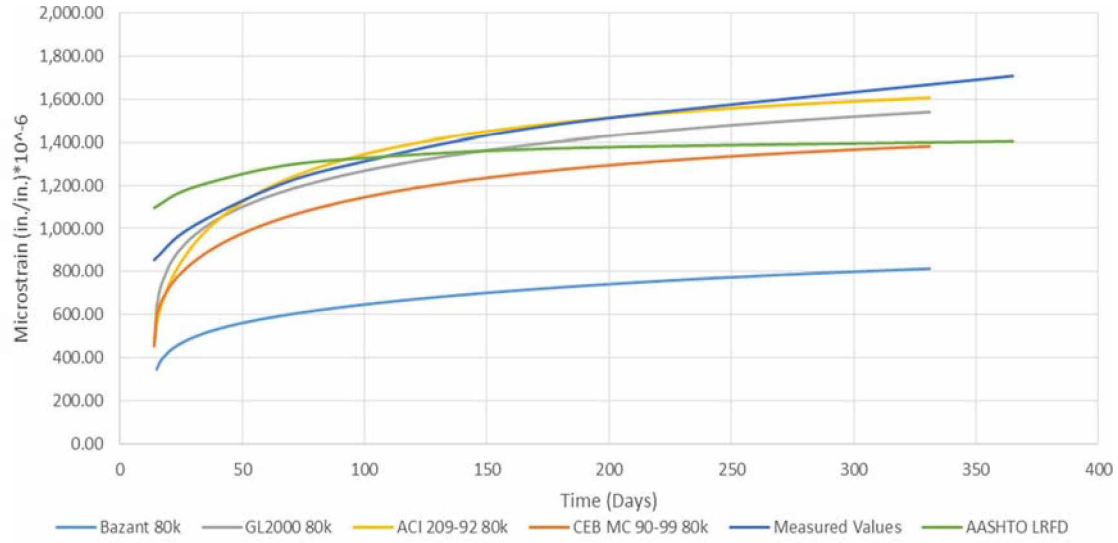

Figure 5-2: Total Strain Comparison (Outdoor, 80kip)

Figures 5-3 and 5-4 represent the range of 70k to 80k that each model predicts, to show the range of measured values during testing.

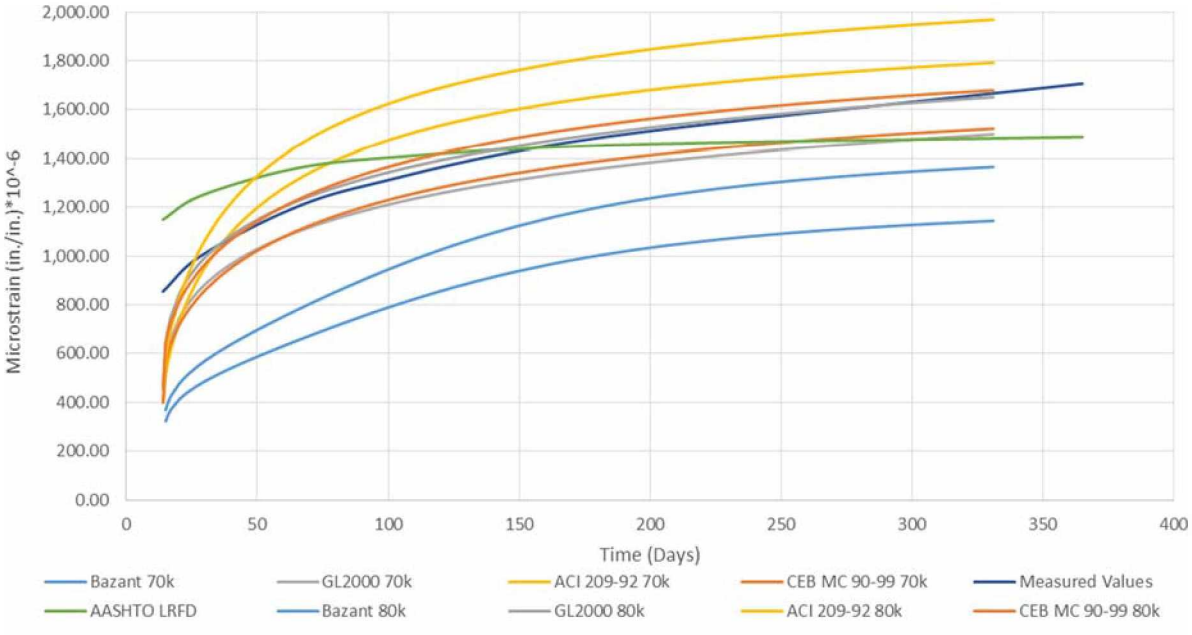

Figure 5-3: Total Strain Comparison (Indoor, 80 kip+70 kip)

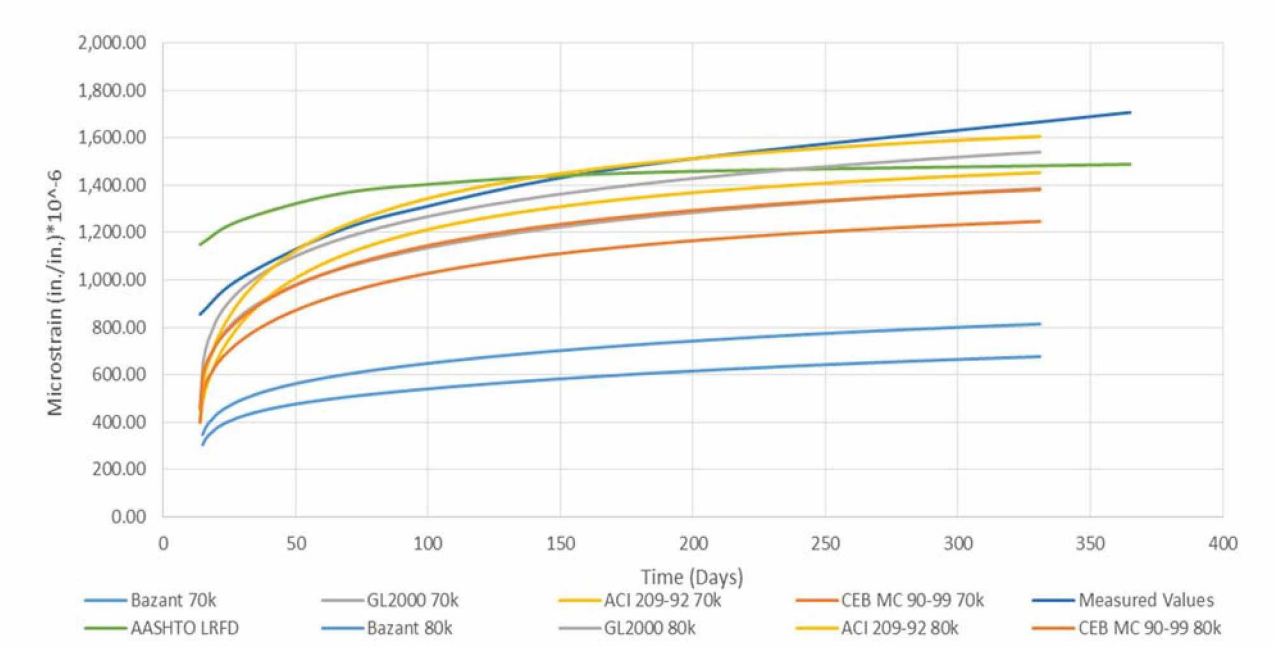

Figure 5-4: Total Strain Comparison (Outdoor, 80 kip+70 kip)

In Figures 5-5 and 5-6, total strains are estimated for the entire 75-year design life expectancy of a DBT bridge girder. The relative humidity values are 0.4 and 0.686, respectively, and the applied stress is $f_{start} = 2829 psi$ for both. Excluding the AASHTO LRFD model prediction, it is revealed that the indoor comparison ranges from approximately 2,000 to 3,100 micro strain, while the outdoor comparison ranges from approximately 1,600 to 2,300 micro strain. It should be noted that the CEB MC90-99 model was the best fit with the measured data for 365 days, and it was the ACI 209-92 model for the outdoor frame case.

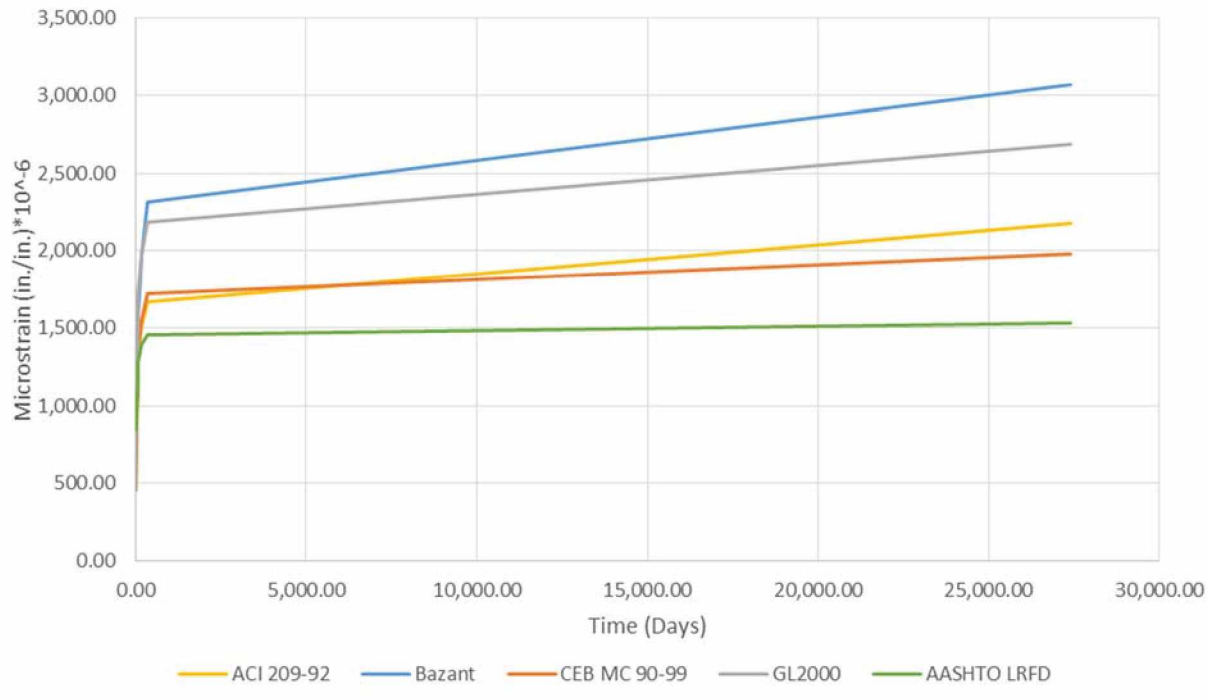

Figure 5-5: Indoor 75-year Prediction Model Comparison

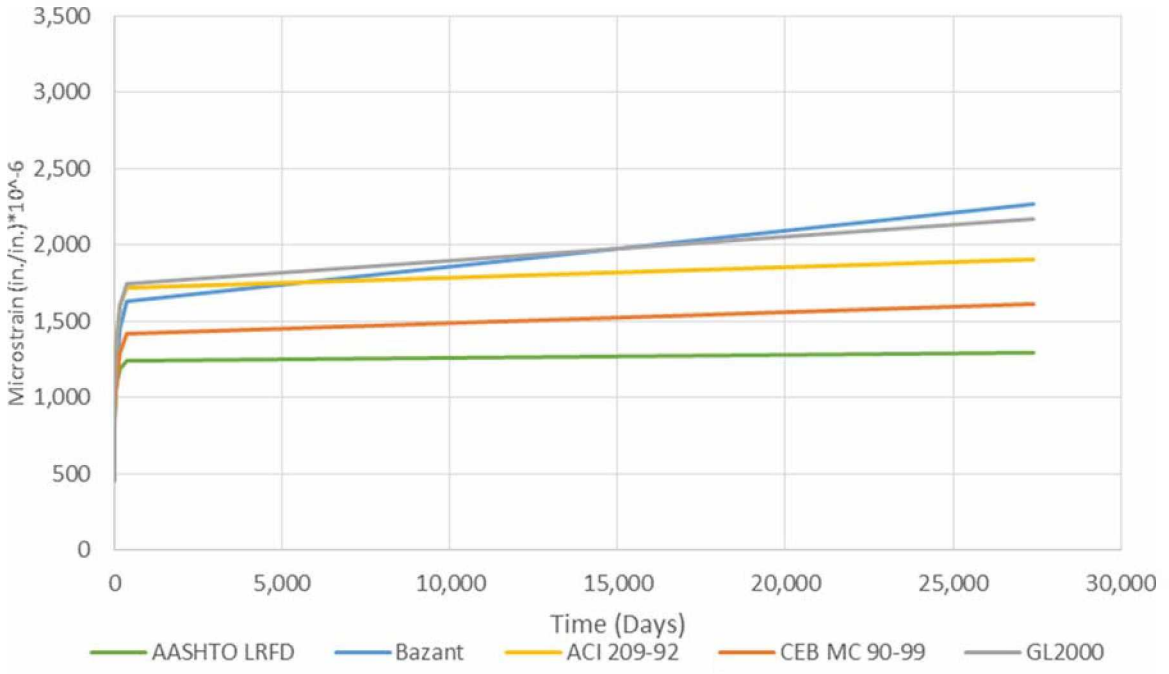

Figure 5-6: Outdoor 75-year Prediction Model Comparison

5.2 Pre-Stress Loss Due to Concrete Creep

In this section, the pre-stress loss due to concrete creep is calculated and compared. Specifically, pre-stress loss from the following three methods are compared.

- 2004 AASHTO LRFD Refined method
- 2017 AASHTO LRFD Refined Estimation
- 2017 AASHTO LRFD Refined Estimation with a modification of creep coefficient from the ACI 209-92 model.

From the comparison with measured total strains, the ACI 209-92 model was the best match in the outdoor frame case. Therefore, the concrete creep coefficients from the ACI 209-92 model were replaced with the ones in the 2017 AASHTO LRFD method.

The overall pre-stress loss estimation must utilize the specific structures properties in terms of geometry and not use the general values. Thus, the section properties of the Tulsona Creek DBT Girder based on the approved submittal can be found in Figure 5-7 for a real life comparison of the pre-stress loss expected. In addition, Table 5-3 shows major input parameters used in concrete creep prediction.

Part	Shape	Height	Width	Ai	yi	Aiyi	I I'	Ai di2	Perimeter length
		in	in				in^4	in^4	in
A	SQ	6.0	66.4	398.3	63.0	25089.8	1194.75	167068.70	78.38
B	SQ	60.0	6.0	360.0	30.0	10800.0	108000.00	56413.27	96.00
C	SQ	1.0	43.0	43.0	59.5	2558.5	3.58	12400.51	2.00
D	TR	3.0	39.0	58.5	58.0	3393.0	29.25	14021.77	39.46
E	SQ	3.0	4.0	12.0	57.5	690.0	9.00	2693.48	0.00
F	TR	2.0	4.0	4.0	55.3	221.3	0.89	656.92	5.66
G	TR	3.0	19.0	28.5	7.0	199.5	14.25	35953.82	19.92
H	SQ	6.0	19.0	114.0	3.0	342.0	342.00	178031.79	31.00
			Sum	1018.25		43294.08	109593.72	467240.26	272.42
					y_bar	42.52	from the bottom		
					I_g	576833.98			

Ap 0.153 in^2

Group	number of strands	CGS	
	ni	in	ni yi
Harped	36	7	252
Straight	28	3.625	101.5
Sum	64		353.5
CGS	5.523	in	from the bottom

Girder

length	1734	in
Section A	1018.25	in^2
Volume	1765645.5	in^3
Side S	472368.568	in^2
End S (two)	2036.5	in^2
Total S	474405.068	in^2

	number	section	per girder	
		in^2	lb/ft	
Rail support	2	180	54.64	
	number	volume	per girder	
		in^3	lb	lb/ft
diaphragm	6	25803	1958.263	13.552

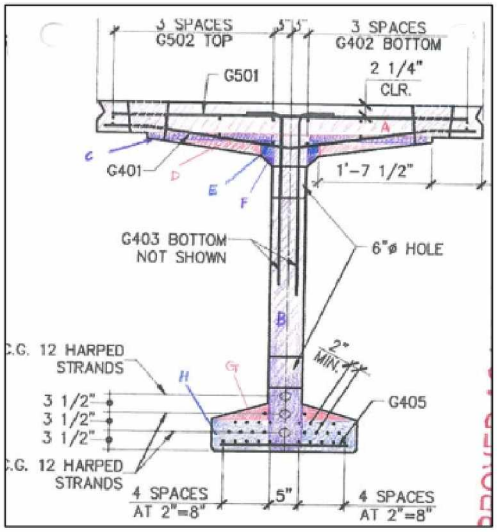

Figure 5-7: Section Properties of Tulsona Creek DBT Girder

Table 5-3: Selected Parameters in Tulsona DBT Girder

Parameter	Value	Remark
unit weight of concrete	$\gamma_c = 153 pcf$	concrete mix document
Concrete compressive strength	$f_c^{'} = 7500 psi$	specified 28day strength
	$f_{ci}^{'} = 6250 psi$	at force transfer
Elastic modulus	$E_{ci} = 5143000 psi$	at force transfer
Relative humidity	$RH=0.7$	AASHTO LRFD
Volume-surface ratio	*3.72 in.*	DBT girder

Table 5-4 shows the pre-stress loss due to concrete creep estimated from the three methods. The value from the 2004 AASHTO method is significantly larger than the others. The 2017 AASHTO method with ACI 209-92 creep coefficients estimates a larger loss when the bridge is in service, which matches well with the measured total strains in the present study.

Table 5-4: Comparison of Pre-Stress Loss Due to Concrete Creep in Tulsona DBT Girder

Method	**0 – Bridge Completion**	**- 75 years**	**Total**
2004 AASHTO	NA	NA	33.9 ksi
2017 AASHTO	10.1 ksi	5.7 ksi	15.8 ksi
2017 AASHTO + ACI Creep Coeff.	10.7 ksi	9.1 ksi	19.8 ksi

Chapter 6 Summary and Conclusions

6.1 Summary

Proper estimations of the behavior of concrete pre-stress loss in cold temperatures directly effects many areas of the country, and the current resources are incomplete to ensure accuracy. Therefore, concrete cylinders were made at AggPro in Anchorage, where girder fabrication is done, and brought to Fairbanks. The cylinders were stored in a lime bath at ADOT&PF Regional Lab and tested for strength and elastic modulus at various days to get a baseline behavior of the concrete. After 14 days, the cylinders were prepped with gauge plugs, two pairs on each specimen, and a thermistor and ready for analysis. Thus, two 6"x12" concrete cylinders, loaded to roughly 80,000 pounds with a hydraulic jack, were left in the outdoor Alaskan environment for one year to be compared to an indoor control set up to measure the differences in creep and shrinkage for future concrete construction applications in the extreme climate. A load cell monitored stress while a weather station, thermometer, and thermistor measured ambient and internal temperature of the concrete specimens. After unloading, all specimen measurements were graphed for concrete creep and shrinkage to identify the total pre-stress loss. Model comparisons from ACI 209R-92, CEM MC 90-99, GL 2000, and Bažant-Baweja B3 were all compared for a best fit analysis for 1 year and 75 years. Section properties were then obtained for a full scale DBT girder in Tulsona Creek that whose values were inputted into the models for a real-life situation.

6.2 Conclusion

Since Alaska bridge construction consists mostly in the summer season and that evidence shows that the majority of the concrete creep takes place within the first 6 months of placement, the winter season should have somewhat minimal effects on the short term creep. However, as the wildly fluctuating winter's cold and summer heat may have more of an effect for the long term creep. The prediction models are not able to accurately predict this long term creep as the relative humidity and temperature are constantly shifting in real life, but are set as one correction factor for evaluation.

It was observed that the natural environment including the ambient air temperature and relative humidity is a big factor in the extent of creep and shrinkage. This is displayed in the

differences of ambient versus internal temperature of the outdoor apparatus. It can be seen from Figure 4-35 that after roughly 80-100 days when the ambient temperature reaches zero degrees, the creep almost stops. This is evidence that the ambient temperature is directly related to the amount of shrinkage and creep within the concrete specimens. Thus, for areas that are more represented by the parameters of the indoor specimen, the ACI 209R-92 or the CEB MC 90-99 models may be the best selection based on the 1 year prediction from Figure 5-3. Whereas areas that are more prone to big variations in temperature and relative humidity may want to refer to the predictions representing the ambient environment for predicting pre-stress loss.

6.3 Implications and Future Studies

The future work regarding concrete shrinkage and creep should be handled with more control over the ambient temperatures to get more quantifiable results of their differences similar to the model predictions. This could be accomplished by placing an apparatus in a cold room where the temperature and relative humidity are maintained throughout the experiment. An additional suggestion would be to load the concrete specimens in the frame earlier than 28 days, a week should be enough time to allow the concrete to harden sufficiently but also allow more movement after loading. This method would display variances of the age when concrete is loaded compared to the creep that it contains short term and long term. The number of specimens that were utilized for this experiment were few and a more accurate representation of the values could be obtained with more frames and in varying locations.

References

AASHTO (2004). *AASHTO LRFD Bridge Design Specifications (3rd ed.)*, American Association of State Highway and Transportation Officials.

AASHTO (2012). *AASHTO LRFD Bridge Design Specifications (6th ed.)*, American Association of State Highway and Transportation Officials.

AASHTO (2014). *AASHTO LRFD Bridge Design Specifications (7th ed.)*, American Association of State Highway and Transportation Officials.

AASHTO (2017). *AASHTO LRFD Bridge Design Specifications (8th ed.)*, American Association of State Highway and Transportation Officials.

ACI (1992). *Prediction of Creep, Shrinkage, and Temperature Effects in Concrete Structures (ACI 209R-92)*. American Concrete Institute, Farmington Hills, MI. 47 pp.

ACI (2005). *Report on Factors Affecting Shrinkage and Creep of Hardened Concrete (ACI 209.1R-05)*. American Concrete Institute.

ACI (2008). *Guide for Modeling and Calculating Shrinkage and Creep in Hardened Concrete (ACI 209.2R-08)*. American Concrete Institute.

ADOT&PF (2017). *Alaska Bridges and Structures Manual*. Alaska Department of Transportation and Public Facilities.

Aguilar, C. (2005). *Study of the Behavior and Development of a Prediction Methodology for Drying Shrinkage of Concretes*. PhD thesis. School of Engineering, Universidad Catolica de Chile, Santiago, Chile.

ASTM (2012). *Standard Practice for Making and Curing Concrete Test Specimens in the Field (ASTM C31 / C31M-12)*. ASTM International

ASTM (2014). *Standard Test Method for Static Modulus of Elasticity and Poisson's Ratio of Concrete in Compression (ASTM C469 / C469M – 14)*. ASTM International.

ASTM (2015). *Standard Test Method for Creep of Concrete in Compression (C 512/C512M-15)*. ASTM International.

ASTM (2018). *C39 / C39M-18, Standard Test Method for Compressive Strength of Cylindrical Concrete Specimens*. ASTM International, West Conshohocken, PA.

Bažant, Z.P. (1987). Statistical Extrapolation of Shrinkage Data – Part I: Regression. *ACI Materials Journal* 84(1):20-34.

Bažant, Z. P. (2000). Criteria for Rational Prediction of Creep and Shrinkage of Concrete. *The Adam Neville Symposium: Creep and Shrinkage-Structural Design Effects, SP-194*, A. Al-Manaseer, ed.:237-260. American Concrete Institute, Farmington Hills, MI.

Bažant, Z.P., and S. Baweja (1995). Creep and Shrinkage Prediction Model for Analysis and Design of Concrete Structures – Model B3. *Materials and Structures* 28:357-365, 415-430, 488-495.

Bažant, Z. P., and S. Baweja (2000). Creep and Shrinkage Prediction Model for Analysis and Design of Concrete Structures: Model B3. *The Adam Neville Symposium: Creep and Shrinkage-Structural Design Effects, SP-194*, A. Al-Manaseer, ed.: 1-83. American Concrete Institute, Farmington Hills, MI.

Brewe, J. E., J. J. Myers and J. Myers (2008). Pre-stress Loss Behavior of High-Strength Self-Consolidating Concrete Girders Subjected to Elevated Compressive Fiber Stresses. *National Bridge Conference*.

CEB (1999). Structural Concrete—Textbook on Behaviour, Design and Performance. Updated Knowledge of the CEB/ FIP Model Code 1990. *fib Bulletin 2*, 2: 37-52. Federation Internationale du Beton, Lausanne, Switzerland.

ClimaTemps (2016). *Climate & Temperature*. http://www.climatemps.com/.

Collins, M. P. and D. Mitchell (1997). *Pre-stressed Concrete Structures*. Response Publications.

Current Results Nexus (2016a). *Humidity Levels in Montana During January*. https://www.currentresults.com/ /Montana/humidity-january.php.

Current Results Nexus (2016b). *Winter Temperature Averages for Every State*. https://www.currentresults.com/Weather/US/average-state-temperatures-in-winter.php

Daugherty, L. and E. Marx (2014). ALASKA Concrete bridges in extreme and remote environments. *ASPIRE* (Summer):34-35.

Figg, L. and W. D. Pate (2004). Precast Concrete Segmental Bridges-America's Beautiful and Affordable Icons. *PCI Journal* 49(5):26-38.

Garber, D. B., J. M. Gallardo, D. J. Deschenes and O. Bayrak (2016). Pre-stress loss calculations: Another perspective. *PCI Journal*(May-June):68-85.

Garber, D., J. Gallardo, D. Deschenes, D. Dunkman and O. Bayrak (2013). *Effect of New Pre-stress Loss Estimates on Pre-tensioned Concrete Bridge Girder Design (FHWA/TX-12/0-6374-2)*. Center for Transportation Research, The University of Texas at Austin; Texas Department of Transportation.

Gardner, N. J., and J. J. Lockman (2001). Design Provisions for Drying Shrinkage and Creep of Normal Strength Concrete. *ACI Materials Journal* 98(2):159-167. Mar.-Apr.

Josten, M. G., W. L. Painter and J. S. Guarre (1995). Precast Pre-stressed Concrete Structure Provides Solution for Getty. *PCI Journal* 40(3):24-39.

Menn, C. (1986). *Pre-stressed Concrete Bridges*, Birkhauser.

Mertol, H. C., S. Rizkalla, P. Zia, and A. Mirmiran (2010). Creep and shrinkage behavior of high-strength concrete and minimum reinforcement ratio for bridge columns. *PCI Journal*(summer):138-154.

Muller, H. S., and H. K. Hilsdorf (1990). *General Task Group 9*. CEB Comité Euro-International du Béton, Paris, France.

Oesterle, R. G., A. F. Elremaily, Z. J. Ma, R. Eriksson and C. Prussack (2009). *Design and Construction Guidelines for Long-Span Decked Precast, Pre-stressed Concrete Girder Bridges (Final Report, NCHRP Project 12-69)*. National Cooperative Highway Research Program; Transportation Research Board.

Park, R. and T. Paulay (1975). *Reinforced Concrete Structures*. John Wiley and Sons.

PCI (2000). *Precast Pre-stressed Concrete Bridge Design Manual*. Precast/Pre-stressed Concrete Institute. Chicago, IL.

PCI (2010). *PCI Design Handbook: Precast and Pre-stressed Concrete. MNL-120 (7th ed.)*. Precast/Pre-stressed Concrete Institute. Chicago, IL.

PCI (2011). *Chapter 6. Preliminary Design. Bridge Design Manual (3rd Ed.)*. Precast/Pre-stressed Concrete Institute. Chicago, IL.

PCINE (2014). *Guidelines for Accelerated Bridge Construction Using Precast/Pre-stressed Concrete Elements Including Guideline Details (2nd ed., PCINE-14-ABC)*. Precast/Pre-stressed Concrete Institute Northeast Bridge Technical Committee.

Roller, J. J., H. G. Russell, R. N. Bruce and W. R. Alaywan (2011). Evaluation of pre-stress losses in high-strength concrete bulb-tee girders for the Rigolets Pass Bridge. *PCI Journal* 56(1):110-134.

Rüsch, H. (1960). Researches Toward a General Flexural Theory for Structural Concrete. *ACI-Journal Proceedings* 57(7):1-28.

Shahawy, M. A. (2003). *Prefabricated Bridge Elements and Systems to Limit Traffic Disruption During Construction (NCHRP Synthesis 324)*. Transportation Research Board.

Tadros, M. K., N. Al-Omashi, S. J. Seguirant and J. G. Gallt (2003). Pre-stress Losses in Pre-tensioned High-Strength Concrete Bridge Girders (NCHRP Report 496). Washington, D.C., Transportation Research Board.

NOWData - *NOAA Online Weather Data. National Oceanic and Atmospheric Administration. Retrieved 19 February 2015.*

Appendices

Appendix A: Submitted and Approved Girder Design

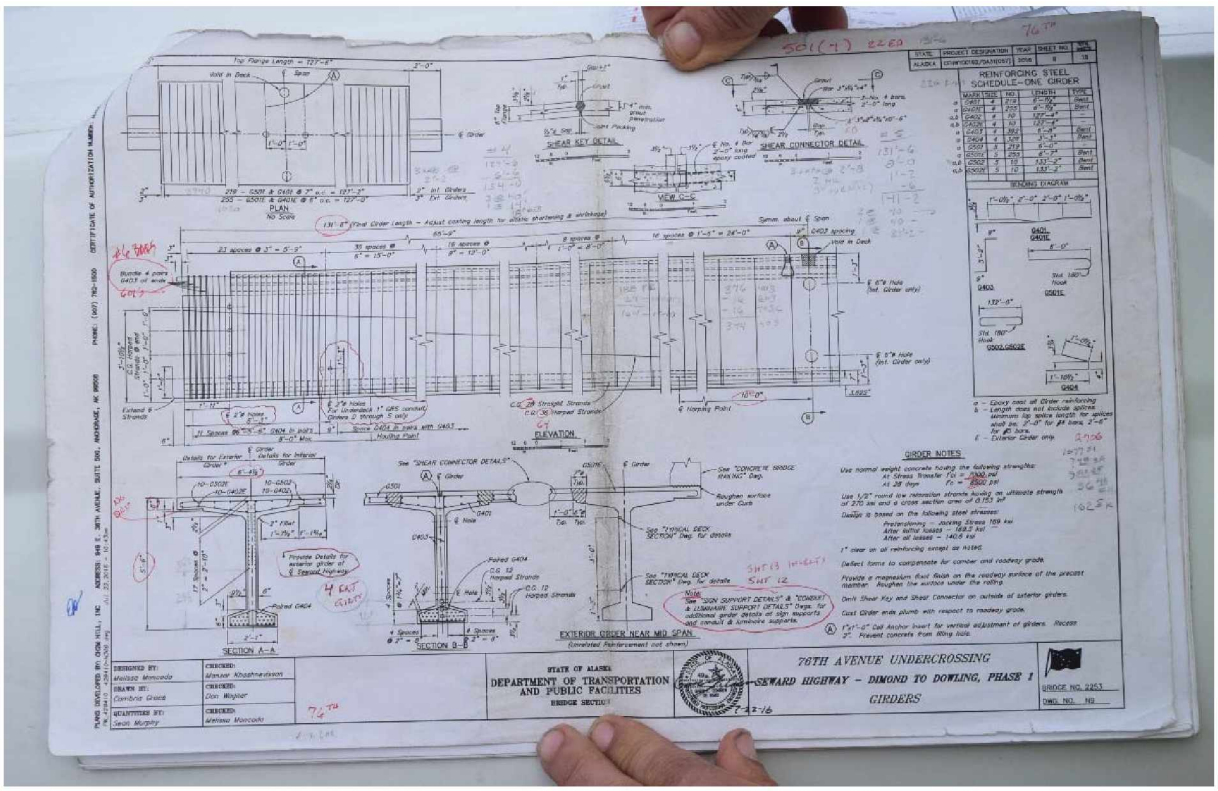

Appendix B: Measured Data

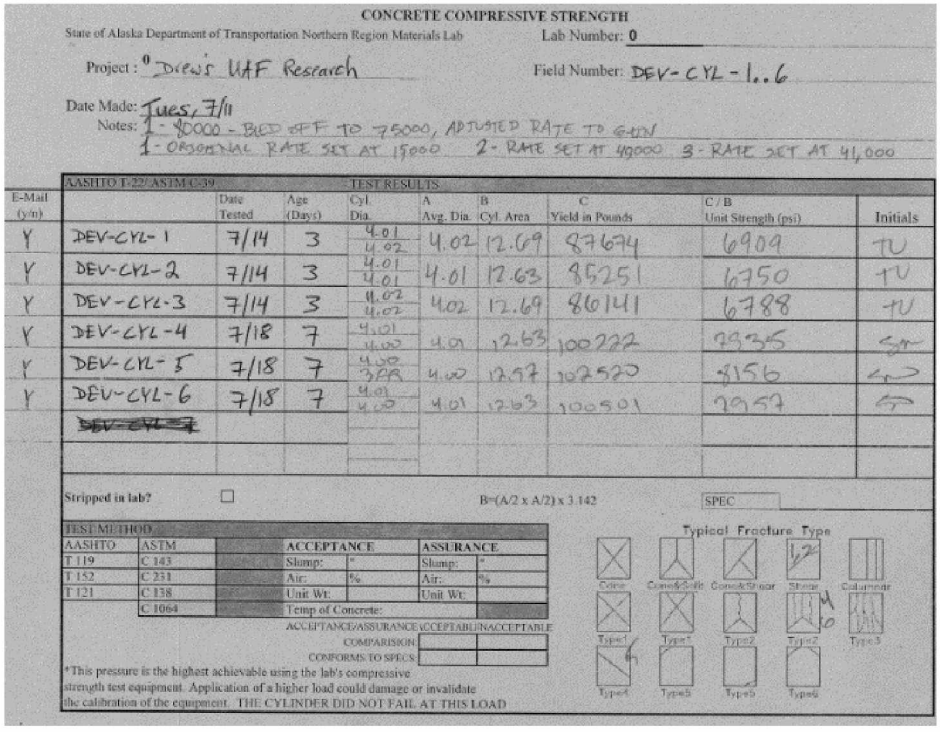

CONCRETE COMPRESSIVE STRENGTH

State of Alaska Department of Transportation Northern Region Materials Lab — Lab Number: 0

Project: 0 Drew's UAF Research — Field Number: DEV-CYL-1..6

Date Made: Tues, 7/11

Notes: 1 - 40000 - BLED OFF TO 75000, ADJUSTED RATE TO 6400
1 - ORIGINAL RATE SET AT 15000 2 - RATE SET AT 40000 3 - RATE SET AT 41,000

AASHTO T-22/ASTM C-39 — TEST RESULTS

E-Mail (y/n)		Date Tested	Age (Days)	Cyl. Dia.	A Avg. Dia.	B Cyl. Area	C Yield in Pounds	C / B Unit Strength (psi)	Initials
Y	DEV-CYL-1	7/14	3	4.01 4.02	4.02	12.69	87674	6909	TV
Y	DEV-CYL-2	7/14	3	4.01 4.01	4.01	12.63	85251	6750	TV
Y	DEV-CYL-3	7/14	3	4.02 4.02	4.02	12.69	86141	6788	TV
Y	DEV-CYL-4	7/18	7	4.01 4.02	4.01	12.63	100222	7935	[illegible]
Y	DEV-CYL-5	7/18	7	4.00 3RR	4.00	12.57	102520	8156	[illegible]
Y	DEV-CYL-6	7/18	7	4.01 4.00	4.01	12.63	100501	7957	[illegible]
	~~DEV-CYL-7~~								

Stripped in lab? ☐ — B=(A/2 x A/2) x 3.142 — SPEC

TEST METHOD		ACCEPTANCE		ASSURANCE	
AASHTO	ASTM	Slump:	"	Slump:	"
T 119	C 143	Air:	%	Air:	%
T 152	C 231	Unit Wt:		Unit Wt:	
T 121	C 138	Temp of Concrete:			
	C 1064	ACCEPTANCE/ASSURANCE		ACCEPTABLE/UNACCEPTABLE	
		COMPARISON:			
		CONFORMS TO SPECS:			

*This pressure is the highest achievable using the lab's compressive strength test equipment. Application of a higher load could damage or invalidate the calibration of the equipment. THE CYLINDER DID NOT FAIL AT THIS LOAD

Typical Fracture Type

Cone | Cone&Split | Cone&Shear | Shear | Columnar
Type1 | Type2 | Type3 | Type4 | Type5 | Type6

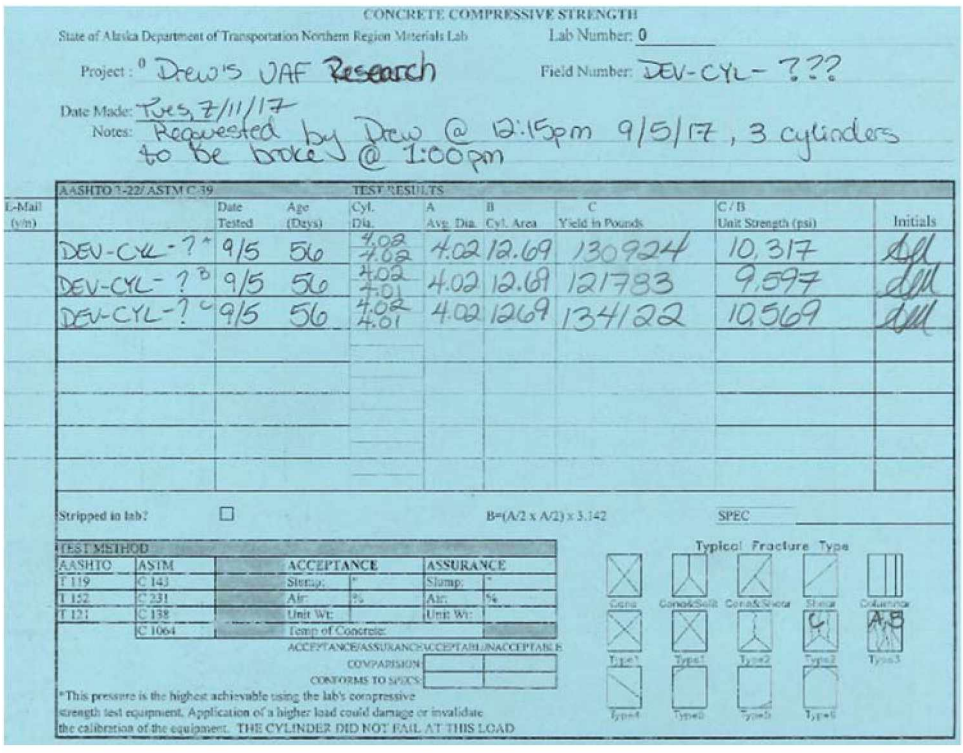

CONCRETE COMPRESSIVE STRENGTH

State of Alaska Department of Transportation Northern Region Materials Lab — Lab Number: 0

Project: 0 Drew's UAF Research — Field Number: DEV-CYL-???

Date Made: Tues, 7/11/17

Notes: Requested by Drew @ 12:15pm 9/5/17, 3 cylinders to be broke @ 1:00pm

AASHTO T-22/ASTM C-39 — TEST RESULTS

E-Mail (y/n)		Date Tested	Age (Days)	Cyl. Dia.	A Avg. Dia.	B Cyl. Area	C Yield in Pounds	C / B Unit Strength (psi)	Initials
	DEV-CYL-?A	9/5	56	4.02 4.02	4.02	12.69	130924	10,317	dll
	DEV-CYL-?B	9/5	56	4.02 4.01	4.02	12.68	121783	9.597	dll
	DEV-CYL-?C	9/5	56	4.02 4.01	4.02	1269	134122	10569	dll

Stripped in lab? ☐ — B=(A/2 x A/2) x 3.142 — SPEC

TEST METHOD		ACCEPTANCE		ASSURANCE	
AASHTO	ASTM	Slump:	"	Slump:	"
T 119	C 143	Air:	%	Air:	%
T 152	C 231	Unit Wt:		Unit Wt:	
T 121	C 138	Temp of Concrete:			
	C 1064	ACCEPTANCE/ASSURANCE		ACCEPTABLE/UNACCEPTABLE	
		COMPARISON:			
		CONFORMS TO SPECS:			

*This pressure is the highest achievable using the lab's compressive strength test equipment. Application of a higher load could damage or invalidate the calibration of the equipment. THE CYLINDER DID NOT FAIL AT THIS LOAD

Typical Fracture Type

Cone | Cone&Split | Cone&Shear | Shear | Columnar
Type1 | Type2 | Type3 | Type4 | Type5 | Type6

CONCRETE COMPRESSIVE STRENGTH

State of Alaska Department of Transportation Northern Region Materials Lab — Lab Number: 0

Project: 0 Drew's UAF Research — Field Number: DEV-CYL-7..12

Date Made: Tues, 7/11

Notes: CYL 10- Rate set at 80000 - stalled at 115k, required adjustment to rate of 200
CYL 11- Rate set at 87,000 - stalled at 103k, required adjustment to rate of 200
CYL 12- Rate set at 87,000 - didn't stall

AASHTO T-22/ ASTM C-39 — TEST RESULTS

E-Mail (y/n)		Date Tested	Age (Days)	Cyl. Dia.	A Avg. Dia.	B Cyl. Area	C Yield in Pounds	C / B Unit Strength (psi)	Initials
Y	DEV-CYL-7	8/8	28	4.03 4.07	4.07	12.69	121939	9609	CS
Y	DEV-CYL-8	8/8	28	4.01 4.02	4.02	12.69	116818	9206	CS
Y	DEV-CYL-9	8/8	28	4.02 4.02	4.02	12.69	108406	8543	CS
Y	DEV-CYL-10	10/9	90	4.01 4.02	4.02	12.69	124937	9845	TV
Y	DEV-CYL-11	10/9	90	4.02 4.02	4.02	12.69	125978	9927	TV
Y	DEV-CYL-12	10/9	90	4.01 4.01	4.01	12.63	123317	9764	TV

Stripped in lab? ☐ — B=(A/2 x A/2) x 3.142 — SPEC

TEST METHOD

AASHTO	ASTM		ACCEPTANCE		ASSURANCE	
T 119	C 143		Slump:	"	Slump:	"
T 152	C 231		Air:	%	Air:	%
T 121	C 138		Unit Wt:		Unit Wt:	
	C 1064		Temp of Concrete:			

ACCEPTANCE/ASSURANCE ACCEPTABLE/UNACCEPTABLE
COMPARISON
CONFORMS TO SPECS

*This pressure is the highest achievable using the lab's compressive strength test equipment. Application of a higher load could damage or invalidate the calibration of the equipment. THE CYLINDER DID NOT FAIL AT THIS LOAD

Typical Fracture Type